Predicting the Settling Velocity of Lime Softening Flocs using Fractal Geometry

by

Arman Vahedi

A thesis submitted to the Faculty of Graduate Studies of the University of Manitoba

in partial fulfillment of the requirements of the degree of

Doctor of Philosophy

Department of Civil Engineering

University of Manitoba

Winnipeg, Manitoba, Canada

Abstract

Stokes' law that is traditionally used for modeling the sedimentation of flocs, incorrectly assumes that the floc is solid and spherical. Consequently the settling rates of flocs cannot be estimated using the Stokes law.

The application of fractal dimensions to study the internal structure and settling of flocs formed in lime softening process was investigated. An optical microscope with motorized stage was used to measure the fractal dimensions of lime softening flocs directly on their images in 2 and 3D space. The fractal dimensions of the lime softening flocs were 1.15-1.27 for floc boundary, 1.49-1.90 for cross-sectional area and 2.55-2.99 for floc volume. Free settling tests were used for indirect determination of 3D fractal dimension. The measured settling velocity of flocs ranged from 0.1 to 7.1 mm/s (average: 2.37 mm/s) for the flocs with equivalent diameters from 10μm to 260μm (average: 124 μm).

Floc settling model incorporating variable floc fractal dimensions as well as variable primary particle size was found to describe the settling velocity of large (>60 μm) lime softening flocs better than Stokes' law. Settling velocities of smaller flocs (<60 μm) could still be quite well predicted by the Stokes' law. The variation of fractal dimensions with lime floc size in this study indicated that two mechanisms are involved in the formation of these flocs: cluster-cluster aggregation for small flocs (>60 μm) and diffusion-limited aggregation for large flocs (<60 μm). Therefore, the relationship between the floc fractal dimension and floc size appears to be determined by floc aggregation mechanisms.

The settling velocity of lime softening flocs was also modeled by a general model that assumes multiple normally distributed fractal dimensions for each floc size. The settling velocities were in the range of 0-10mm/s and in good agreement with measured settling velocities (0.1-7.1mm/s). The Stokes' law overestimates the settling velocity of lime flocs. It seems that the settling velocity of flocs is mainly controlled by aggregation mechanisms and forming large floc does not guarantee improved sedimentation.

The multifractal analysis of lime softening flocs showed that these aggregates are multifractal and a spectrum of fractal dimensions is required to describe the structure of an individual floc.

Acknowledgment

First and foremost, I would like to thank my advisor, Dr. Beata Gorczyca. You were the one who initiated the idea of this research and you were always my first resource for creative ideas and helpful advices. You helped me to grow as a student and engineer and it is not easy to recount all that I have learnt from you.

Also, I would like to thank my advisory committee. Dr. Cicek, thank you for your great ideas on practical application of my research and also your valuable comments on development of models. Dr. Morrison, thank you for your help in understanding the mathematical parts of my thesis and your valuable comments on my papers. Dr. Sherriff, thank you for your help with the chemical analysis part of my thesis and your valuable help with my papers and my annual committee meetings.

I really appreciate the help of two undergraduate students, Graeme and Latoya, who helped me in summer terms with experimental part of my thesis.

I spent four years of my life in the Environmental Engineering group of University of Manitoba and I had the chance to meet a wonderful group of graduate students, staff and professors. I would like to thank you all for providing such an environment. I would like to especially thank my office mates in the past four years, Charles, Steven, Justin, and Maryam. I also appreciate the friendship of other colleagues in Environmental Engineering group, Victor, Quyan, Dominika, Magda, Stan, Lukasz, Mehrnaz, Joe, Pouria, Kerry, Michelle and Elsie.

My PhD program and my research were funded by a number of resources. I received financial assistance through University of Manitoba, the City of Portage la Prairie and R.M. Macdonald

water treatment plants, MB's Graduate Research Internship Program (MITACS) and NSERC Collaborative Research and Development Grant.

My research was in collaboration with the City of Portage la Prairie water treatment plant. I would like to thank Mr. Kelly Braden, the director of operations at the city of Portage la Prairie and Mr. Doug Campbell, the manager of the Portage La Prairie water treatment plant.

Finally I would like to acknowledge the role that my family and particularly my parents had in all my life and also in the past four years in completion of my graduate studies. Mom and Dad, you were always very supportive for the decisions that I have made in my life. Keyvan and Saba, you are the best brother and sister anyone can have. I love you all and I am always grateful for having such a wonderful family.

Table of Contents

List of Tables

List of Figures

List of Symbols

F_b	Buoyant force acting on a falling particle in a liquid, N
F_g	Gravitational force acting a falling particle in a liquid, N
F_d	Drag force acting a falling particle in a liquid, N
v_s	Floc settling velocity, $m.s^{-1}$
ρ_f	Particle (floc) density, $kg.m^{-3}$
ρ_w	Water density, $kg.m^{-3}$
ρ_m	Solid density of floc, kg/m^3
ρ_m	Solid density of floc, kg/m^3
V_p	Volume of primary particles, m^3
V_S	Volume of solid component in an aggregate, m^3
g	Gravitational acceleration, $m.s^{-2}$
μ	Dynamic viscosity, $kg.m^{-1}.s^{-1}$
υ	Kinematic viscosity, $m^2.s^{-1}$
C_D	Drag coefficient
Ω	Correction factor in Stokes' Law for porous particles
ε	Floc porosity
d	Particle (floc) diameter, m
d_{50}	Median size of the component particles within floc, m
d_p	Size of primary particles, m
v_{zs}	Sludge settling velocity, $m.s^{-1}$
C	Sludge concentration
K,n	Constants in sludge settling model
N_r	Number of floc covering elements
r	Size of floc covering elements, m
D_H	Hausdorff fractal dimension
D_B	Boundary fractal dimension
D_S	Cross-sectional area fractal dimension
D_V	Volume fractal dimension
D_M	Mass fractal dimension
D_{ST}	Mass fractal dimension estimated from settling tests
D_q	Rényi dimension
M_P	Mass of floc covering elements, kg
ρ_f	density of a floc, kg/m^3
k	Permeability of the aggregate (m^2)
k^*	Dimensionless permeability
N	Number of primary particles in an aggregate
P	Floc perimeter, m
A	Floc projected area, m^2
M	Floc mass, kg
V	Floc volume, m^3
S	Floc cross-sectional area, m^2
D_P	Perimeter-based fractal dimension
D_A	Fractal dimension associated with the projected area

δ	Volume fractal dimension of the primary particles
γ	Distance from self-similarity
l	Dimensionless floc size
θ	Dimensionless particle shape factor
ρ_s	Density of the primary particles, kg/m^3
Φ	The effect of the size distribution of the primary particles
Re	Particle Reynolds number
Q	The scattering momentum (wave vector)
n	The reflective index of surrounding medium
ω	Angle of light
λ	Wave length of the light
I	Scattered intensity
D_{SC}	Fractal dimension from light scattering
H_r	Information entropy of the fractal
P_{rj}	Relative frequency
α_q	Singularity strength
f_q	Singularity spectrum
D_I	Information Dimension
D_C	Correlation Dimension
ECD	Equivalent Circular Diameter, m

Chapter 1
Background

The success of removal of substances by coagulation/flocculation processes is usually determined by the success of soli/liquid separation. The key concept in coagulation and precipitative softening processes is that the suspended and dissolved impurities or unwanted elements aggregate into larger and heavier aggregates (flocs) which subsequently are separated from the water typically by gravity settling (sedimentation).

In design of sedimentation tanks, the settling velocity of individual flocs is the critical parameter that determines the size of the tank. Traditionally, the settling velocity of an individual aggregate in a fluid is described by Stokes' law. There is much evidence that Stokes' law cannot fully describe the settling velocity of flocs. In this thesis Stokes' law is modified to model the settling velocity of chemical coagulation flocs. In this chapter Stokes' law is briefly described. Also the objectives and outline of this thesis are presented.

1.1. Stokes' law

According to Stokes' law, the terminal velocity of a falling object in a viscous fluid is reached when the friction forces combined with the buoyant force exactly balance the gravitational force (Figure **1.1**). For a falling particle in a liquid, the buoyant force, gravitational force and drag force are calculated from the following equations (Batchelor 1967):

$$F_b = \frac{2gM\rho_w V}{M + \rho_w V} \tag{1.1}$$

$$F_g = Mg \tag{1.2}$$

$$F_d = \frac{1}{2}\rho_w v_s^2 C_D A \tag{1.3}$$

where F_b is the buoyant force, g is the gravitational acceleration, M is the particle (floc) mass, V is the particle volume, F_g is the gravitational force, F_d is the drag force, ρ_w is the fluid (water) density, v_s is the settling velocity and C_D is the drag coefficient that is a dimensionless parameter. The drag coefficient is used for quantifying the drag force and is usually a function of Reynolds number (Re).

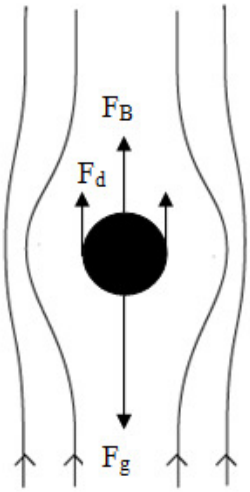

Figure 1.1. Forces acting on a falling object in a viscous fluid; F_d, F_B, and F_g are drag (friction) force, buoyant force and gravitational force respectively (The image was created by author)

For a solid spherical particle, George Gabriel Stokes (1819-1903) calculated the buoyant and drag forces and derived the terminal settling velocity of the particle. Assuming a very low Reynolds number for flocs (Re<<1), he estimated the drag coefficient by using the following equation (Batchelor 1967, Johnson et al. 1996):

$$C_D = \frac{24}{Re} \tag{1.4}$$

where *Re* is the Reynolds number that can be calculated from Eq. (1.5):

$$Re = \frac{\rho_w v_s d}{\mu} \tag{1.5}$$

where d is the particle size (diameter of the spherical particle) and μ is the dynamic viscosity. Therefore, the buoyant force, gravitational force and drag force on the solid spherical particle can be described by the following equations:

$$F_b = \frac{1}{6}\pi d^3 \rho_w g \tag{1.6}$$

$$F_g = mg = \frac{1}{6}\pi d^3 \rho_f g \tag{1.7}$$

$$F_d = 6\pi\mu v_s d \tag{1.8}$$

where ρ_f is the floc density. The settling velocity determined by Stokes' law is presented in Eq. (1.9) (Batchelor 1967).

$$v_s = \frac{(\rho_p - \rho_w)}{18\mu} g d^2 \tag{1.9}$$

1.2. Problem Statement

In derivation of Eq. (1.9) it is assumed that the falling particle is a solid and spherical object. However, the aggregation mechanisms of flocs result in a heterogeneous and porous structure (Figure **1.2**). Therefore, the forces acting on a settling floc will be different from the forces acting on a solid spherical object and consequently the settling velocity of flocs may not follow the Eq. (**1.9**) (Li and Ganczarczyk 1987, Logan 1999).

Many conventional water treatment plants in Manitoba use precipitative lime softening process for hardness removal. The process results in formation of highly heterogeneous flocs that are usually removed by sedimentation. The preliminary settling velocity measurements in our study indicate that the Stokes' law and its modifications generally overestimate the settling velocity of lime softening flocs. Therefore, the designed sedimentation tanks do not remove the flocs effectively. The lime flocs that are not removed may cause filter clogging in the following filtration processes.

1.3. Fractal Structure of Flocs

The internal arrangement of primary particles inside the aggregate, that is the floc structure, determines the drag, mass, porosity, density and dewatering properties of flocs. The internal structure of a floc has been shown to be well described by fractal models that are characterized by distinctive fractal dimensions (Li and Ganczarczyk 1989, Logan B.E. 1999, Kim et al. 2001, Gorczyca and Ganczarczyk 2001 and 2002, Chung and Lee 2003, Maggi et al. 2006, Vahedi and Gorczyca 2010).

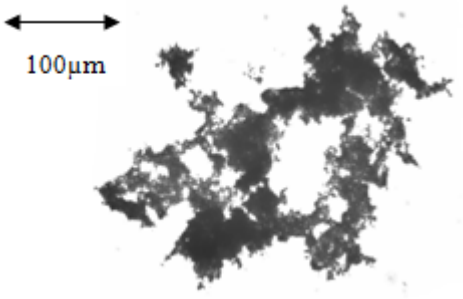

Figure 1.2. Fractal structure of a lime softening floc (The microscopy image was prepared by author)

A fractal dimension can be interpreted as the degree of meandering or irregularity of an object (Gomes and Selman 1999, Kinsner 2005,). A floc's fractal dimensions may indicate a particular structural model that can be used to simulate its hydrodynamic behaviours such as gravity settling and flow-through.

1.4. Objectives

Lime softening flocs have fractal structure andtheir settling velocity cannot be predicted accurately by Stokes' law. A model that considers the fractal structure of flocs must be used for predicting the settling velocity of these aggregates. The generation of such models will be discussed in Chapter 2. In this thesis we will start from a model that was suggested for cohesive sediment flocs and we will make appropriate modifications and improvements to the model for lime softening flocs. The objectives of this thesis are:

- Analyzing the sedimentation processes at Portage la Prairie lime softening water treatment plant.
- Evaluating the existing models for settling velocity of flocs.
- Modeling the settling velocity of lime softening flocs by using a model that incorporates the fractal dimensions of flocs.
- Applying appropriate modifications to the model and deriving a general model for settling velocity of lime softening flocs.

1.5. Thesis outline

The main contributions of this thesis are presented in Chapters 3, 4, 5 and 6. In each chapter the related experimental procedures and analytical methods are presented. Chapter 2 is the literature review that mainly focuses on the application of fractal geometry in modeling the behaviour of flocs.

In Chapter 3, Floc separation processes are evaluated at a conventional lime softening plant located at Portage la Prairie (Manitoba, Canada). The mechanisms of particle formation in different processes of Portage plant are investigated.

Chapter 4 focuses on the separation of lime flocs by sedimentation as a critical solid/liquid separation process in the plant. The application of fractal dimensions in modeling of settling velocity of individual lime softening flocs is presented in this chapter.

Chapter 5 presents findings related to characterization of the structure of lime softening flocs by multifractals.

In Chapter 6, a general model for describing the settling velocity of flocs formed in chemical coagulation processes is presented.

The main contributions, conclusions and recommendations for future studies are presented in Chapter 7.

Chapter 2

Literature Review

This chapter mainly focuses on previous studies on properties of flocs such as size, structure and settling velocity. The mechanisms of flocculation and precipitative softening are also briefly described.

2.1. Flocculation and Precipitative Softening

2.1.1. Coagulation/Flocculation

In conventional water treatment plants, coagulation is usually a pre-treatment process and the first step of the treatment. In most cases, the action of coagulant depends on the formation of an amorphous precipitate that traps the impurities by sweep flocculation (De Julio and Gregory 2009). Sweep flocculation is a non-selective aggregation of particles within the floc. Sweep flocs can be described as large aggregates that are formed when a coagulant such as alum or ferric is added to water (Rattanakawin 2005).

Different sources of water may need different coagulants, but the most commonly used are aluminum sulfate (alum; $Al_2(SO_4)_3$) and ferric sulfate (ferric; $Fe_2(SO_4)_3$). The mechanism of coagulation involves two steps: (1) destabilization of particles by adding a coagulant; (2) collision of destabilized particles to form a larger aggregate (floc). The collision of particles starts by Brownian diffusion (perikinetic aggregation) and is followed by induced fluid motion

(orthokinetic aggregation). The flocculation mechanism is illustrated in Figure **2.1** (Bartby 2006; Gregory 2009).

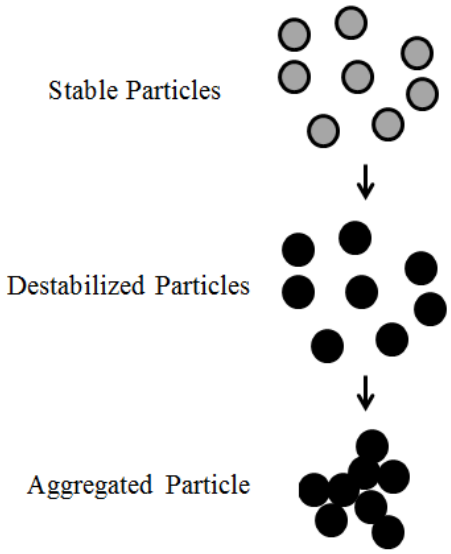

Figure 2.1. Mechanism of particle aggregation in enhanced coagulation. (The idea of the image was taken from Gregory 2009)

The random collision of particles in flocculation results in highly heterogeneous porous aggregates. The hydrodynamic behaviour of these aggregates such as their sedimentation determines the success of the treatment process.

2.1.2. Precipitative Lime-softening

Softening is the treatment process of removing cations (primarily Ca^{+2} and Mg^{+2}) that cause hardness from water. The hardness removal is usually accomplished by chemical precipitation of ions to insoluble salts.

In precipitative lime softening, lime (CaO) or hydrated lime ($Ca(OH)_2$) is added to the source water to increase the pH and decrease the solubility of hardness-causing ions. The ions may precipitate in the forms of calcium carbonate ($CaCO_3$) or magnesium hydroxide ($Mg(OH)_2$) that can be removed by sedimentation or filtration. Eq. (2.1) shows the general chemical reactions in the lime softening process (Benefield et al 1982).

$$CaO + H_2O \rightleftharpoons Ca(OH)_2$$
$$Ca(OH)_2 + CO_2 \rightleftharpoons CaCO_3 + H_2O \tag{2.1}$$

Even though the primary purpose of lime softening is hardness removal, particles and organic matter may also be removed in the lime softening process by attachment to the precipitated calcium carbonate aggregates. Similar to the mechanism of flocculation, during the lime softening process, the calcium carbonate particles and other impurities in the source water collide and form a heterogeneous porous aggregate (floc). The flocs are removed from water by sedimentation or filtration.

2.2. Size Analysis of Flocs

Stokes' law identifies floc size as one of the key variables defining the settling velocity of the floc. Because of the irregular shapes of flocs, it is necessary to have a definition for the size. The size of a floc can be defined in different ways generally based on the instruments and methods used to measure the size. Many definitions have been used in the literature for the size of flocs. For example, length or maximum size that means the longest distance between two points of the circumference of the floc in a single plane. Some researchers inversely use breadth as the size

that is the shortest distance between two points on the circumference of the floc. Equivalent Circular Diameter (*ECD*) is a common definition for floc size that is the equivalent diameter of a circle that has the same area as the original floc (Allen 1997, Markus 2009, Mikeš 2011):

$$ECD = \sqrt{\frac{4A}{\pi}} \tag{2.2}$$

where *A* is the floc projected area.

Many researchers have tried to determine the size distribution of particles formed in water and wastewater treatment using different methods. Some of the techniques that have been used to measure the size distribution of particles in water and wastewater treatment are listed in Table **2.1**.

Fluid turbulence in water and wastewater treatment reactors is one of the main factors determining the size of aggregates. Turbulence is a fluid regime that is characterized by stochastic changes of fluid properties such as velocity, diffusion and pressure. The turbulence may cause shear force on flocs, breakage and formation of eddies. Eddies are swirling of fluid that are caused by chaotic motion of fluid or when the current hits an obstacle. The size of eddies can control the maximum size of aggregates in a fluid (Thomas 2004, Bouyer et al. 2004).

Parker et al (1972) developed the floc break-up theories and showed that the size and structure of flocs are controlled by shear forces acting on flocs. Increased shear force decreases the average floc size (Spicer and Pratsinis 1996).

Table 2.1. Some studies on size distribution analysis of floc

Researcher	Method	Size range & type of flocs
Li and Ganczarczyk (1989)	Microscopy Image Processing	20-1000µm (activated sludge flocs)
Li and Ganczarczyk (1987)	Stroboscopic Imaging	50-1000µm (activated sludge flocs)
Ganczarczyk and Rizzi (1996)	Microscopy Image Processing	30-1500µm (activated sludge flocs)
Nies and Tiehm (1997)	Light Scattering	0.1-125µm (activated sludge flocs)
Hilligardt and Hoffmann (1997)	Light Scattering	0.5-1200µm (activated sludge flocs)
Van Gelder et al,1999	Multiple Particle Counters	1-50µm (particles in water)
Gorczyca and Ganczarczyk (1999)	Microscopy Image Processing	10-220µm (Alum coagulation flocs in Water treatment)
Kim et al. (2001)	Microscopy Image Processing	200-3000µm Alum coagulation flocs in Water treatment)
Motta et al. (2001)	Light Scattering	1-1000µm (activated sludge flocs)
Annadurai et al. (2003)	Light Scattering	5-200µm (Flocs of coagulation by polyaluminum in water)
Zhang 2007	Light Scattering	0.4-340µm (activated sludge flocs)
Gorczyca and Klassen, 2008	Dynamic Image Analysis (DIA) Microscopy	1-1000µm Activated sludge flocs Coagulation flocs
Coufort et al. 2008	Optical Imaging by CCD camera	10-1000µm Alum coagulation flocs
Vahedi and Gorczyca, 2009	Dynamic Image Analysis (DIA) Light Scattering Microscopy	0.02-300µm (lime softening flocs)
Govoreanu et al 2009	Light Scattering Time of Transition Dynamic Image Analysis (DIA)	0.1-1000µm Activated sludge flocs
Manning et al. 2010	Optical Imaging by CCD camera	20-300µm (mud flocs)
Yu et al. 2011	Microscopy	10-400µm Alum coagulation flocs

2.3. Fractal Dimensions of Flocs

Fractal dimensions are parameters that are used to characterize the fractals. Mandelbrot (1982) applied fractal dimensions to describe the surface or boundary roughness of shapes. Mandelbrot developed mathematical definitions for a variety of fractals. Many studies have shown that flocs formed in water and wastewater treatment have fractal properties (Li and Ganczarczyk 1989, Thill et al. 1998, Kim 2001, Gorczyca and Ganczarczyk 2001, Tang et al, 2002, Chu et al 2004, Khelifa and Hill 2006, Weiying et al. 2011, Vahedi and Gorczyca 2011).

2.3.1. Methods for determination of fractal dimensions

In general, the fractal dimensions can be determined directly on the images of flocs or indirectly from other properties of flocs. The widely used methods for determination of fractal dimensions of flocs are box-counting (direct method), settling tests (indirect method) and light scattering (indirect method).

2.3.1.1. Box-counting method: Direct method for measuring fractal dimensions

Eq. (2.3) shows the Hausdorff method for the determination of the fractal dimension of a floc directly by covering its image by N_r elements of size r (Kaye 1993, Kinsner 2005):

$$D_{B,S,V} = \lim_{r \to 0} \frac{\log (N_r)}{\log (1/r)} \tag{2.3}$$

The Hausdorff fractal dimension can be calculated for the boundary (perimeter), surface or volume of a fractal object. A variation of the Hausdorff dimension, the box-counting fractal

dimension, uses squares in 2D and cubes in 3D as covering or filling elements. In this thesis, the box-counting fractal dimensions are labelled as D_B, D_S and D_V for floc boundary, cross-section area and volume respectively. D_V is an example of a 3D fractal dimension or capacity dimension (Maggi and Winterwerp 2004) which provides direct information of 3D structure of the floc and can be used directly to model floc's hydrodynamic behaviours such as gravity settling and flow through the floc.

Li and Ganczarczyk (1989) used optical microscopy imaging and box-counting method to measure the perimeter fractal dimension of activated sludge flocs in the size range of 30-1000 μm. Their results showed that the activated sludge flocs had the perimeter fractal dimension of 1.13-1.22. The results of later study on chemical coagulation flocs (alum flocs) by Gorczyca and Ganczarczyk (1996, 1999) showed similar results. Bahrami and Gorczyca (2008) used the same technique to measure the perimeter fractal dimension of alum and ferric coagulation flocs in water treatment. The perimeter fractal dimension of chemical coagulation flocs was 1.11-1.16 in their study.

Ganczarczyk and Rizzi (1996) measured the surface fractal dimension of activated sludge flocs directly on aggregate images by using microscopy imaging and box-counting method. The surface fractal dimension of activated sludge flocs was 1.88-1.97 in their study. Similar studies by Gorczyca and Ganczarczyk (1996, 1999) and Cousin and Ganczarczyk (1998) showed similar results. Bahrami and Gorczyca (2008) measured the surface fractal dimension of ferric and alum coagulation flocs. The surface fractal dimension of coagulation flocs was 1.94-1.99 in their study.

When perimeter or boundary of the floc is being covered with the line elements (sticks) of size *r*, Eq. (2.3) results in the following power law:

$$P \sim (1/r)^{D_B} \tag{2.4}$$

where *P* is the floc perimeter. The projected area of the floc is sometimes used for fractal analysis. The similar power law can be written for the projected area of the floc. Note that the projected area may be different from the cross-sectional area. The cross-sectional area of a floc is the floc intersection with a plane in 3D but the projected area of a floc is simply the 2D projection from any direction; projected area is what is usually captured in microscopy imaging but the cross-sectional area imaging requires floc sections. The projected area and associated fractal dimension are labelled as *A* and D_A respectively.

$$A \sim (1/r)^{D_A} \tag{2.5}$$

Combining Eq. (2.4) and Eq. (2.5) results in the following power law between the perimeter and projected area of the floc:

$$A \sim P^{\frac{D_A}{D_B}} \tag{2.6}$$

The projected area of a floc is sometimes used to determine the perimeter-based fractal dimension D_P:

$$A \sim P^{\frac{2}{D_P}} \tag{2.7}$$

Eq. (2.6) and Eq. (2.7) show that D_P is equal to the boundary fractal dimension (D_B) only when $A \sim d^2$. For fractals this assumption is not necessarily correct (Imre 2006). In this thesis, D_P is referred to as perimeter-based floc fractal dimension.

Several researchers used Eq. (2.3) and Eq. (2.7) to measure the boundary and cross-sectional area and perimeter-based fractal dimensions of chemical coagulation and activated sludge flocs directly on images of projections of these flocs (Li and Ganczarczyk 1989, Thill et al. 1998, Gorczyca and Ganczarczyk 1996, 1999, Kim et al. 2001, Gorczyca and Ganczarczyk 2001, Maggi and Winterwerp 2004, Dong et al. 2011).

Of all of the fractal dimensions discussed above, only 3D volume fractal dimensions of flocs have practical applications for modeling the settling and other hydrodynamic characteristics. Unfortunately, this particular dimension is extremely difficult to measure directly as it requires 3D reconstruction of flocs. Confocal microscopy has been used for 3D imaging of biological aggregates (Snidaro et al. 1997, Thill et al. 1998, Schmid et al. 2003). Chu et al (2004) used confocal microscopy to obtain cross-sectional surface area images of activated sludge flocs and measured the surface fractal dimension directly on floc images. Chu et. al (2004) also reconstructed 3D images of flocs by stacking 2D cross-sectional images obtained by confocal microscopy and measured the volume fractal dimension of activated sludge flocs by covering the floc volume with volume elements. The reported surface and volume fractal dimensions of activated sludge flocs were 1.72-1.81 and 2.46-2.70 in their study. There are several limitations associated with the use of confocal microscopy for floc imaging. The samples have to be stained

with fluorescent stain which attaches only to the organic parts of the floc making inorganic parts invisible. This is especially limiting for the analysis of chemical coagulation flocs which are predominantly inorganic. The staining process can be considerably elaborative and change the moisture content of flocs which may result in altering their fragile structure. Therefore, D_V has not yet been directly measured for chemical coagulation flocs. However, the indirect estimation of three-dimensional volume fractal dimension (D_V) of a floc from the boundary (D_B), perimeter (D_P) and cross-sectional area fractal dimensions (D_S) has been attempted by some researchers.

The Hausdorff dimension is sometimes referred to as self-similarity dimension or Sierpinski fractal dimension named after the Polish mathematician, Wacław Sierpinski (1882-1962).

2.3.1.2. Estimation of volume fractal dimension (D_V) from other dimensions

Few researchers have attempted to estimate the volume fractal dimension of flocs from other dimensions. Two methods that use different approaches for the estimation of volume fractal dimensions are presented below.

Estimation of D_V from surface fractal dimension (Ds) (Thill et al. 1998)

The "*Codim*" of a fractal set (X) is defined as:

$$Codim\,(X) = fdim\,(X) - E \tag{2.8}$$

where *fdim (X)* is the fractal dimension of the fractal set X and E is the Euclidian dimension of the space that the fractal set is defined in. According to Mandelbrot (1985), the intersection of a

fractal set X and a plane P is also a fractal with the fractal dimension of $D_{P\cap X}$ and the following relationship exists:

$$Codim\,(P \cap X) = Codim\,(P) + Codim\,(X) \tag{2.9}$$

Therefore the fractal dimension of intersection of a three-dimensional floc with a plane that is D_S can be derived as follows:

$$Codim\,(Intersection) = Codim\,(Plane) + Codim\,(3D\ floc) \tag{2.10}$$

Since the plane and the floc are defined in the 3D space, E for plane, floc and intersection will be the same and equal to 3.

$$fdim\,(Intersection) - 3 = fdim\,(Plane) - 3 + fdim\,(3D\ floc) - 3$$

$$(D_S - 3) = (2 - 3) + (D_V - 3)$$

$$D_S = D_V - 1 \tag{2.11}$$

Thill et al. (1998) used Eq. (2.11) to estimate the volume fractal dimension of activated sludge flocs. In the derivation of Eq. (2.11), D_S was assumed to be the fractal dimension of cross-sectional surface area determined by using Eq. (2.3).

Estimation of D_V from perimeter based fractal dimensions (Dp) Maggi and Winterwerp (2004)

Maggi and Winterwerp (2004) estimated the volume fractal dimension from the floc perimeter-based fractal dimension by using the following relationship:

$$D_V = \sqrt{\frac{a(l)}{D_P - b(l)}} \quad for \quad D_P < 2 \tag{2.12}$$

where $l=d/r$ is the dimensionless floc size, d is the floc size, r is the pixel size in the two-dimensional projection of the floc and $a(l)$ and $b(l)$ are calculated from the following equations:

$$a(l) = 9\left(z(l) - \frac{2[k(l)]^2 - 9z(l)}{[k(l)]^2 - 9}\right), \quad b(l) = \frac{2[k(l)]^2 - 9z(l)}{[k(l)]^2 - 9} \tag{2.13}$$

where

$$k(l) = z(l)[z(l) - 1] + 1, \quad z(l) = D_P \frac{\log[4l - 4]}{\log[l]} \tag{2.14}$$

They simply assumed that $A = P^{\frac{2}{D_P}}$.

2.3.1.3. Free settling test: Indirect method for measuring fractal dimensions

Another form of 3D fractal dimension is called mass fractal dimension (D_M) that can be derived directly from Eq. (2.3) by substituting the number of volume filling elements with the mass of

filling elements. The floc volume (V) scales with the size of aggregate according to the following power law:

$$V \sim d^{D_V} \tag{2.15}$$

Assuming a constant density for floc's elements (pixels), the following power law is obtained:

$$M \sim d^{D_M} \tag{2.16}$$

where M and D_M are floc mass and floc mass fractal dimension respectively.

If we assume the density of the primary particle (filling elements) of the floc to be constant, the floc mass (M) and volume (V) are linearly correlated and 3D mass fractal dimension (D_M) and volume fractal dimension (D_V) should be identical.

Many researchers have used the following equation to estimate the mass fractal dimension of flocs from their settling velocities (Li and Ganczarczyk 1989, Logan 1999, Bushel et al. 2002, Tang et al. 2002, Chu et al. 2004, Liao et al 2005):

$$v_s \propto d^{D_M - 1} \tag{2.17}$$

In Chapter 4 of this thesis the Eq. (2.17) is critically evaluated.

2.3.1.4. Fractal dimension determined indirectly from light scattering properties of flocs (D_{SC})

Light scattering has been used as an indirect method to measure the mass fractal dimension of flocs by a number of researchers (Kim et al. 2001, Tang et al. 2002, Annadurai et al. 2003, Chu et al. 2004, Wu and He 2010, Wang et al. 2010). Eq. (2.18) and Eq. (2.19) are used to measure the mass fractal dimension by light scattering.

$$Q = \frac{4\pi n}{\lambda} \sin\left(\frac{\omega}{2}\right) \tag{2.18}$$

where, Q is the scattering momentum (wave vector), n is the reflective index of surrounding medium, ω is the angle of light, and λ is the wave length of the light, and

$$I(Q) \propto Q^{-D_{SC}} \tag{2.19}$$

where, I is the scattered intensity, and D_{SC} is the fractal dimension from light scattering. The mass fractal dimension is obtained from the slope of scattering intensity (I), versus scattering momentum (Q) for different angles. The light scattering method is based on moving a certain wavelength of light through the media. The assumption in light scattering is that the particles do not move during the scattering. This assumption is not necessarily correct for large flocs that can rapidly settle. Tang et al. (2002) suggested using light scattering only for small particles. They used a combination of light scattering (for large flocs >10μm) and settling test (for small flocs<10 μm) to measure the mass fractal dimension of flocs. They also compared the mass fractal dimensions obtained from settling test and light scattering and showed that the results of light scattering and settling test are comparable for small flocs (<10 μm).

2.3.2. Variability of fractal dimensions with flocs size

Several studies have suggested that the fractal dimensions of flocs vary with the floc size (Gorczyca and Ganczarczyk 2001, Chakraborti et al. 2003, Maggi and Winterwerp 2004, Khelifa and Hill 2006, Maggi et al. 2007, Son and Hsu 2008). This variation is a natural consequence of the difference in the structure of small and large flocs which is consistent with the theory of multi-level floc aggregation.

Many studies have shown that the aggregation mechanism affects the morphology and fractal dimension of aggregates (Meakin 1984, Jullien et al 1987, Thouy and Jullien 1994, Snidaro et al 1997, Gorczyca and Ganczarczyk 2002). The aggregation mechanism is determined by many factors such as the properties of primary particles, hydrodynamic conditions in the reactor and so on. In the first stage of flocculation processes, the primary particles of flocculent collide and form the primary clusters. After this stage the flocculation becomes more complex and can be described by particle-cluster aggregation or cluster-cluster aggregation models (Meakin 1985). Therefore, the aggregation mechanism is different for smaller flocs and large flocs. The diffusion-limited aggregation (DLA) is an extension of these models in which the particles undergoing a random walk due to Brownian motion collide to form aggregates (Witten and Sander 1981). DLA has been shown to be consistent with aggregation of large activated sludge flocs (Thill et al 1998, Snidaro et al 1997).

As the aggregates grow, both cluster-cluster aggregation and particle-cluster aggregation might occur and form different structures. In the case of particle-cluster aggregation, the small primary particles can easily penetrate into and fill in a fractal structure via either linear or random trajectory and form a compact structure with fractal dimensions closer to Euclidean dimensions.

On the other hand in cluster-cluster aggregation the clusters cannot penetrate each other via any trajectory and simply stick to each other and usually form a larger aggregate with lower fractal dimension (Meakin 1984). The probability of penetration in particle-cluster aggregation or sticking in cluster-cluster aggregation depends on many factors.

Floc restructuring, for example, due to breakup and re-aggregation, can also change the fractal dimension of aggregates (Meakin and Jullien 1988). Since the breakup and restructuring pattern depend on the hydrodynamic conditions that define the aggregate size, the relationship between the size and fractal dimension of aggregates can be affected by many phenomena.

Gorczyca and Ganczarczyk (1999, 2001) investigated Sierpinski fractal dimensions of alum coagulation and activated sludge flocs. According to their study, the flocs formed in different stages and the relationship between the size and fractal dimension is linear for each stage but different from other stages. Sierpinski fractal dimension is equivalent to *Ds* as discussed in this chapter. They also showed that the flocs become more irregular and their fractal dimensions deviates from Euclidean dimensions as their size increases.

Maggi (2005) suggested that a floc's volume fractal dimension changes with aggregate size according to the following power law:

$$D_V = \delta l^{\gamma} \tag{2.20}$$

where δ is the volume fractal dimension of the primary particles, which is normally close to or equal to 3 but no larger than 3, and γ is a parameter called distance from self-similarity. The

parameters δ and γ can be calculated by fitting Eq. (2.20) to the floc's fractal dimension and size data.

2.3.3. Multifractal analysis of flocs

Highly heterogeneous fractal objects with varying density patterns cannot be fully characterized by a single fractal dimension. Such fractals are too complex to be described by one fractal dimension.

Here we should distinguish between two types of fractal dimensions: morphological fractal dimensions and entropy fractal dimensions. Box-counting fractal dimensions are morphological fractal dimensions and only use the information about the geometry of fractal objects and provide no information about the distribution of a measure or time behaviour of a system (Kinsner 2005).

Using the concept of information entropy a number of other fractal dimensions can be defined that can be used to characterize very complex fractals. Information entropy is the amount of information needed to specify the state of a system. If a fractal is covered by N_r elements with size of r, the first order measure of information entropy of a system can be written as (Shannon 1948):

$$H_r = -\sum_{j=1}^{N_r} P_{rj} log P_{rj} \tag{2.21}$$

where H_r is the information entropy of the fractal, P_{rj} is the relative frequency n_{rj} with which the fractal enters (intersects) the jth covering element at a given r, divided to the total number N_{rT} of intersects of the fractal with all elements at that r when N_r is large enough (r is very small):

$$P_{rj} = \lim_{N_r \to \infty} \frac{n_{rj}}{N_{rT}} \tag{2.22}$$

$$N_{rT} = \sum_{i=1}^{N_r} n_{rj} \tag{2.23}$$

In other words, P_{rj} is the probability of intersecting the fractal with the jth covering element at a given r. For any fractal object that is covered by N_r elements with size of r, the entropy based fractal dimensions can be defined using the following power-law relation:

$$D_q = \lim_{r \to 0} \frac{1}{q-1} \frac{log \sum_{j=1}^{N_r} \left(P_{rj}^q\right)}{log(r)} \qquad -\infty \leq q \leq +\infty \tag{2.24}$$

Eq. (2.24) is the generic equation of various fractal dimensions of a multifractal object. The fractal dimension D_q is often called Rényi dimension in the literature (Hentschel and Procaccia 1983, Grassberger 1985, Kinsner 2005). To achieve a bounded spectrum for different fractal dimensions the following transformation is used (Kinsner 2005):

$$\alpha_q = \frac{d}{dq}\left[(q-1)D_q\right] \tag{2.25}$$

$$f_q = q\alpha_q - (q-1)D_q \tag{2.26}$$

The parameters α_q and f_q are called singularity strength and singularity spectrum respectively. Each point on the singularity spectrum represents a specific fractal dimension. By rearranging the Eq. (2.26) the fractal dimension associated to a given point on the singularity spectrum can be derived:

$$D_q = \frac{f_q - q\alpha_q}{1-q} \tag{2.27}$$

A typical spectrum resembles the graph shown in Figure **2.2**.

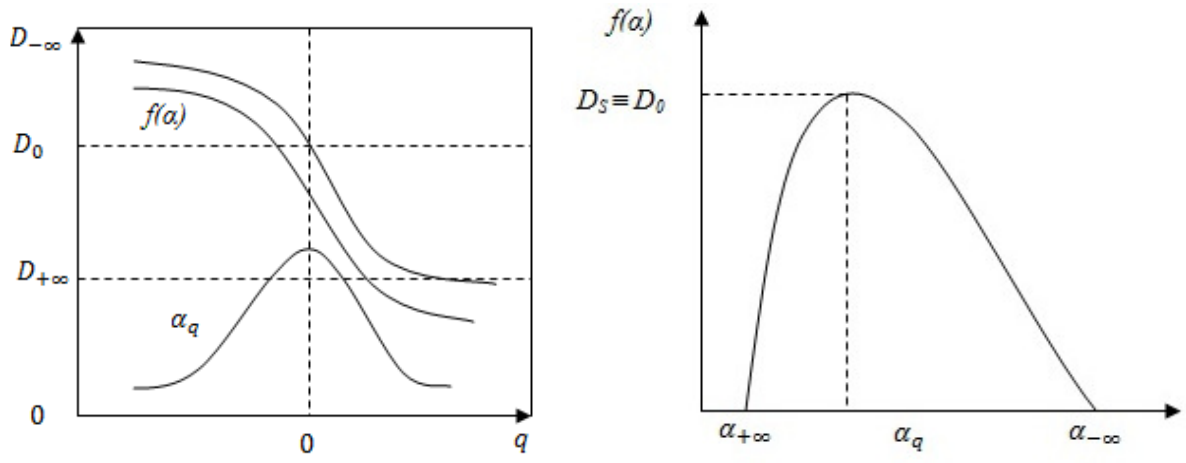

Figure 2.2. Rényi fractal dimensions (Left) and bounded singularity spectrum (right) (Images were created by author)

2.3.3.1. Important points on the multifractal spectrum

For *q=0*, the Rényi dimension is equivalent to the self-similarity or box-counting dimension.

$$D_0 = \lim_{r\to 0} \frac{1}{0-1} \frac{log \sum_{j=1}^{N_r} \left(P_{rj}^0\right)}{log(r)} = \lim_{r\to 0} - \frac{logN_r}{logr} = \lim_{r\to 0} \frac{logN_r}{(1/r)} \tag{2.28}$$

For *q=1* the Rényi dimension is:

$$D_1 = \lim_{r\to 0} \frac{\sum_{j=1}^{N_r} P_{rj} \log\left(P_{rj}\right)}{log(r)} = \lim_{r\to 0} \frac{H_1}{\log\left(1/r\right)} \tag{2.29}$$

In the literature D_1 is often called "Information Dimension" (D_I) (Hentschel and Procaccia 1983, Grassberger 1985, Kinsner 2005).

For *q=2* the Rényi dimension is:

$$D_2 = \lim_{r\to 0} \frac{1}{2-1} \frac{log \sum_{j=1}^{N_r} {P_{rj}}^2}{log(r)} = \lim_{r\to 0} \frac{log \sum_{j=1}^{N_r} {P_{rj}}^2}{log(r)} \tag{2.30}$$

In the literature D_2 is often called "Correlation Dimension" (D_C) (Hentschel and Procaccia 1983, Grassberger 1985, Kinsner 2005).

2.3.3.2. Probability-based multifractal analysis

Chhabra and Jensen (1989) developed a method for determination of singularity spectrum from an image of a fractal object by using the concept of probabilities. For an image covered by N_r elements with size of r, let's define moment ($\mu_i(q,r)$) as:

$$\mu_i(q,r) = \frac{[P_{ri}]^q}{\sum_j [P_{rj}]^q} \tag{2.31}$$

Note that the probabilities in Eq. (2.31) are the same as Eq. (2.24). The singularity strength α_q and singularity spectrum f_q then can be calculated by using the following equations:

$$\alpha_q = \lim_{r\to 0} \frac{\sum_i \mu_i(q,r) log[P_i(r)]}{log(r)} \tag{2.32}$$

$$f_q = -\lim_{r\to 0} \frac{\sum_i \mu_i(q,r) log[\mu_i(q,r)]}{log(r)} \tag{2.33}$$

Maggi et al. (2007) performed a multifractal analysis for mud flocs and successfully derived the multifractal spectrum of the aggregates using the Chhabra and Jensen (1989) method.

Yang et al. (2008) used the same technique for multifractal analysis of images of activated sludge flocs and two deterministic (artificial) fractal sets. Even though the method properly interpreted the singularity spectrum for deterministic fractal systems, the singularity spectrum obtained for naturally occurring sludge flocs showed extremely large values or large errors at the

boundaries ($q \rightarrow \pm\infty$). They suggested that this discrepancy is due to the highly heterogeneous distribution of biomass inside the floc and inappropriate size of the box used in their analysis.

Perrier et al (2006) developed a computer program for multifractal analysis of two-dimensional binary images in 2D. In their algorithm, they used Eq. (2.24) and determined the singularity spectrum by computing the values of D_q.

2.3.3.3. Wavelet-based multifractal analysis

In late 1980s and early 1990s, Stephane Mallat made some fundamental contributions to the application of wavelet theory for image processing by developing the theory of multiresolution signal decomposition (Mallat 1989). The use of wavelets in multiresolution analysis is an important characteristic that can be used for the analysis of any phenomenon that is self-similar over a certain time or scale range.

A multifractal can be treated as a signal that is self-similar in both time and frequency. In the past two decades many researchers have tried to use the wavelet transform for multifractal analysis (Holschneider 1988, Arneodo et al 1988, Daubechies and Lagrias 1992, Riedi et al 1999, Murguia and Urias 2001, Chavez et al 2010). It appears that the wavelet transform is able to capture the full information of a self-similar multifractal.

Any digital image can be considered as a signal or series of numbers that are stored in a 2D or 3D matrix. To extract information from any signal, an appropriate signal processing technique is needed. Typically, in the process of any signal processing, the time-domain signal is transformed into another domain that can reveal some characteristic information of the signal that is not observable in the original form (Gao and Yan 2010). The most common transform techniques

use a form of integral transform in order to simplify the analysis of a signal by reducing the number of dimensions of differential equations. Fourier transform and Laplace transform are popular examples of such transform techniques.

The wavelet transform of a signal *x(t)* can be written as:

$$w(s,\tau) = \langle x, \psi_{s,\tau} \rangle = \frac{1}{\sqrt{s}} \int_{-\infty}^{+\infty} x(t) \psi^* \left(\frac{t-\tau}{s} \right) dt \tag{2.34}$$

where $s > 0$ is the scaling parameter and τ is the shift parameter. The symbol ψ^* denotes the complex conjugation of the base wavelet $\psi(t)$. The main difference between wavelet transform and Fourier transform is that wavelets are localized in both time and frequency whereas the standard Fourier transform is only localized in frequency (Gao and Yan 2010).

In the reviewed studies, there were few studies on the possibility of unifying various fractal dimensions of flocs into a singularity spectrum. For chemical coagulation flocs, there was no study on direct measurement of a singularity spectrum or Rényi dimension among the reviewed papers. Such analysis can provide numerical measures for the complexity and the mass distribution in flocs.

2.4. Linkage of Fractal Dimensions and Settling Velocity

Many attempts to model the settling velocity of individual flocs have been undertaken. These models are mainly modifications of Stokes' law, such as Eq. (2.35) that includes a correction factor for porous particles (Ω) (Lee et al. 1996, Bushell et al. 2002, Gorczyca and Ganczarczyk 2001):

$$v_S{}^2 = \frac{4g(\rho_f - \rho_w)}{3\Omega C_D \rho_w}\, d \tag{2.35}$$

where v_S is the settling velocity, ρ_f is the floc density, ρ_w is the water density, g is the gravitational acceleration, C_D is the drag coefficient, Ω is a correction factor for porous particles and d is the floc size.

The correction factor (Ω) in the modified Stokes' law for permeable aggregates (Eq. (2.35)) reflects the effect of the floc permeability and shape in the aggregate settling velocity. For a highly porous sphere moving steadily through an infinite medium, Neale et al. (1973) theoretically derived the following value for the correction factor (Ω):

$$\Omega = \frac{2\beta^2[1 - (\tan\beta)/\beta]}{2\beta^2 + 3[1 - (\tan\beta)/\beta]} \tag{2.36}$$

where

$$\beta = \frac{\mathrm{d}}{2\sqrt{\mathrm{k}}} \tag{2.37}$$

where k is the permeability of the aggregate (m^2) and d is the floc size.

There is much evidence showing that Stokes' law does not adequately describe the floc settling velocity (Logan 1999). The correction factor (Ω) modifying the original Stokes' law has not been widely applied due to its limited effectiveness (Namer and Ganczarczyk 1993, Brown and Lawler 2003, Khelifa and Hill 2006).

Several researchers have incorporated floc fractal dimensions into Stokes' law to improve the settling velocity predictions (Winterwerp 1998, Logan 1999, Li and Yuan 2002, Bushell et al. 2002, Tang et al. 2002, Li et al. 2003, Sterling 2005, Khelifa et al 2006).

For a digitized image of a floc in a 3D embedding space with characteristic diameter of d, if a unit mass is associated with each pixel of the image, the total mass (M) corresponds to its volume and its density ($\rho=M/d^3$) is a measure of the fraction of the space that is occupied by the floc (Stanley and Meakin 1988). For a fractal structure the total mass can be related to the characteristic diameter by the following relationship (Bushell et al 2002):

$$M \sim d^{d_M} \tag{2.38}$$

For a fractal $d_M<d$, therefore the total mass increases more slowly than d^3. For flocs, this characteristic of fractal structures may result in their irregular hydrodynamic behaviours such as their settling velocity (Logan 1999, Bushell 2002). Now, let us see how this characteristic can be used to modify Stokes' law for fractal objects.

The relationship between the number of primary particles within a floc (N) and floc mass (M) can be written as:

$$N.m_p = M \tag{2.39}$$

where m_p is the mass of one primary particle. According to the theory of fractals the following relationships can be written for the mass and size of a floc (Kay 1993, Kinsner 2005):

$$M \sim d^{D_M} \tag{2.40}$$

Similar relationship can be written for the primary particles:

$$m_p \sim {d_p}^{D_{M,p}} \tag{2.41}$$

Where d_p and $D_{M,p}$ are the size and mass fractal dimension of primary particles respectively. In the literature it is assumed that D_M=$D_{M,p}$ (Kranenburg 1994, Li and Logan 2001) and therefore:

$$N \sim \left(\frac{d}{d_P}\right)^{D_M} \tag{2.42}$$

However, it has been shown that the fractal dimension of primary particles is close to the Euclidean dimension and different from the fractal dimension of the floc aggregate (Maggi and Winterwerp 2004, Vahedi and Gorczyca 2011).

Assuming that the floc is composed of solid and water, therefore, the density of the aggregate, ρ_f, can be expressed as follows:

$$\rho_f = \frac{\left(N.V_p.\rho_p\right) + (V - V_S)\rho_w}{V} \tag{2.43}$$

where V_p is the volume of the primary particles, V_S is the volume of the solid component in the aggregate N. V_p and V is the total aggregate (floc) volume and ρ_p is the density of the primary particles forming the flocs. Therefore:

$$(\rho_f - \rho_w) = \frac{\left(N.V_p.\rho_p\right) - (V_S)\rho_w}{V} \tag{2.44}$$

Hence:

$$(\rho_f - \rho_w) = \frac{N.V_p(\rho_p - \rho_w)}{V} \tag{2.45}$$

From Eq. (2.42) and Eq. (2.45) Kranenburg (1994) suggested the following relationship between the floc density and the density of primary particles within the floc:

$$\Delta\rho_f = (\rho_f - \rho_w) \sim (\rho_p - \rho_w)\left[\frac{d_p}{d}\right]^{3-D_M} \tag{2.46}$$

Winterwerp (1998) modified the drag force (Eq. (1.3)) and gravitational force (Eq. (1.6)) acting on flocs by introducing two parameters (α and β):

$$F_g = \frac{\alpha}{6}\pi d^3 \rho_f g \tag{2.47}$$

$$F_d = \beta\frac{1}{2}\rho_w v_s^2 C_D \frac{\pi d^2}{4} \tag{2.48}$$

The parameters α and β are coefficients depending on the sphericity of the particles.

He also assumed that the Reynolds number of flocs falls within 0.2≤Re≤1000 which is called transitional Stokes' regime and used the following empirical expression for drag coefficient that was suggested by previous researchers for flocs in that regime (Graf 1977).

$$C_D = \frac{24}{Re}(1 + 0.15Re^{0.687}) \tag{2.49}$$

According to Eq. (2.47) – Eq. (2.49), Winterwerp (1998) suggested the following equation for the settling velocity of flocs that incorporates the aggregate fractal dimension into the Stokes' law:

$$v_{st} = \frac{\alpha}{18\beta}\frac{(\rho_p - \rho_W)g}{\mu} d_0^{3-D_M} \frac{d^{D_M-1}}{1 + 0.15Re^{0.687}} \tag{2.50}$$

However, the correction coefficients (α, β) and the methods for estimating these factors were not discussed in details in Winterwerp's (1998) study. For spherical (α=β=1) and solid particles (D_V=3) in the Stokes' regime (Re<<1), Eq. (2.50) reduces to original Stokes' law:

$$v_{st} = \frac{1}{18}\frac{(\rho_p - \rho_W)g}{\mu} d^2 \tag{2.51}$$

Logan (1999) conducted extensive study of settling velocities of microbial aggregates. He found that microbial flocs settle much faster than Stokes' law predicts. Li and Yuan (2002) performed a settling test for microbiological aggregates ranging from 1000-2500 µm and found that the settling velocity for these aggregates are very close and slightly faster than the velocity predicted

by Stokes' law for impermeable particles (Eq. (1.9)). Li et al (2003) also concluded that the settling velocity of activated sludge flocs can be closely predicted by Stokes' law. Although the results in their study show that the settling velocity of biological fractal aggregates can be predicted by the Stokes' law it may not be correct for the much smaller chemical coagulation flocs formed in water treatment processes. The faster settling velocity of permeable particles than impermeable shows that Stokes' law may not be reliable for predicting the settling velocity of all fractal aggregates.

Based on the assumption of Li and Yuan (2002) and Li et al (2003) that Stokes' law closely predicts the settling velocity of fractal aggregates, Sterling et al (2005) suggested the following equation for settling velocity of fractal aggregates:

$$v_{st} = \frac{1}{18}\frac{(\rho_p - \rho_W)g}{\mu} d_p^{3-D_M} d^{D_M-1} \tag{2.52}$$

Khelifa and Hill (2006) successfully modified the Eq. (2.50) by assuming that floc fractal dimensions varied with the floc size according to Eq. (2.53) :

$$D_M = a\left(\frac{d}{d_p}\right)^b \tag{2.53}$$

They suggested the following equation to estimate the settling velocity of individual flocs:

$$v_s = \frac{1}{18}\theta g \frac{\rho_P - \rho_w}{\mu} d_{50}^{3-D_M} \frac{d^{D_M-1}}{1 + 0.15Re^{0.687}}\psi \tag{2.54}$$

where d_{50} is the median size of the component particles within the floc, θ is a dimensionless particle shape factor replacing α and β in Eq. (2.50) and $Re=v_s d/\nu$ is the particle Reynolds number in which ν is the kinematic viscosity of the water. $\psi = m_3/m_F^{3/D_M}$, represents the effect of the size distribution of the primary particles in the floc, where $m_3 = \left(\sum_{i=1}^{k} d_i^3\right)/k$ and $m_F = \left(\sum_{i=1}^{k} d_i^{D_M}\right)/k$.

2.5. Linkage of fractal dimensions to floc permeability, porosity and flow though flocs

Flow through flocs affects the drag force acting on a settling aggregate; it also provides for advective transport of substances inside the flocs. In water treatment, this may play an important role, for example in the transport of disinfecting chlorine inside the floc. The flux through a floc depends on floc material permeability, which in turn is determined by floc porosity.

2.5.1. Permeability

Attempts have been undertaken to model the permeability and flow through water and wastewater flocs (Li and Ganczarczyk 1987, Li and Logan 2001, Gorczyca and Ganczarczyk 2002, Chu et al. 2005).

The permeability of flocs has been estimated using mathematical models that are in general in the form of $k=d_0 f(\varepsilon)$ where ε is the porosity of the floc and d_0 is the size of the primary particles forming the floc. Some of these mathematical models are listed in Table **2.2**. The main limitation of these equations is the estimation of floc porosity.

Table 2.2. Floc permeability models (Lee et al. 1996)

Model	Primary particle shape	Permeability function
Binkman	Sphere	$k = \frac{d_0^2}{72} \times \left[3 + \frac{4}{1-\varepsilon} - 3\sqrt{\frac{8}{1-\varepsilon} - 3}\right]$
Carman-Kozeny	Sphere	$k = \frac{\varepsilon^3}{5S_0^2(1-\varepsilon)^2}$
Happel (or cell model)	Sphere	$k = \frac{d_0^2}{18\gamma^3} \times 3\frac{3 - 4.5\gamma + 4.5\gamma^5 - 3\gamma^6}{3 + 2\gamma^5}$
Happel	Fiberous	$k = \frac{3d_0^2}{32\varphi} \times \left[-\ln\varphi - \frac{\varphi^2 - 1}{\varphi^2 + 1}\right]$
Davies	Fiberous	$k = \frac{d_0^2}{4} \times \frac{1}{16\varphi^{3/2}(1 + 56\varphi^3)}$
Iberall	Fiberous	$k = \frac{3}{16} \times \frac{\varepsilon d_0^2}{1-\varepsilon}\frac{2 - \ln Re_p}{4 - \ln Re_p}$

The symbol d_0=primary particle diameter; $\varphi=1-\varepsilon$ = solid fraction of floc; $\gamma = \varphi^{1/3}$; S_0 = specific surface area of the primary particle = $6/d_0$; $Re_p = d_0\rho_w v/\mu\varepsilon$ = Reynolds Number based on the primary particle and internal flow velocity

2.5.2. Porosity

A common and simple method for estimating the density and porosity of flocs using the modified Stokes' law for porous aggregates (Eq. (2.51)) has been used by several researchers (Li and Ganczarczyk 1987, Lee et al. 1996, Ganczarczyk and Rizzi 1996, Wu and Lee 2003).

$$\left(\rho_f - \rho_w\right) = \frac{3\Omega C_D \rho_w}{4gd} {v_S}^2 \tag{2.55}$$

and

$$\varepsilon = \frac{(\rho_f - \rho_w)}{(\rho_p - \rho_w)} \tag{2.56}$$

It has been shown that the modified Stokes' law may not adequately describe the settling velocity of flocs (Li and Ganczarczyk 1987, Johnson et al. 1996, Logan 1999, Khelifa and Hill 2006, Vahedi and Gorczyca 2011). Therefore, Eq. (2.55) and Eq. (2.56) cannot perfectly estimate the flocs density and porosity.

From Eq. (2.42) and Eq. (2.43), Li and Logan (2001) suggested Eq. (2.57) for the porosity of aggregates:

$$\varepsilon = 1 - c\left(\frac{d}{d_P}\right)^{D_M - 3} \tag{2.57}$$

The estimated porosity in Eq. (2.57) can be used to estimate the floc permeability from the equations presented in Table 2. However, in derivation of Eq. (2.57), Li and Logan (2001) assumed a spherical shape for the aggregate and that the volume of the aggregate could be calculated from the following equation:

$$V = \frac{\pi d^3}{6} \tag{2.58}$$

Eq. (2.58) is not necessarily correct for fractal aggregates and is in contrast with Eq. (2.15) which is a fundamental equation for fractal objects.

Floc porosity is determined by the internal arrangement of primary particles and clusters that is determined by the mechanism of aggregation. The fractal dimensions of flocculated aggregates have been theoretically determined by a number of researchers and it has been shown that the aggregation mechanism determines the fractal dimension of flocs (Witten and Sander 1981, 1983, Meakin 1983[a], Brown and ball 1985, Turkevich and Scher 1985, Tan et al 1999, Hasley 2000, Weipeng et al 2009).

The porosity and the number of primary particles within the flocs are correlated. Therefore, since the number of primary particles and fractal dimension are correlated according to Eq. **Error! Reference source not found.**, the floc porosity and floc fractal dimension are also correlated. Therefore, the aggregation mechanism determines the floc porosity. The aggregation mechanisms and their effect on the structure of flocculated aggregates are discussed in greater detail in Section 6.2 of Chapter 6.

It has been shown that the porosity and permeability of activated sludge flocs increase as the floc size increases (Hriberesk et al 2011). According to Eq. (2.57), the fractal dimension decreases as the porosity increases. It means that the fractal dimension of studied activated sludge flocs by Hriberesk et al (2011) decreases as the floc size increases. This conclusion is in agreement with the theory of variable fractal dimensions that was presented in Section 2.3.2.

2.5.3. Flow through flocs

Li and Ganczarczyk (1987) compared the settling velocity of activated sludge aggregates with impermeable solid particles and found experimental evidence for the possibility of fluid flow through flocs. Li and Ganczarczyk (1992) used free settling tests to estimate the permeability of

activated sludge flocs. They concluded that, generally, small flocs were not permeable, but all flocs in the size range from 100 to 500 µm were permeable. During the gravitational settling, flocs with the longest dimension in the range of 50 to 1000 µm showed a drainage rate of 10^2 - 10^7 µm^3/s. Wu et al. (2000) performed a similar study and for activated sludge flocs in the size range of 150-800 µm their estimated permeability ranged from 2.5×10^2 to 8×10^7 m^2. Similar research was also performed by Lee et al (1996).

The Sierpinski carpet fractal model has been successfully used to represent the structure of flocs (Gorczyca and Ganczarczyk 1999, 2001) and predict the flow through activated sludge and alum coagulation flocs.

Adler (1986) suggested the following form of the Carmen-Kozeny equation to calculate the permeability of an ideal Sierpinski carpet:

$$k^* = (1/3.51)[(b^2 - l^2 - b)/4]^2[(b^2 - l^2)/b^4]^N \quad (2.59)$$

where, $k^*=k/D^2$ is dimensionless permeability; b^2 is the number of squares in the carpet; l^2 is the number of squares removed from the carpet; and N is the construction stage. Gorczyca and Ganczarczyk (2002) estimated the permeability of alum coagulation flocs and activated sludge flocs from Eq. (2.59). The flow rates through flocs were 0.7×10^9 µm^3/s and 3×10^7 µm^3/s for activated sludge flocs and alum coagulation flocs respectively. The estimated permeability values were comparable with previous studies.

Li and Logan (2001) incorporated the porosity determined from Eq. (2.57) into equations existing for the permeability models of Table 2. They used two methods, single-particle fractal

model for flocs with uniformly distributed particles in an aggregate and cluster-fractal model for flocs where the primary particles within the aggregate are not uniformly distributed within the volume but are instead separated into smaller clusters. Table **2.3** shows the suggested equations for the permeability factor $\beta = d/2\sqrt{k}$ derived from the models. The permeability ($k=(d/2\beta)^2$) can be determined based on size (d) and β.

Table 2.3. Permeability factors (β) derived from single-fractal and cluster-fractal models (Li and Logan 2001)

Model	**Permeability function (single-fractal)**	**Permeability function (cluster-fractal)**
Caeman-Kozeny	$\beta = 6.7c\left(\frac{d}{d_0}\right)^{D_V-2}\left[1-c\left(\frac{d}{d_0}\right)^{D_V-3}\right]^{-3/2}$	$\beta = 6.7c\left(\frac{N}{c}\right)^{(D_V-2)/D_V}\left[1-c\left(\frac{N}{c}\right)^{(D_V-3)/D_V}\right]^{-3/2}$
Brinkman	$\beta = 4.2c\left(\frac{d}{d_0}\right)\left[3+\frac{4}{c}\left(\frac{d}{d_0}\right)^{3-D_V}-3\sqrt{\frac{8}{c}\left(\frac{d}{d_0}\right)^{3-D_V}}-3\right]^{-1/2}$	$\beta = 4.2\left(\frac{N}{c}\right)^{1/D_V}\left[3+\frac{4}{c}\left(\frac{N}{c}\right)^{(3-D_V)/D_V}-3\sqrt{\frac{8}{c}\left(\frac{N}{c}\right)^{\frac{(3-D_V)}{D_V}}}-3\right]^{-1/2}$
Happel	$\beta = 2.1\left(\frac{d}{d_0}\right)\left[\frac{3-4.5\gamma_p+4.5\gamma_p^5-3\gamma_p^6}{\gamma_p^3(3+2\gamma_p^5)}\right]^{-1/2}$ where $\gamma_p=c^{1/3}(d/d_0)^{(Dv-3)/3}$	$\beta = 2.1\left(\frac{N}{c}\right)^{1/D_V}\left[\frac{3-4.5\gamma_c+4.5\gamma_c^5-3\gamma_c^6}{\gamma_c^3(3+2\gamma_c^5)}\right]^{-1/2}$ where $\gamma_p=c^{1/3}(N/c)^{(Dv-3)/3Dv}$

They found that Brinkman and Happel permeability equations provided more realistic predictions of the actual permeability of aggregates. However, they did not directly measure the volume fractal dimension (D_V) in their paper.

Chu et al. (2005) and Yang et al. (2007) used confocal microscopy to obtain a three dimensional reconstructed floc and then modeled the flow through the floc by using the equations governing the fluid flow through a porous media. If a uniform fluid flow U is imposed at the entry plane and at the side-walls of the floc model, the governing equations of the fluid flow are stated as follows:

$$(\vec{u}^* \cdot \nabla^*)\vec{u}^* + \left(\frac{P_0}{\rho U^2}\right)\nabla^* \mathrm{P}^* = \frac{\mu}{\rho U d_f}\nabla^{*2}\vec{u}^* \tag{2.60}$$

$$\vec{u}^* = \frac{\vec{u}}{U} \tag{2.61}$$

$$\nabla^* = \frac{\nabla}{\mathrm{d_f}} \tag{2.62}$$

$$\mathrm{P}^* = \frac{\mathrm{P}}{\mathrm{P_0}} \tag{2.63}$$

where u is the fluid velocity, P_0 is the pressure at the inlet plane, P is the pressure, d_f is the geometric mean of the length, width and height of the floc. The boundary conditions of the model are:

$$\vec{u}^* = U\vec{\imath} \qquad at\ inlet\ plane\ and\ side\ walls \tag{2.64}$$

$$\vec{u}^* = 0 \qquad at\ solids\ surface \tag{2.65}$$

Chu et al. (2005) used FLUENT 6.0 (Fluent Inc., USA) to solve Eq. (2.60) to determine the pressure difference between the inlet and outlet of their floc model. Once Eq. (2.60) is solved the permeability of the floc can be calculated using Darcy's law:

$$q = \frac{k}{\mu}\nabla P \tag{2.66}$$

where q is the flux (flow per area unit) of flow, k is the permeability and ∇P is the pressure difference between the inlet and outlet of the floc. Their estimation of permeability for activated sludge flocs ranging from 78-113 µm was 10^{-12}-10^{-10} m^2.

2.6. Sludge Sedimentation

The sedimentation process usually occurs through two different mechanisms: (1) individual floc settling; (2) sludge zone settling (Figure **2.3**).

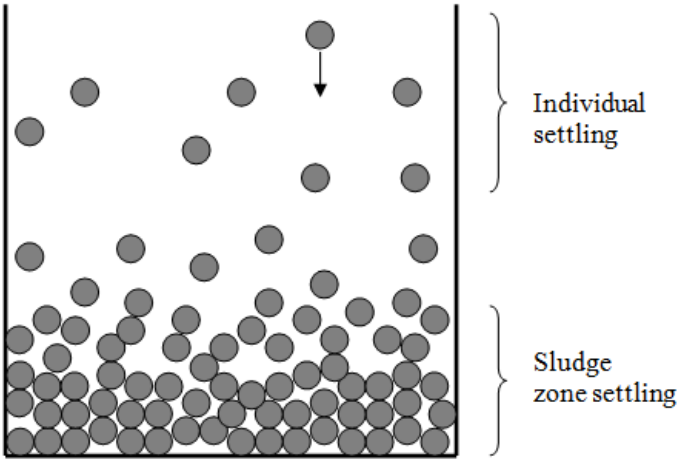

Figure 2.3. Individual floc settling and sludge zone settling

Based on the concentration of settling particles, the sedimentation process is classified into four common classes that are presented in

Table **2.4**.

Table 2.4. Common sedimentation classifications

Class I	Unlimited settling of discrete particles
Class II	Settling of dilute suspension of flocculated particles
Class III	Hindered settling and zone settling
Class IV	Compression settling (compaction)

Floc properties determine the settling of the sludge; this is especially pronounced at low sludge concentrations (type I settling) and very high sludge concentration (type IV settling). In type I settling flocs settle as individual aggregates; in type IV settling, a blanket of flocs settles. Effectiveness of type I settling depends on settling velocities of individual flocs, while type IV settling is predominantly determined by the dewatering properties of flocs. The sludge settling process is typically modeled using the sediment flux theory. In this theory, all properties of flocs are reduced to one parameter – sludge solid concentration (Ekama et al. 1997).

According to the flux theory, the settling of a concentrated suspension of flocs, i.e. sludge, has been modeled. Eq. (2.67) shows one of many mathematical expressions linking the sludge zone settling velocity to the concentration of the sludge (Ekama et al. 1997):

$$v_{ZS} = Ke^{-nC} \tag{2.67}$$

where v_{zs} is the sludge settling velocity, C is the sludge concentration and K and n are constants related to the characteristics of particular sludge. The physical meaning of K and n is not known but it has been suggested that these parameters might represent some properties of the flocs such

as settling velocity and drainage (Gorczyca and Ganczarczyk 2002). Knowledge about the structure of individual flocs may help us understand the mechanism of sludge settling.

Chapter 3

Analysis of Particle Separation and Filtration at Portage la Prairie Water Treatment Plant

The main objective of this study was to evaluate the effectiveness of solid/liquid separation at a conventional lime softening plant located in Portage la Prairie (Manitoba, Canada). This plant suffers from frequent clogging of the sand filters. An improvement in solid/liquid separation results in more effective filtration and a significant energy saving in backwashing. The plant also experiences a scale deposition on recarbonation tank and pipelines.

3.1. Introduction

Sand filters are widely used in water purification for the removal of solid particles. With an appropriate coagulation pre-treatment, the sand filters can also be used to remove dissolved organic carbon and many other dissolved contaminants such as heavy metals, pesticides and pharmaceutical products (Wotton 2002, Thirunavukkarasu et al. 2003, Rooklidge et al. 2005, Aslan et al. 2007).

There are three main types of sand filters that are used in water treatment: rapid (gravity) sand filters, upflow sand filters and slow sand filters. Sand filters may function either as physical treatment units by trapping particles or as biological treatment units through the formation of a gelatinous layer (biofilm) that provides an effective removal of organic matter and pathogens.

Sand filters function as depth filters i.e. the particles are trapped inside the pores of the filter media. The grain size of each layer of the sand filter is determined from the target particle size.

The accumulation of particles on the surface of sand filters may cause filter clogging. The size and structure of particles play the key role in all filtration mechanisms. The properties of the individual flocs such as flow-through, compressibility and size may also determine the properties of the clogging layer and the effectiveness of the filtration (Li and Ganczarczyk 1992). The clogging layer formed on the filter media is essentially a cake of compressed flocs. The linkage of flocs individual properties and properties of clogging cake on filters and membranes has been studied by a number of researchers (Barbot et al. 2008, Choi et al. 2008, Ji et al. 2008, Huang et al. 2011).

Frequent filter clogging requires more filter backwashing and media maintenance, which may negatively impact the operational cost of the plant. Filter clogging is affected by physical or biological factors. Physical clogging usually occurs when solid particles adhere to the sand grains, form a cake on the sand filter surface or accumulate inside the pores of the filter. Biological clogging is related to the growth of biofilm on the sand media; this is usually the case in the filtration of raw water with a high concentration of dissolved organic carbon (Huisman and Wood 1974, Reddi et al 2000).

In general, several factors can affect the sand filter performance: the raw water content, the pre-treatment processes, and many other environmental conditions such as pH and temperature (Darby and Lawler 1990, Platzer et al 1997, Gorczyca and London 2003, Lawler and Nason 2006). The raw water content and pre-treatment processes determine the characteristics of the

filter inflow suspensions such as the number, size, chemical composition and charge of solid particles.

In this study all water samples were taken from the Portage la Prairie water treatment plant (Manitoba, Canada). In this chapter an overview of the treatment processes as well as the water quality at the Portage la Prairie plant is presented. The particle separation and the problem of filter clogging at the plant are also evaluated in this chapter.

3.2. Portage la Prairie water treatment plant

The city of Portage la Prairie is located approximately 70km (45mi) west of Winnipeg (Manitoba, Canada). The population of the city is about 13000. The city of Portage la Prairie and its surrounding communities with a total population of 50000 are served by a conventional lime softening water treatment plant that acquires its raw water from the Assiniboine River (City of Portage la Prairie 2009).

3.2.1. Raw water quality

Seasonal turbidity spikes, high total organic carbon (TOC) and high total hardness are the main characteristics of Assiniboine River. These characteristics represent serious challenges for the Portage la Prairie water treatment plant.

Table **3.1** shows the Assiniboine River raw water quality and representative particle sizes. Standard methods for measuring pH, alkalinity, turbidity, color and TDS were used (APHA, 2005). Also two particle counters (Brightwell Technologies and Spectrex 2200) and the methods developed by Gorczyca and Klassen (2008) were used for particle size distribution analysis of

raw water. According to the archived data, for the same season no significant fluctuation in the raw water quality data occurred from 2007-2010.

Table **3.1** shows the average raw water quality that was taken from the plant lab in 2009 and measured in 2009 and 2010 at University of Manitoba Environmental Engineering laboratory.

Table 3.1. Raw water quality of the Portage La Prairie Plant

Parameter	Raw Water	Finished Water
pH	7.5-8.5	7-8
Alkalinity (mg/l CaCO3)	250-300	50-100
Total Hardness (mg/l CaCO3)	300-450	150-200
Total Dissolved Solid (mg/l)	300-600	200-300
Turbidity (NTU)	0.5-50	<0.5
Color (TCU)	25-60	<5
DOC (mg/l)	9-20	2-7
Particle Size Range (μm)	10-90	<15
Standard Deviation of Particle Size (μm)	3.05	-
d50 of Particle Size Distribution (μm)	64	-

3.2.2. Water Treatment Processes

The schematic diagram of the Portage La Prairie water treatment plant is shown in Figure **3.1**. The first step in the treatment process is sand ballasted flocculation. The plant uses alufer as coagulant which is a mixture of alum and ferric chloride. After the flocculation clarification, water flows into clarifiers for hardness removal.

The plant uses a lime softening process for hardness removal (about 320mg/l of hydrated lime is added). The clarifier effluent at a pH of around 10.5-11 then enters the re-carbonation contactor where pH is lowered to about 7.5-8.0 (dosage of CO_2 is about 45 mg/l). After that water flows

into the ozone contactor for disinfection. The ozone residual is usually between 1 to 3 mg/l. Then the water passes through sand gravity filters and granular activated carbon (GAC) filters respectively. There is a clear well between sand filters and GAC filters that stores enough water for backwashing of the sand filters. Fluoride, orthophosphates and chlorine are added to the water before it enters the storage reservoir. This reservoir provides enough contact time for chlorination. Finished water is then pumped from the storage reservoir to the distribution system.

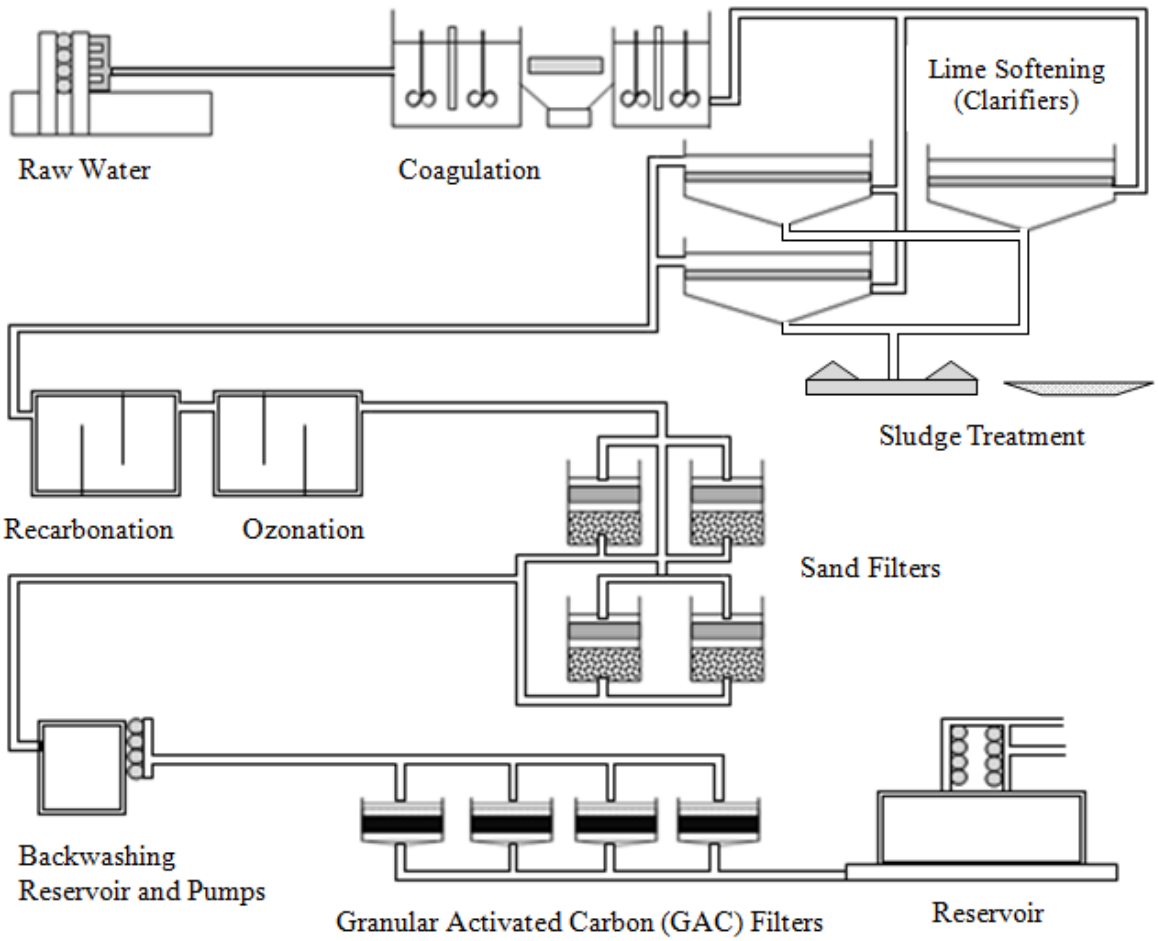

Figure 3.1. Portage water treatment plant schematic diagram (Diagram was reproduced by author according to visitor brochure of Portage la Prairie water treatment plant, 2009)

3.2.3. The issue of filter clogging at Portage plant

The Portage la Prairie water treatment plant has the problem of needing frequent filter backwashing at the sand filters. The plant also experiences a scale deposition on the recarbonation tank and pipelines. An improvement in filtration would result in saving significant energy for backwashing. In this chapter, the origin of sand filter clogging at the Portage la Prairie water treatment plant as well as the mechanisms of particle formation and particle separation in pre-treatment processes is analyzed.

3.3. Experimental procedures and results

The experiments were performed in two stages; (1) analysis of filter medium deposits and water quality changes throughout the plant; (2) bench scale modeling of treatment processes in the laboratory.

3.3.1. Analysis of filter media and water quality changes throughout the plant

3.3.1.1. Analyses of deposited material on sand filters

X-ray diffraction, Scanning Electron Microscopy (SEM) equipped with an Energy Dispersive Spectrometer (EDS) and Inductivity-Coupled Plasma Ion Chromatography (ICPIC) were used to determine the chemical composition of the clogging material deposited on the sand filter media.

X-ray diffraction was used to determine the molecular structure of compounds. EDS is a method used to determine the identity of elements in compounds. Application of X-ray diffraction in combination with EDS allows for determination of the chemical composition and molecular

structure of the material. However, none of these methods provide exact information about the relative quantity of each element or compound; therefore ICPIC was used to establish the quantities of elements and compounds in the sample.

A 250 mg sample of the filter media was taken from Portage La Prairie water treatment plant in August 2009. Samples were kept at 4°C until analysis. The cake deposited on the filter was separated from the filter media by suspending the media sample in ethanol. The deposit was separated from sand and was dried at room temperature. The dried sample of the filter deposit was used for chemical composition analysis.

X-ray diffraction

The in situ powder X-ray diffraction instrument (Bragg-Brentano powder X-ray diffractometer, PANalytical X'Pert Pro, PANalytical B.V., Netherland) at the Department of Geological Science of University of Manitoba was used to determine the crystal structure of the material clogging the sand filters (diffractometer radius = 240 mm).

Scanning Electron Microscopy (SEM) and Energy Dispersive Spectrometry (EDS)

In this study, a combination of SEM (Cambridge Stereoscan 120, Cambridge, United Kingdom) and EDS at the Department of Geological Science, University of Manitoba, was used for elemental analysis of the material clogging the sand filters.

ICPIC

Inductivity-Coupled Plasma Ion Chromatography (ICPIC) was used to determine the chemical composition of clogging material. A suspension of 1 mg of the clogging material in 50ml of

HCL (5%) was prepared and the ICPIC analysis was performed at the Department of Animal Science of the University of Manitoba.

3.3.1.2. Analyses of particle size distribution and water quality changes in the plant

In August 2009, particle analysis was conducted throughout the plant to observe the particle formation during each water treatment process. Three replicate 100 ml samples were collected at eight accessible points of the plant. A Spectrex 2200 particle counter (Laser particle counter, Spectrex 2200, Spectrex Corp., CA, USA) that utilizes the principles of light scattering was brought to the plant to measure the number and size of particles of samples on-site.

Turbidity and pH measurements were also conducted on samples collected throughout the plant between November 2010 and January 2011. Standard methods for measuring pH, and turbidity were used (APHA, 2005). 250 ml samples were collected at eight accessible points of the plant and were kept at 4 ºC. The turbidity and pH were measured within 48 hours of sampling.

3.3.1.3. Results and discussion

Figure **3.2** shows the result of the X-ray diffraction of the cake layer on the sand filter media. The pattern of the diffracted X-ray indicates the crystal structure of the sample. The horizontal axis of the graph is 2-theta (2θ) and the vertical axis is intensity of spinal .The X-ray analyses indicated that the filter clog material is predominantly composed of calcite, a stable form of $CaCO_3$.

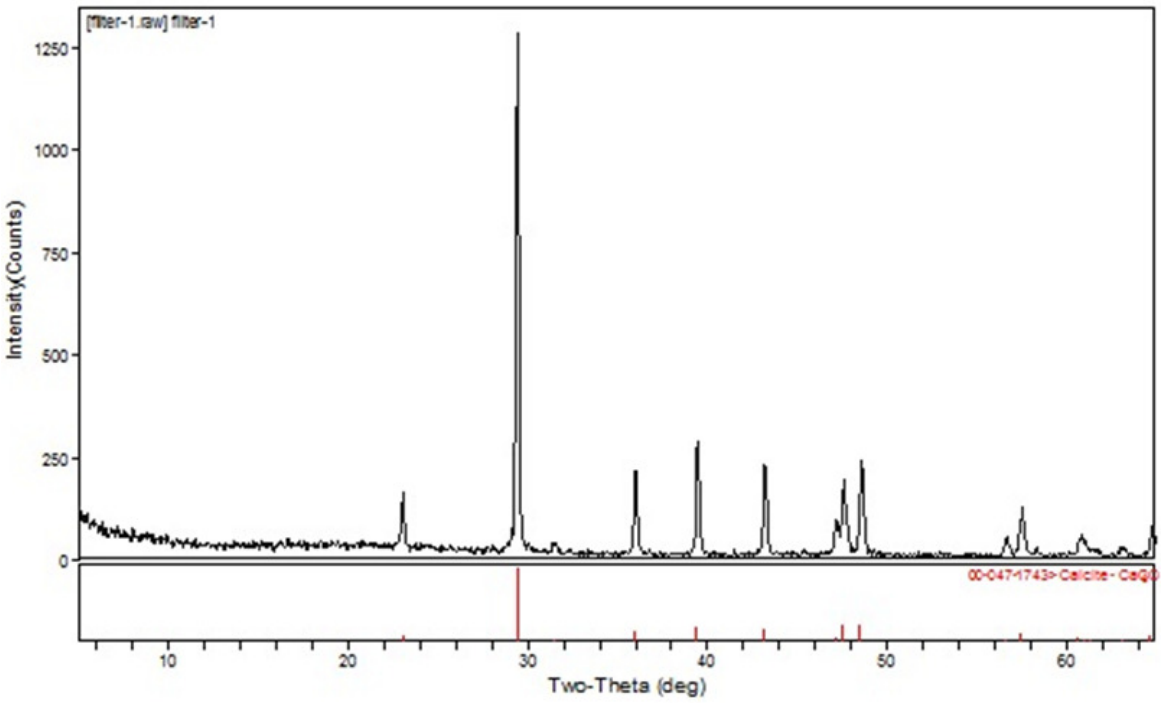

Figure 3.2. X-ray diffraction result of the sand filter clogging material

The filter deposit image captured by SEM and the results of elemental analysis are shown in Figure **3.3** and Figure **3.4**.

The EDS results confirm that the clogging particles are mainly composed of calcium compounds. Lower amounts of Fe, Al, Mg and Si were also identified in the sample of clogging material. Since alum and ferric coagulants were added in the pre-treatment process their existence was expected. The source of silica could be due to either the sand filter media or the sand that was used in the sand ballasted flocculation during the pre-treatment process.

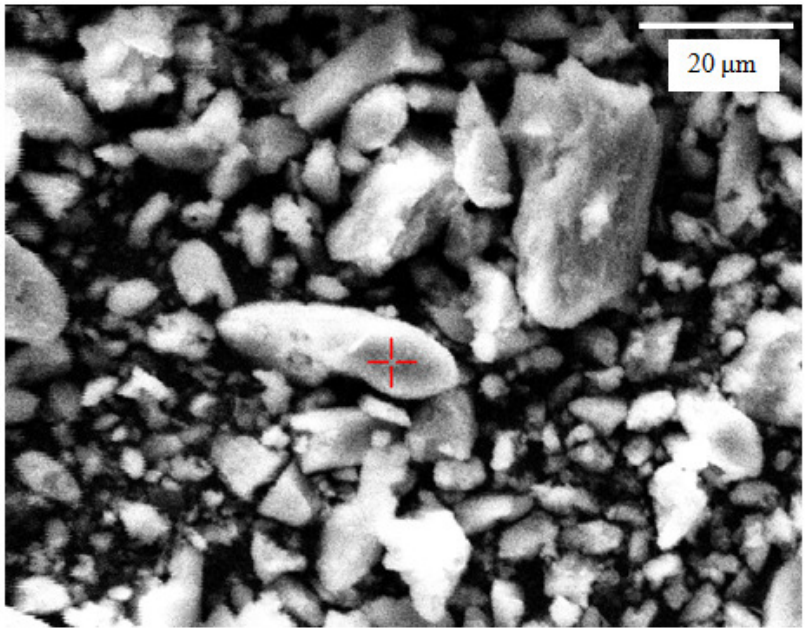

Figure 3.3. SEM Image of clogging particles separated from the filter media

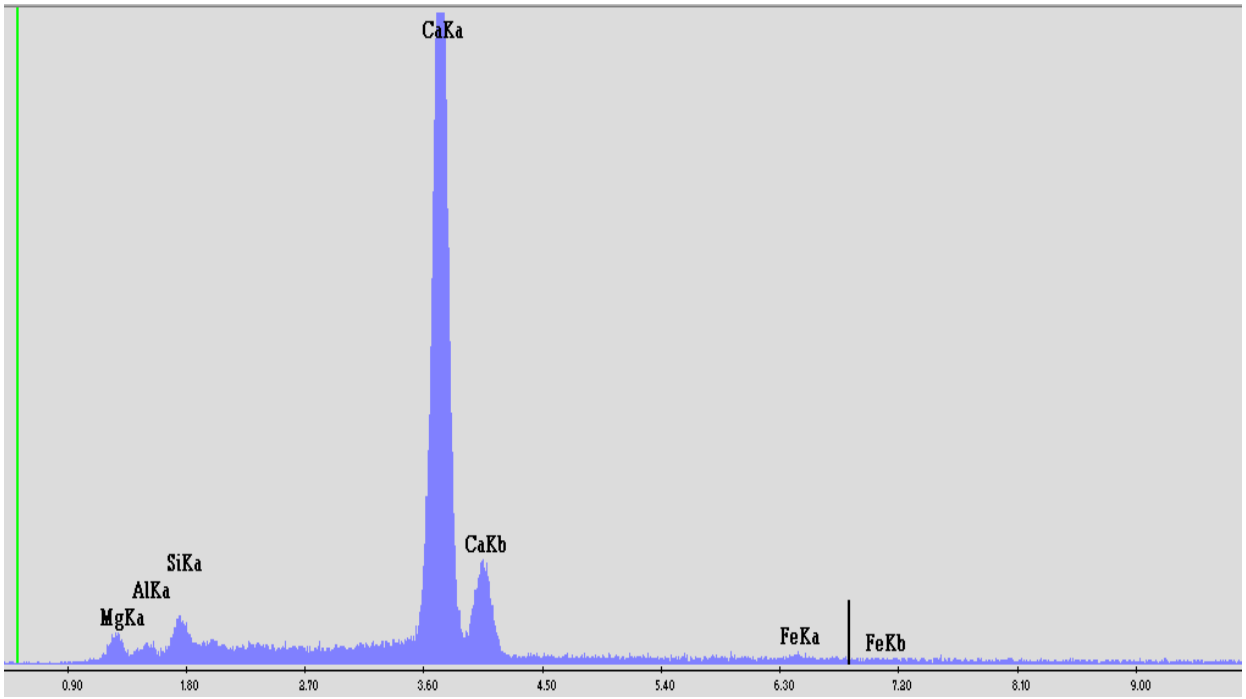

Figure 3.4. Analysis of elements of clogging particles by Energy Dispersive Spectrometry (EDS).

The Inductivity-Coupled Plasma Ion Chromatography (ICPIC) results showed that the metals in the samples were mainly calcium (95%), Mg (3%), Fe (1.5%) and small amounts of other elements including Al (0.5%).

Figure **3.5**-Figure **3.6** show the changes in turbidity, pH and particle sizes throughout the plant.

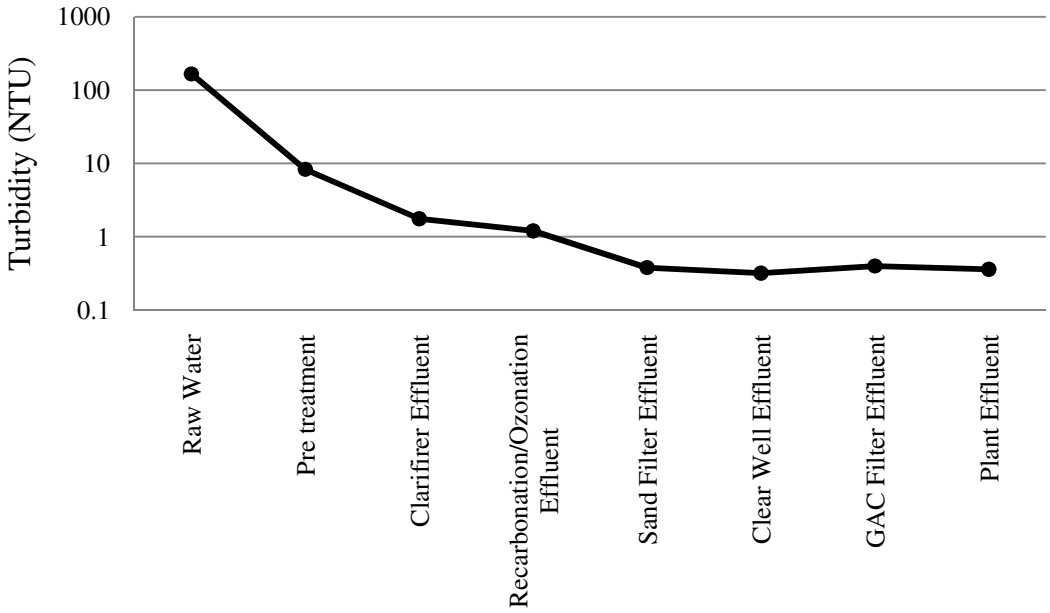

Figure 3.5. Turbidity in Portage La Prairie plant (January 2011)

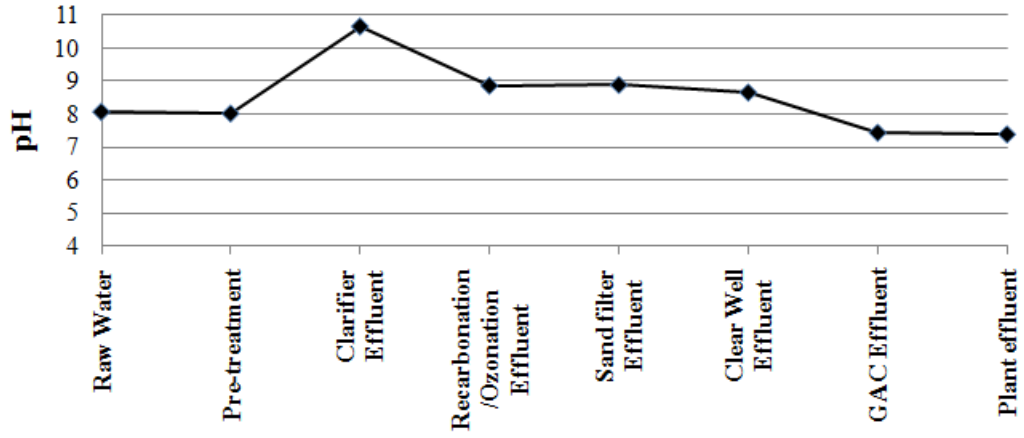

Figure 3.6. pH in Portage La Prairie plant (January 2011)

The results of particle counting throughout the plant are shown in Figure **3.7** which indicates that there is a significant increase in the size of particles in recarbonation and ozonation processes. It seems that the particle size is increasing inside the recarbonation and ozonation chambers.

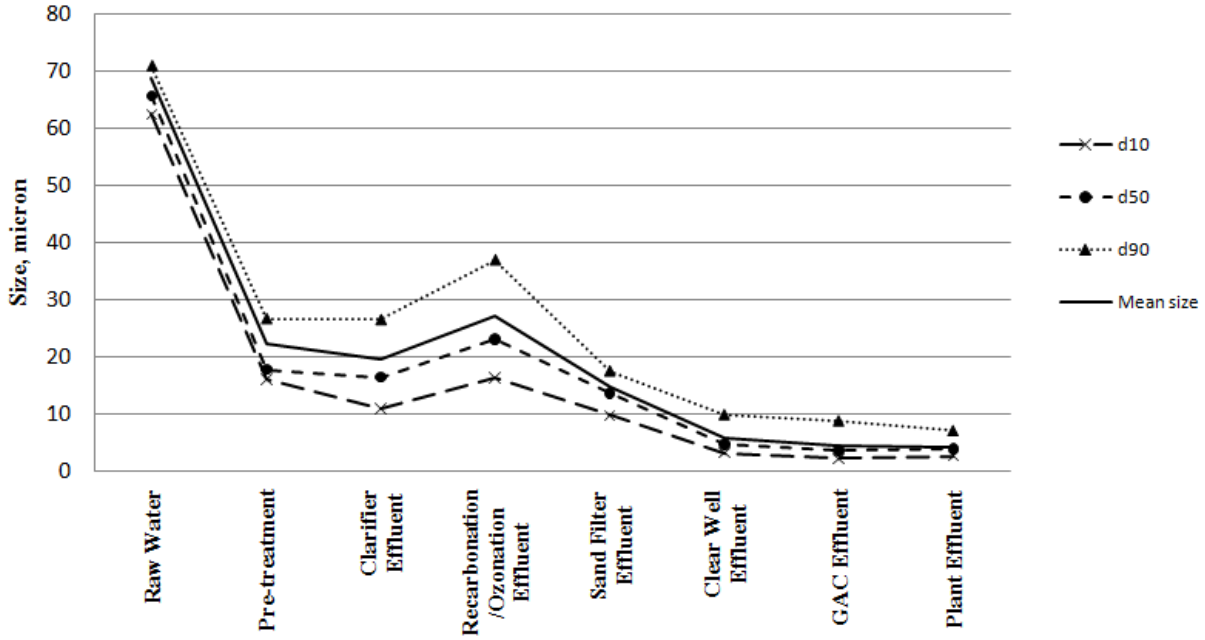

Figure 3.7. Change in representative sizes of particles in Portage la Prairie plant (August 2009)

Figure **3.5** shows that the sand filters are lowering the turbidity from 1.2 to about 0.4 NTU. Figure **3.6** indicates that in the softening process, the pH of water is raised to about 10.5-11 which causes the precipitation of calcium carbonate particles. After the lime softening process, the pH of water is lowered to about 8-9 by dissolving carbon dioxide gas (recarbonation). Figure **3.7** shows an increase in particle size during recarbonation and ozonation processes. It was hypothesized that during the time required for pH to be lowered from 11 to the guidelines level of 6.5 – 8.5 (Health Canada, 2008) a continuous formation of calcium carbonate precipitates in water occurred; these precipitates would clog the sand filters and deposit in the pipes. Another

hypothesis was that ozone promoted precipitation of calcium carbonate and increased the rate of particle formation. Laboratory experiments were conducted to investigate the above hypotheses in greater detail.

3.3.2. Bench scale modeling of treatment processes

3.3.2.1. Investigating the impact of the recarbonation process on particle formation

The recarbonation process of Portage plant was modeled on a bench scale at the Environmental Engineering Laboratory of University of Manitoba. The clarifier effluent was delivered from the plant in the first week of August 2009 and samples were kept at 4°C. The tests were performed within 3-4 days of the water delivery.

A dynamic particle analyzer (DPA 4100) was used to monitor the formation of particles during the recarbonation process. In the measurements with DPA 4100, the suspension passes through a flow cell where the particles can be detected (Figure **3.8**).

Figure 3.8. Bench scale recarbonation model and particle counting

A 1-liter beaker was placed on the platform of the particle counter. Carbon dioxide was applied to the water sample through a small stone diffuser in seven steps to reduce the pH by about 1 pH unit in each step. The recarbonation was continued until the pH of the sample was down to 6.5. At each pH level, three tests were conducted. The final pH of 6.5 was chosen based on the plant data (May 2008-May2009) and water quality standards. Particle counting was performed after each addition of carbon dioxide.

3.3.2.2. Investigating the impact of ozonation process on particle formation

The ozonation experiments were also conducted at the Environmental Engineering Laboratory at the University of Manitoba. The recarbonated effluent was delivered from the plant on August 10, 2009 and was kept in 4°C. The tests were performed within 3-4 days of water delivery.

An ozone generator (OZO 100 VTTL, Ozomax Ltd, Quebec, Canada) was used for ozonation modeling (Figure **3.9**).

Figure 3.9. Bench scale ozonation model

The ozone generator was calibrated by using the traps that are shown in Figure **3.9**. Three different doses of ozone (2.4, 3.2 and 5.4 mg/l) were added to one litre of the sample through a small stone diffuser and the particle counting was performed every five minutes for 25 minutes. The ozone doses were selected to achieve an ozone residual between 1 mg/l and 3 mg/l. A DPA 4100 particle counter was used to monitor the formation of particles during the ozonation process.

3.3.2.3. Results and discussion

The size distribution of the particles for different pH levels in recarbonation process were obtained. The relationships between the pH and the number as well as representative sizes of the particles (d_{10}, d_{50}, d_{90}) are shown in Figure **3.10** and Figure **3.11**. These figures show that the size and number of particles in recarbonation process are constant indicating no formation of new particles in the process.

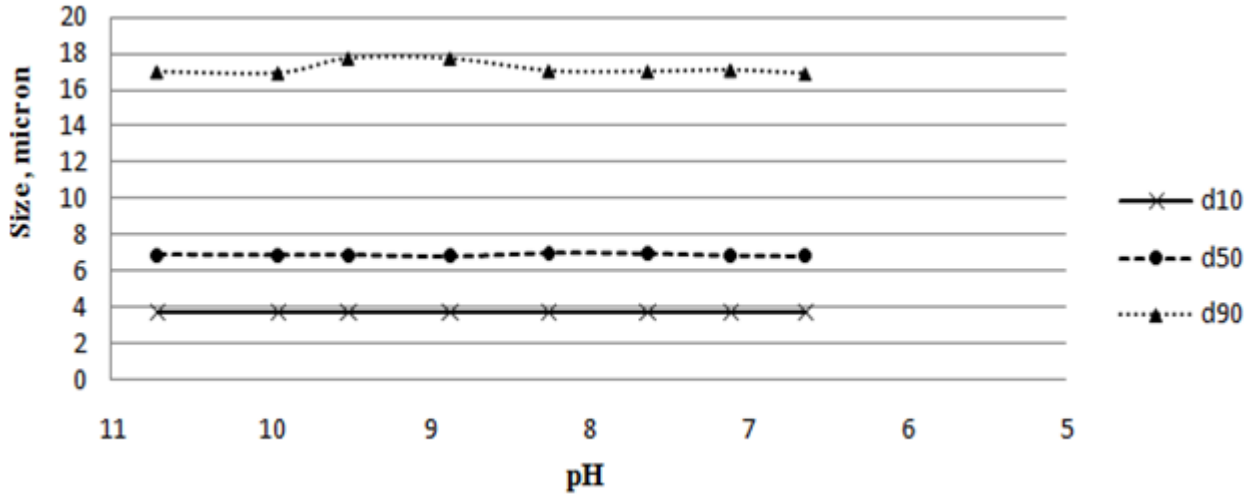

Figure 3.10. Change of representative particle sizes during the recarbonation process for Portage la Prairie water

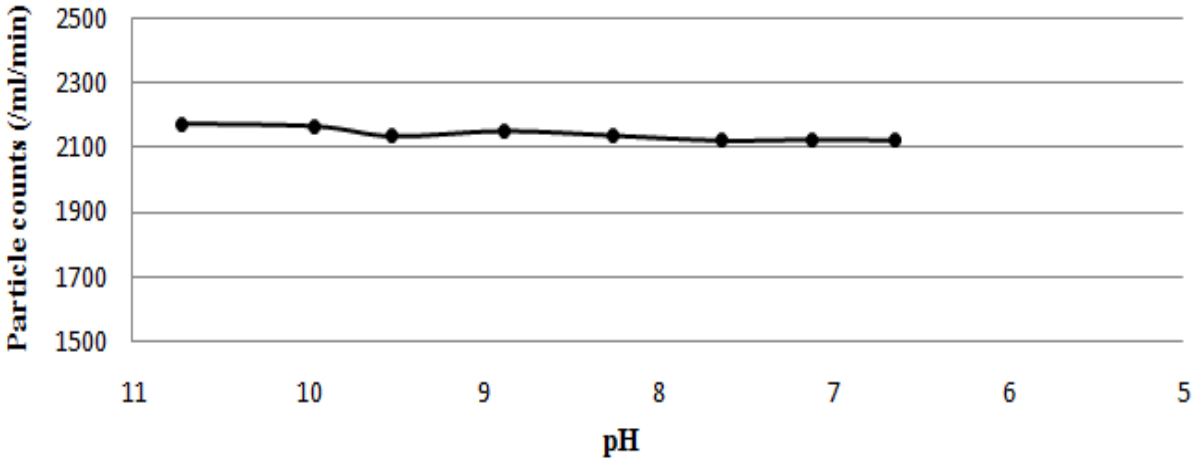

Figure 3.11. Effect of pH on particle count during recarbonation for Portage la Prairie water

The results of the ozonation experiments are presented in Figure **3.12** and Figure **3.13**. They show that the ozonation dose does not have any significant effect on the number or size of the particles.

Although an increase in the size of the particles in the recarbonation and ozonation process at the plant was observed, the laboratory experiments showed no correlation between pH or ozone dose and size or number of particles.

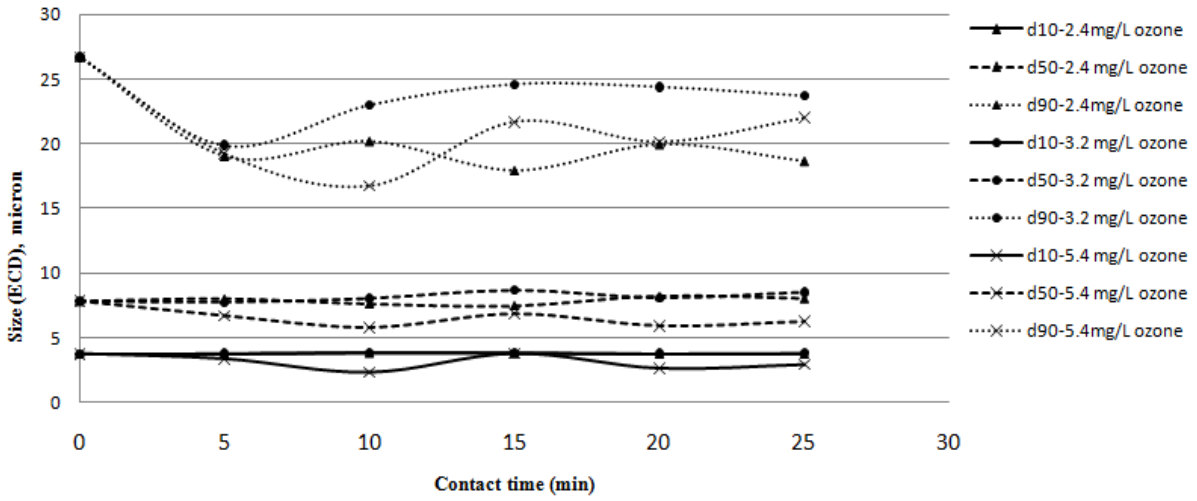

Figure 3.12. Change of representative particle sizes during the ozonation process for Portage la Prairie water

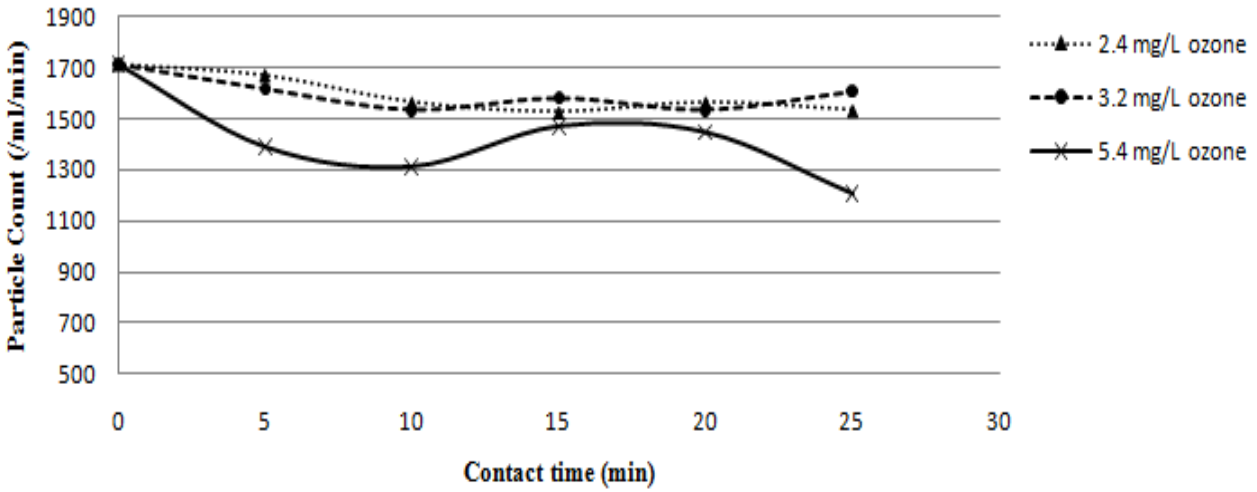

Figure 3.13. Change of particle counts during ozonation process for Portage la Prairie water

Further investigation of the results represented in Figure **3.13** shows that the total number of particles has slightly decreased as contact time in the ozonation process increased. This slight change in the number of particles is probably due to the sedimentation of larger particles inside the ozonation reactor. The decrease in d90 in Figure **3.12** indicates that there were fewer number of large particles (>20µm) after few minutes of ozonation. The large flocs flowing into the ozonation chamber must have been formed during the recarbonation process conducted at the plant; however, the formation of particles during recarbonation was not observed in the bench scale experiments. The main differences between the laboratory batch model and actual recarbonation reactor in plants are the size and hydrodynamic conditions of the process. The continuous flow reactor at the plant allows for more effective particle contacts and formation of flocs. The detention time of recarbonation and ozonation at Portage la Prairie plant is about 20 minutes for each process. Therefore, the recarbonation and ozonation chambers may provide mixing conditions promoting the formation of new flocs. A portion of these newly formed

particles sediment inside both recarbonation and ozonation processes and the remaining particles flow onto the filters forming the clogging cake on the filter media.

Improving the hydrodynamic conditions of recarbonation and ozonation processes may prevent the particle formation. For instance, decreasing the retention time in recarbonation and ozonation units may increase the mixing and reduce the particle formation.

The large flocs formed in recarbonation and ozonation processes essentially originate from smaller particles that are not removed in the preceding lime softening clarifier. Therefore, optimization of coagulation and sedimentation processes may decrease the particle formation inside the recarbonation and ozonation chambers.

Our other studies on the Portage la Prairie plant revealed that the coagulation processes do not remove the dissolved organic carbon (DOC) properly. Figure **3.14** shows the DOC removal at different processes of the plant. The high DOC in the treated water reacts with the chlorine that is added in the final stage and causes high Trihalomethane (THMs) concentration in the distribution system. High THMs concentration in distribution system has been reported repeatedly by the City of Portage la Prairie.

We also believe that the high organic content of water causes biological growth on the GAC filter media that subsequently results in pre-mature exhaustion of GAC media and frequent filter backwashing. Improving the effectiveness of coagulation and sedimentation in pre-treatment processes may also reduce the THMs formation potential of treated water and improve the GAC filtration.

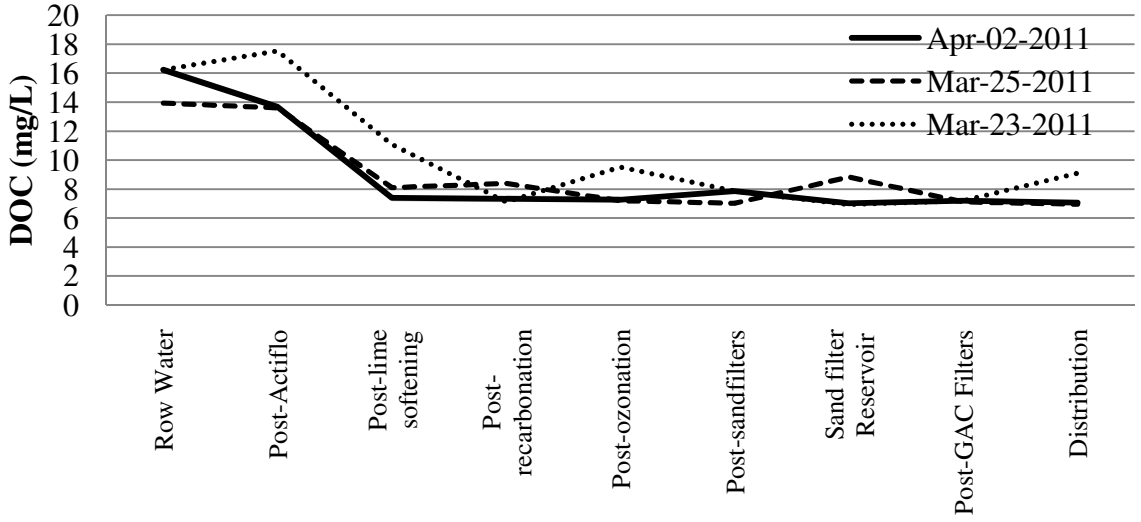

Figure 3.14. DOC change in Portage La Prairie plant (January 2011)

According to recent studies (Vahedi and Gorczyca 2011), the flocs formed in the lime softening process have fractal structure and their sedimentation can be described best by the models that incorporate the fractal characteristics of these particles. However, Vahedi and Gorczyca (2011) demonstrated that the settling velocity of small lime flocs (<50μm) can be predicted by Stokes' law. The specifications of the existing clarifiers at Portage la Prairie water treatment plant are presented in Table **2.1** (GENIVAR 2010). The smallest floc that, according to Stokes' law, can be removed by the clarifiers are calculated and shown in Table **3.2**.

Table 3.2. Portage la Prairie clarifiers

	Clarifier #1	Clarifier #2	Clarifier #3
Effective capacity (m^3/day)	9000	9000	20000
Diameter (m)	14	14	16.5
Surface overflow (m/hr)	3	3	3.25
Smallest floc that theoretically is removed (Stokes' law) (μm)	38	38	39.5

The surface overflow rates for the clarifiers at Portage la Prairie plant have been recently improved with 60º 0.5m tall ABS tube settlers; therefore, in practice, the clarifiers are capable of removing smaller particles resulting in d_{90} of about 28µm in clarifiers' effluent (Figure **3.7**).

According to Stokes' law, the settling velocity of flocs and the floc size have the following relationship:

$$v_{st} \sim d^2 \tag{3.1}$$

Also, for a given flow rate, the average surface overflow rate and the total surface area of clarifiers have the following relationship:

$$SOR \sim \frac{1}{S} \tag{3.2}$$

where S is the total surface area of clarifiers. By equating the surface overflow rate of the clarifier and the settling velocity of flocs, the following relationship is obtained:

$$\frac{1}{S} \sim d^2 \tag{3.3}$$

It is understood that the current design of clarifiers has resulted in d_{90} of about 28 µm for the particle size distribution of clarifiers' effluent (Figure **3.7**). The expected d_{90} for different diameters of clarifiers can be estimated by using the Eq. (3.3). Figure **3.15** shows the relationship between the total surface area of clarifiers and the estimated d_{90} in clarifiers' effluent. It is

assumed that the total flow rate is constant and is equal to the sum of effective flow rates of existing clarifiers.

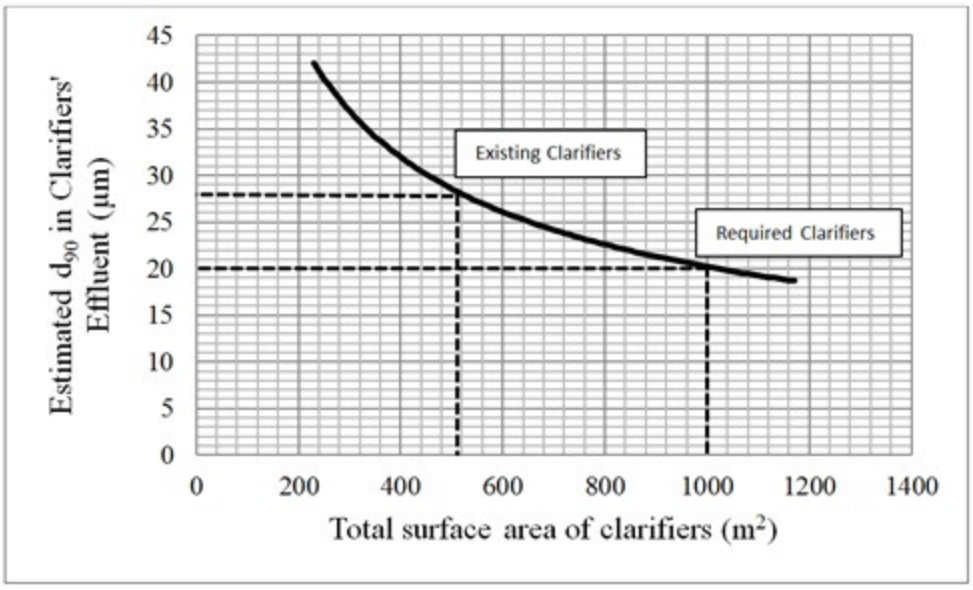

Figure 3.15. Relationship of the total surface area of clarifiers and the estimated d_{90} of clarifiers' effluent at Portage la Prairie water treatment plant

According to Figure **3.15**, reducing the d_{90} of size distribution of flocs in clarifiers' effluent to 20 µm requires the total surface area of almost two times larger than the total surface area of the existing clarifiers. Therefore, the change of the capacity of clarifiers for reducing the size of flocs in clarifiers' effluent may not be economically feasible.

Another recommendation for preventing the sand filter clogging is to rearrange the sequence of the treatment processes by applying sand filtration before recarbonation and ozonation. According to Figure **3.14**, there is no significant change in DOC before and after recarbonation and ozonation and the sand filters should not have problem with the organic load if they are used

right after clarifiers. However, since the pH of clarifiers' effluent is about 10.5-11, the effect of high pH water on sand filters should be investigated.

Reducing the contact time in recarbonation and ozonation chambers by reducing the capacity of these units and applying rapid mixing may also reduce the chance of sand filter clogging.

3.4. Conclusions

The Portage la Prairie water treatment plant experiences significant sand filter clogging and deposition inside the pipelines. The objective of this research was to study the reasons for frequent filter clogging. The following conclusions can be made from this work:

The flocs formed in the lime softening process are responsible for clogging of the sand filters and deposition inside the pipes at the Portage la Prairie water treatment plant.

The flocs not removed by the clarifier are allowed to flocculate to the size of about 40µm during the recarbonation and ozonation processes.

Increasing the effectiveness of clarifiers and filtering water prior to recarbonation and ozonation units may reduce the chance of sand filter clogging.

Improving the mixing conditions in the recarbonation and ozonation tanks by decreasing the water detention time in each process and rapid mixing may reduce the chance of sand filter clogging.

Changes in pH during the recarbonation as well as ozone dose did not affect the number or the size of the particles. This finding may be important because the plant also has the problem with the pH and lead corrosion control.

Chapter 4

Application of Fractal Dimensions to Model the Settling Velocity of Lime Softening Flocs

The application of fractal dimensions to study the settling velocity of lime softening flocs was investigated. The linkage between the fractal dimensions of flocs and their settling velocities is well documented (Ganczarczyk 1995, Lee et al. 1996, Gorczyca and Ganczarczyk 1996, Logan 1999, Gorczyca and Ganczarczyk 2000, Bushell et al. 2002, Tang et al. 2002, Chu et al. 2004, Jarvis et al. 2005, Khelifa et al. 2006, Bugni et al. 2007, Chakraborti et al. 2007). However, the methods for the measurement of fractal dimensions have not been well-established. In this study, the fractal dimensions of flocs formed in water lime softening process were determined directly on floc images and indirectly from settling velocities of aggregates. These fractal dimensions were compared to those of other flocs formed in water/wastewater treatment processes. Finally the application of various fractal dimensions to predict the floc settling velocity was investigated.

It is assumed that the Reynolds number of lime softening flocs follows the transitional Stokes' regime ($0.2 \leq Re \leq 1000$) and therefore, their drag coefficient can be determined from Eq. (2.49). It is also assumed that the mass fractal dimension of flocs in 3D is estimated by their Hausdorff dimension for the volume of flocs.

The model of settling velocity that we use in this chapter for modeling the settling velocity of lime softening flocs is based on the model suggested by Khelifa and Hill (2006) that was discussed in Chapter 2 with some modifications. The model is presented below:

$$v_s = \frac{1}{18}\theta g \frac{\rho_P - \rho_w}{\mu} d_{50}^{3-D_M} \frac{d^{D_M-1}}{1 + 0.15Re^{0.687}}\psi \qquad (4.1)$$

Here, we assume that the mass fractal dimension is equivalent to the Hausdorff fractal dimension for volume which is a correct assumption for self-similar fractals. Hausdorrf fractal dimensions for the volume of flocs are measured directly on their images. We also consider the variation of fractal dimensions with floc size. Further, we assume different primary particle sizes in the model.

In order to model the settling velocity of lime softening flocs the information about size of the flocs, fractal dimensions of flocs in 3D and density of primary particles were needed. In the following sections the experimental procedures for obtaining the required information are explained.

4.1. Experimental Procedure and Analytical Methods

The studied flocs were collected in May and August 2008 as well as January and August 2009 from the sedimentation tanks of Portage la Prairie plant. The samples were collected from the upper portion of the circular solid blanket clarifiers where the solid concentration is relatively low and individual floc settling is predominant.

The qualitative data as well as the size distribution characteristics of the raw and clarifier water are presented in Table **4.1**.

Table 4.1. Raw and clarifier water quality at Portage La Prairie Plant

	Raw Water	Clarifier Influent	Clarifier	Clarifier Effluent
pH	7.5-8.5	-	10.5-11	-
Alkalinity (mg/l CaCO3)	250-300	-	60-100	-
Total Hardness (mg/l CaCO3)	300-450	-	150-200	-
Total Dissolved Solid (mg/l)	300-600	-	-	-
Turbidity (NTU)	0.5-50	-	-	-
True Color (TCU)	25-60	-	-	-
DOC (mg/l)	9-20			
Particle Size Range (μm)	2-90	2-85	-	2-62
Standard Deviation of Particle Size (μm)	3.05	8.6	-	8
d50 of Particle Size Distribution (μm)	64	17	-	16

4.1.1. Chemical composition analysis of lime softening flocs

The chemical composition of flocs determines the density of the primary particles that subsequently affects the floc density and floc settling velocity. The analysis of chemical composition of studied flocs also provides information about the possible charges of the primary particles and flocculation mechanisms.

The collected floc samples were preserved at 4 °C and their chemical composition were analyzed within one day from the time of sampling. Multiple methods were used to obtain adequate information about the chemical composition of flocs (Table **4.2**).

Table 4.2. Instruments used for determination of chemical composition of flocs

Instrument/Technique	**Intention**
X-ray Diffraction	Determination of the crystal structure of the molecules and comparing with known structures
Scanning Electron Microscopy (SEM) equipped with Energy Dispersive Spectrometer (EDS)	Determination of the elements in the sample
Inductivity-Coupled Plasma Ion Chromatography (ICPIC)	Quantitative analysis of elements in the sample

4.1.1.1. X-ray diffraction, SEM/XRD and ICICP

X-ray diffraction, Scanning Electron Microscopy (SEM) equipped with Energy Dispersive Spectrometer (EDS) and Inductivity-Coupled Plasma Ion Chromatography (ICPIC) were used to determine the chemical composition of lime softening flocs. The procedures were similar to the chemical composition analysis of filter media. The details were explained in Section 3.3.1.

4.1.2. Floc Size Distribution Analysis

The floc samples were preserved at 4 °C and their size distributions were analyzed within 6 hours from the time of sampling. A combination of particle counting, optical microscopy and small angle light scattering was used to determine the full size distribution of the flocs with each instrument detecting particles in a specific size range, optimal for that particular method (Table **4.3**). The equivalent circular diameter (ECD) of a floc is considered to be the representative size.

Table 4.3. Instruments used for each size of flocs

Floc size range	Instruments
0.002 µm – 2 µm	Dynamic Light Scattering (Photocor Tech) Malvern Mastersizer 2000
2 µm-20 µm	Particle Counter (DPA) Particle Counter (Spectrex 2200)
> 20 µm	Microscopy Imaging (SMZ 800) Particle Counter (Spectrex 2200)

4.1.2.1. Size distribution analysis of flocs smaller than 2 µm

The flocs samples were analyzed by two instruments in order to determine the existence and distribution of submicron particles. Both instruments use light scattering technique to measure the size distribution.

Dynamic light scattering

A dynamic light scattering instrument (Photocor Tech, Department of physics and astronomy, University of Manitoba) was used mainly to detect flocs smaller than 2 µm. About 5 mL of floc suspension was analyzed in each test. The sample was placed in a small transparent rectangular tube that was placed in the instrument where the laser beam passes through the sample. The angle at which the laser hits the sample can be adjusted. The equivalent floc diameter distribution obtained from the measurements at five different angles (30°, 50°, 70°, 90° and 110°) was averaged to obtain the relative size distribution of the flocs. For each angle two tests were conducted and the average was used in the analysis.

Malvern Mastersizer 2000 (light scattering)

The Malvern Mastersizer utilizes light scattering to detect the particles from 0.02 to 2000 µm, however, in this study the instrument was used to detect the particles from 0.02 to 2 µm. The reason that the instrument was not used for larger flocs is that the settling velocity of large particles is high and the significant movement of these particles may cause error in the results. Even though the instrument has a stirrer, the large particles still settle to the bottom of the container and result in errors. A small drop of the suspension (50 mL) was placed in the detection tube and the instrument measured the proportion of the total particle volume within

each class size. It is possible to convert this volume distribution to a frequency distribution, but it should be noted that small particles which are present in floc suspensions in very large numbers represent a relatively small volume. Even a small error in volume measurement due, for example to the background noise, can be translated into an apparently large number of small size particles. To avoid the transformation error, this instrument was not directly used for the determination of the size distribution of flocs but to investigate the existence of the sub-micron flocs. The Malvern Mastersizer 2000 at the Richardson centre for functional foods and nutraceuticals (RCFFN) at the University of Manitoba was used in this study.

4.1.2.2. Size distribution analysis of flocs larger than 2 µm

Two particle counters and microscopy imaging were used to determine the size distribution of lime softening flocs larger than 2 µm. Previous experience showed the results from two particle counters (Spectrex 2200 and DLA 4100) and microscopy imaging to be comparable (Gorczyca and Klassen 2008). The equivalent circular diameter (ECD) of a floc was considered as the representative size.

Dynamic Particle Analyzer (DLA 4100)

A dynamic particle analyzer (DLA 4100) at the department of civil engineering of University of Manitoba was used to determine the size distribution of lime softening flocs in the size range of 2-20 µm. (Figure **4.1**). The 8 ml/s flow of suspension was analyzed for 60 seconds in five separate tests. About 3770 particles were counted in the range of 2-20µm. In order to avoid clogging of pipes, very large flocs were separated from the samples for 10 seconds sedimentation in a 50 cm column of water. According to the preliminary results of settling tests, the flocs that

are smaller than 30 µm move less than 1cm in 10 seconds and can be preserved in the samples that are taken from the upper portion of the sedimentation column.

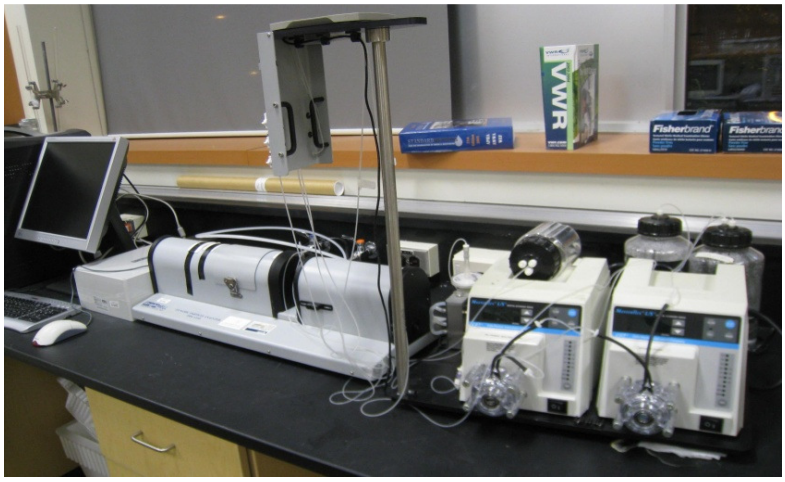

Figure 4.1. Dynamic particle analyzer (DLA 4100) used in this study

Spectrex 2200 particle counter

The particle counter (Spectrex 2200) at the department of civil engineering of University of Manitoba was used to determine the size distribution of lime softening flocs in the size range of 2-92 µm. The Spectrex 2200 particle counter utilizes the principles of light scattering to count the number and measure the sizes of particles in a suspension. A 100 mL of sample in a transparent container is placed in the instrument where the laser beam passes through the sample (Figure **4.2**). Five tests were performed for lime softening flocs. About 1530 particles were counted in the range of 2-92 µm.

Figure 4.2. Particle counter (Spectrex 2200) used in this study

Microscopic imaging

The size distribution of the flocs larger than 20µm was obtained by using an optical microscope (SMZ 800) with the magnification of 6.3X. The microscope was equipped with a digital camera (Olympus DP70) and ProPlus 5.0 software for image processing. The numerical aperture (N.A.) of the microscope was 1.4 with the display resolution of 4080×3072 pixels. About 1 ml of the diluted floc suspension in a Petri dish was placed on the microscope for imaging. 30 images were taken from 5 samples and about 1680 flocs were counted. The distribution of flocs per field was found to be a Poisson distribution. For such a distribution, when the total counts increased to 200 to 300, the precision of the measurement increased to approximately 0.05 (Parker 1970). The number of images per field of view was chosen to be 30 to achieve a standard error of less than 0.05 for the data. Additional random areas are chosen if the standard error exceeds 0.05.

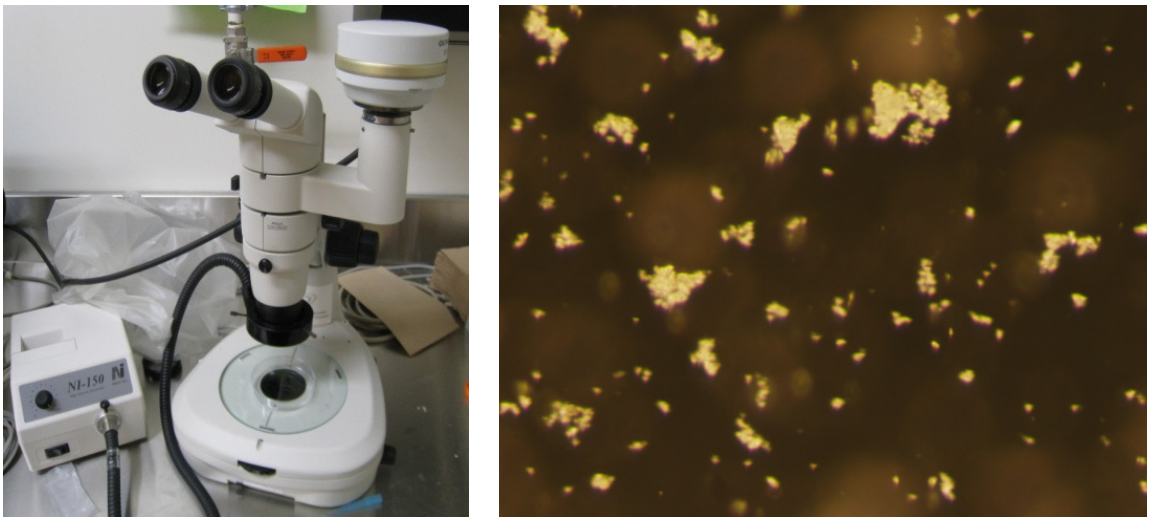

Figure 4.3. SMZ800 microscope and a sample image of lime softening flocs

To ensure the reliability of the measurement of the particle sizes, a certain number of particles should be measured. To have a reliable number of flocs, the standard error of the data was considered to be 0.05. At least 20 random areas were chosen for microscopy and the following equations were used to determine the reliability of the data. Additional random areas were chosen if the standard error exceeds 0.05.

$$\bar{X} = \frac{1}{n}\sum_{i=1}^{n} \bar{X}_i \tag{4.2}$$

where $\bar{X}_i$ is the mean value of the sizes of random area i, n is the number of random areas, and $\bar{X}$ is the mean value of all data. The standard error was calculated using the following equation:

$$SE(\bar{X}) = \frac{S(\bar{X}_i)}{\sqrt{n}} \tag{4.3}$$

where, $S(\overline{X}_i)$ is the standard deviation of data from the random area *i*. In this study 30 images were taken from 5 samples and about 1680 flocs were counted.

4.1.2.3. Combining the distributions obtained by various instruments

Previous experience showed that the results of microscopy and particle counting are comparable (Gorczyca and Klassen, 2008). The linear opinion pool method (Eq. (4.4); Stone 1961) was used to combine the overlapped parts of distributions obtained from microscopy and particle counters.

$$p(x) = \sum_{i=1}^{n} w_i p_i(x) \tag{4.4}$$

where n is the number of probability distributions, $p_i(x)$ is the value of the probability distribution *i* for the uncertain quantity *x*, the weightings (w_i) sum to one, and $p(x)$ represents the combined probability distribution. In this study for combining two instruments the weightings were considered to be 0.5.

4.1.3. Direct determination of fractal dimensions

The box-counting fractal dimension of lime softening flocs was measured for perimeter, cross-sectional surface area and volume of flocs directly on the flocs' images.

4.1.3.1. Obtaining floc images

3D images of flocs were needed to measure the volume fractal dimension (D_V) of flocs directly. A CCD camera and an optical microscope equipped with a motorized stage (Zeiss AxioImager Z1) were used for acquisition of floc's section images at different depths (Figure **4.4**).

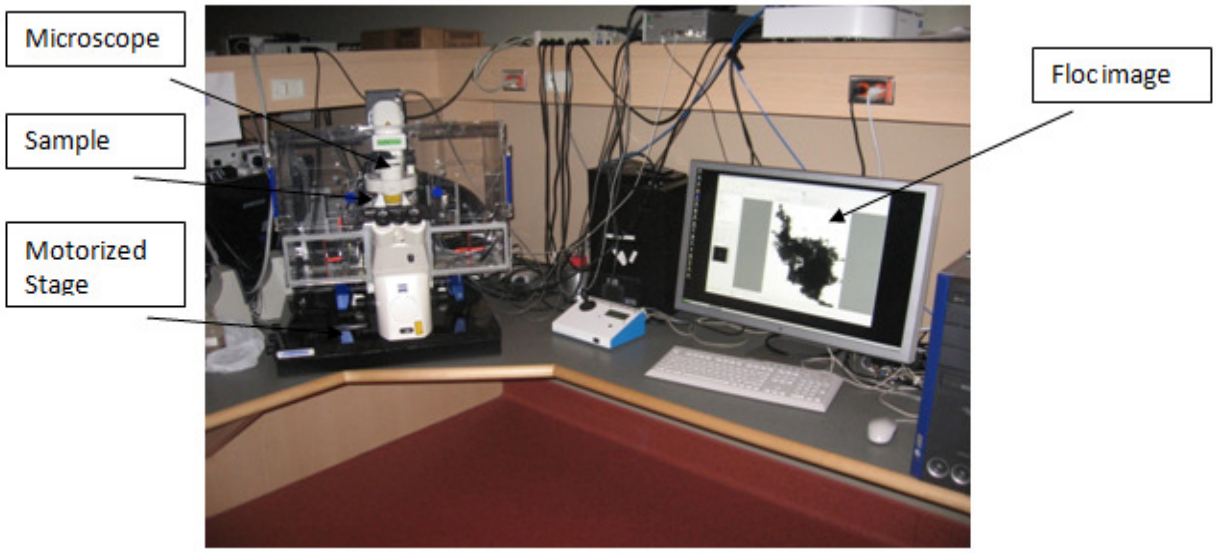

Figure 4.4. 3D imaging of lime softening floc by using the motorized stage microscope

The microscope had inverted lenses that allowed direct imaging of flocs in the suspension while preserving the floc structure. The microscope was equipped with a temperature and moisture controlled chamber. A small volume of floc suspension (<1mL) was placed in a petri dish and viewed in bright field. The smallest possible distance between two focal planes was 50 nm but in this study the distance between the levels of imaging varied from 100 nm to 1000 nm. The maximum image resolution of camera was 6250 pixels/mm and the numerical aperture (N.A.) of the microscope was 1.4. The magnifications of lenses used in this study were 10X, 20X and

40X. Axio Vision 4.5 Software was used for deconvolution of the images. Table **4.4** shows the floc sampling details.

Table 4.4. The experimental details of 3D imaging of lime softening flocs

Number of flocs analyzed	85
Size of flocs (ECD for 2D images)	8µm-260µm
Distance between the sections	100nm-1000nm
Number of the sections per floc	50-75

4.1.3.2. 3D reconstruction of flocs

The 3D-doctor software made by Able Software Corporation (Lexington, MA, USA) commonly used for 3D reconstruction of MRI images, was used for reconstruction of 3D images of flocs. The 3D-doctor acquires the 2D section images as well as the distance between the sections and provides the 3D image of the object.

4.1.3.3. Measurements of fractal dimensions

Any 2D black and white image can be defined and stored as a 2D matrix of numbers. The value of each element of the matrix is the greyscale level that can be any integer from 0 (black) to 255 (white). Figure **4.5** shows a small 8×8 pixels 2D image and its matrix.

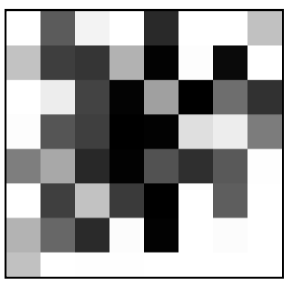

$$\begin{bmatrix} 255 & 91 & 243 & 255 & 41 & 255 & 255 & 193 \\ 194 & 62 & 53 & 178 & 2 & 253 & 10 & 255 \\ 255 & 237 & 67 & 4 & 160 & 0 & 110 & 49 \\ 253 & 85 & 63 & 0 & 2 & 223 & 237 & 124 \\ 126 & 168 & 40 & 2 & 82 & 47 & 89 & 254 \\ 255 & 63 & 194 & 58 & 0 & 255 & 94 & 255 \\ 179 & 103 & 42 & 252 & 2 & 255 & 252 & 255 \\ 193 & 255 & 254 & 254 & 254 & 255 & 255 & 255 \end{bmatrix}$$

Figure 4.5. Sample image and matrix

In order to simplify the box counting fractal analysis, the images were first processed in MATLAB 7.8 R2009a (developed by MathWorks Inc., USA). For simplicity the original floc images were converted to binary images by using "im2bw" command in MATLAB. This command uses the threshold value equal to 127. Therefore, the matrix of a floc image will have only 1s (black) and 0s (white). Figure **4.6** shows the binary matrix of the image shown in Figure **4.5**.

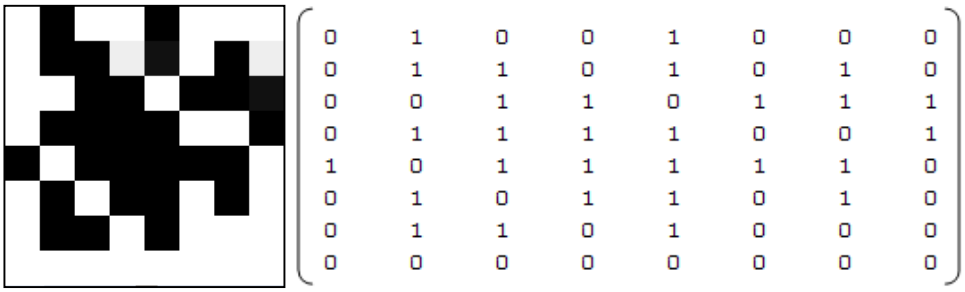

Figure 4.6. Binary image and matrix

Figure **4.7** shows an original floc image and its binarized image that is covered by 64 covering elements of size $r=1.6\mu m$.

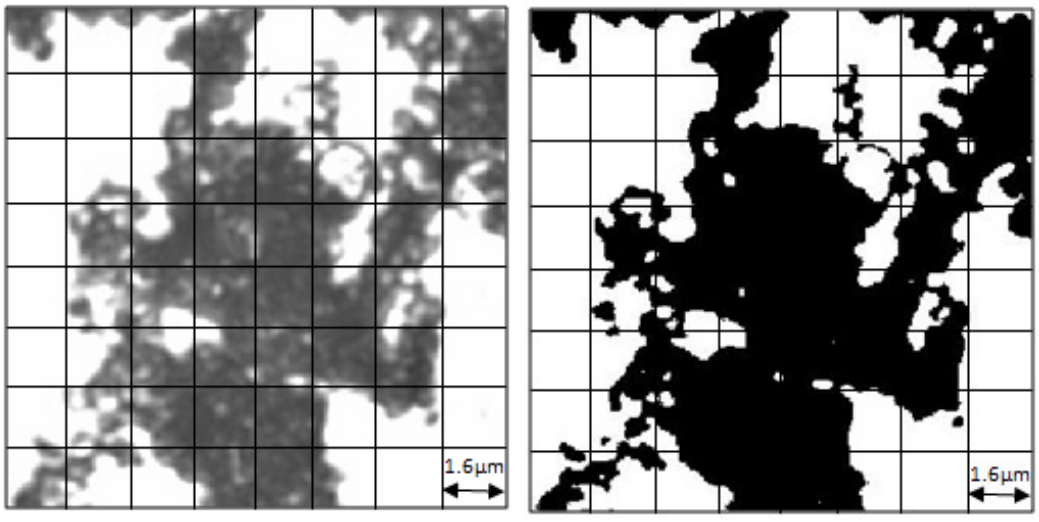

Figure 4.7. Original floc image covered by 64 elements (left); Binary floc image (right)

For fractal analysis, the holes inside the images were deducted from the area for measuring the cross-sectional area or volume of flocs.

The boundary box-counting fractal dimension (D_B) was determined on the images of flocs by using the image analysis system Image ProPlus 5.0 that uses Eq. (2.3) (box-counting dimension) for fractal analysis. The cross-sectional and volume box-counting fractal dimensions of the binary images were calculated by using the "boxcount" toolbox in MATLAB 7.8 R2009a. This toolbox takes a 2D or 3D image as a 2D or 3D array and calculates the box-counting dimensions. The 3D array was built by stacking the 2D arrays and assuming that the space between two sequential images is similar to the lower level image. The 2D or 3D images were covered by pixel (voxel) sizes ranging from 0.16 µm to 3.2 µm. For each pixel size, the "boxcount" toolbox counts the number of 2D pixels covering the cross-sectional area of the floc image or 3D cubes (voxels) covering the volume of the floc. Figure **4.8** illustrates the steps of box-counting method for a 2D floc image.

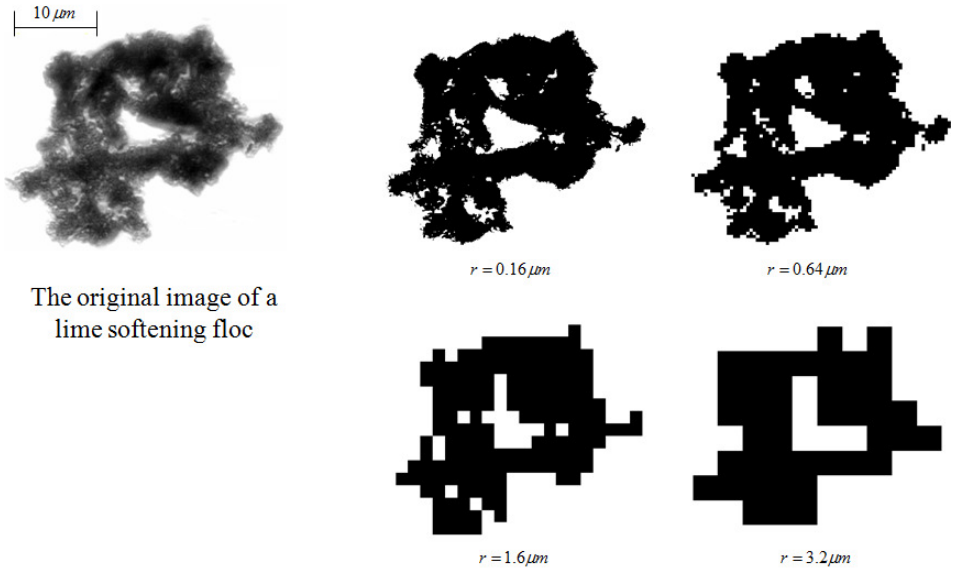

Figure 4.8. Illustration of box-counting method for a 2D lime softening floc image

The "boxcount" toolbox calculates the fractal dimension of flocs in 2D and 3D according to Eq. (2.3), by plotting the number of covering elements against the inverse size of elements in a log-log plot. For each individual floc, the perimeter-based fractal dimension of flocs (D_P) was also simply estimated assuming that $A=P^{2/Dp}$. This assumption has been used in other studies (Maggi and Winterwerp 2004).

4.1.3.4. Estimating the volume fractal dimension of lime softening flocs based on other dimensions

The methods suggested by Maggi and Winterwerp (2004) and Thill (1998) were applied to the data to estimate the volume fractal dimension of flocs from their other fractal dimensions (Eq. (2.11), Eq. (2.12)). The results were compared to directly measured volume fractal dimensions.

4.1.3.5. Indirect determination of volume fractal dimension of flocs from settling velocity

Terminal settling velocities of flocs were measured in free settling tests and the mass fractal dimension of individual flocs was calculated by using Eq. (2.17).

The free settling tests were performed by combining a high speed camera (Fastec Imaging, Fastec Inline Camera, Innovation Systems Inc., CA, USA) and a cylinder equipped with a flat window made of Plexiglas (Figure **4.9**). The camera is capable of recording images with the rates of 60, 125, 250, 500 and 1000 frame per second. In this study the rate was set as 60 frames per second. The maximum CMOS sensor resolution of the camera is 640×480. With a proper lens it was possible to detect and capture images of flocs that were larger than 5 µm. The camera works with two operation software programs MIDAS 2.0 and FIMS 3.0.

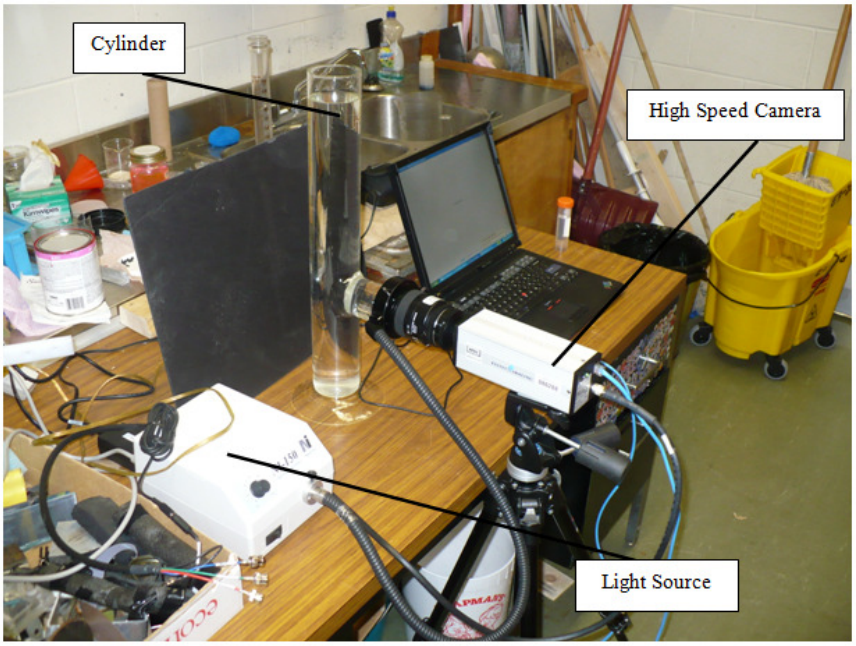

Figure 4.9. The set-up of free settling test

Figure **4.10** shows a sample image of a falling lime softening floc that is captured by the high speed camera.

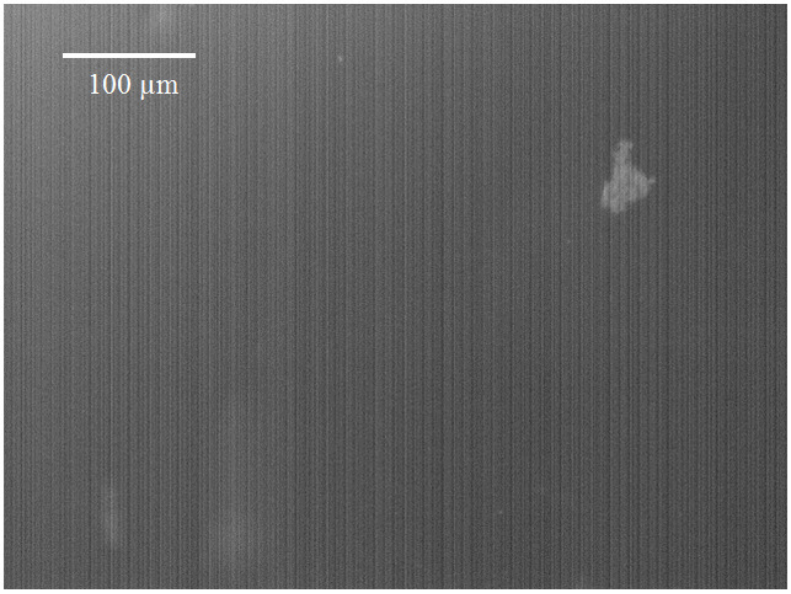

Figure 4.10. A falling lime softening floc in free settling test (Floc size = 46µm)

The image processing, detection of falling particles and size measurements were carried out by Image ProPlus 5.0. Figure **4.11** shows a sample of processed images for one studied floc in two different locations.

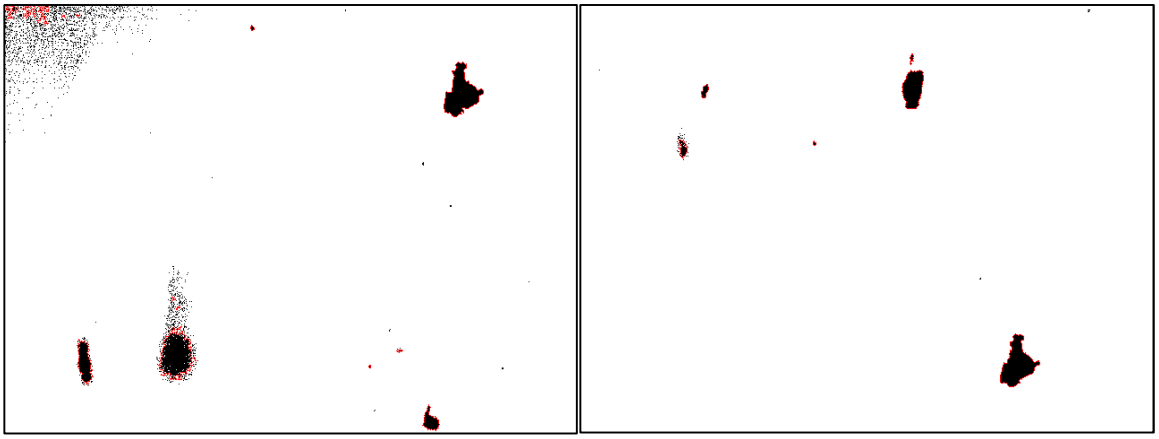

Figure 4.11. Processed images of a falling floc in different locations (Floc size =46µm)

In about 30 tests, the settling velocities of about 100 lime softening flocs with sizes ranging from 10µm to 260µm were measured.

4.2. Results

4.2.1. Results of chemical composition analysis of lime softening flocs

4.2.1.1. Results of X-ray diffraction for lime flocs deposited on sand filters

Figure **4.12** shows the result of the X-ray diffraction of lime softening flocs. The X-ray analyses indicated that the lime softening flocs are predominantly composed of calcite, a stable polymer of calcium carbonate ($CaCO_3$).

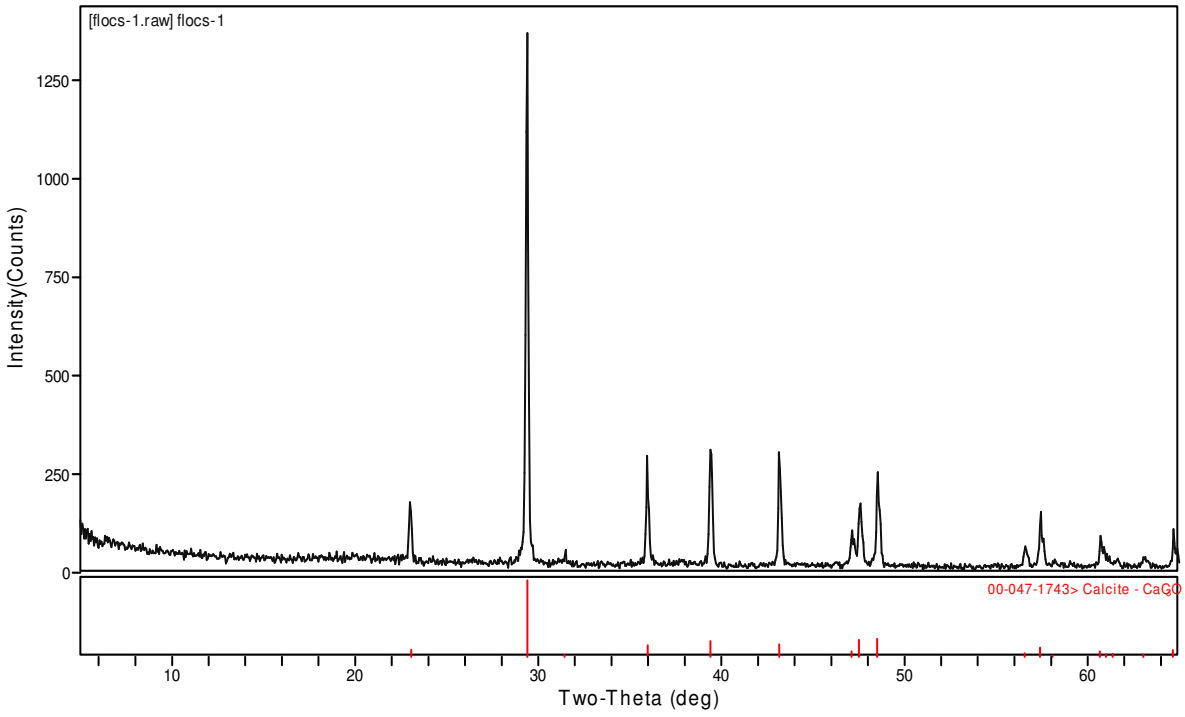

Figure 4.12. X-ray diffraction result of the lime softening flocs

4.2.1.2. Results of SEM and EDS for lime flocs

The image of dried lime flocs captured by SEM is shown in Figure **4.13**. Also the result of elemental analysis is shown in Figure **4.14**.

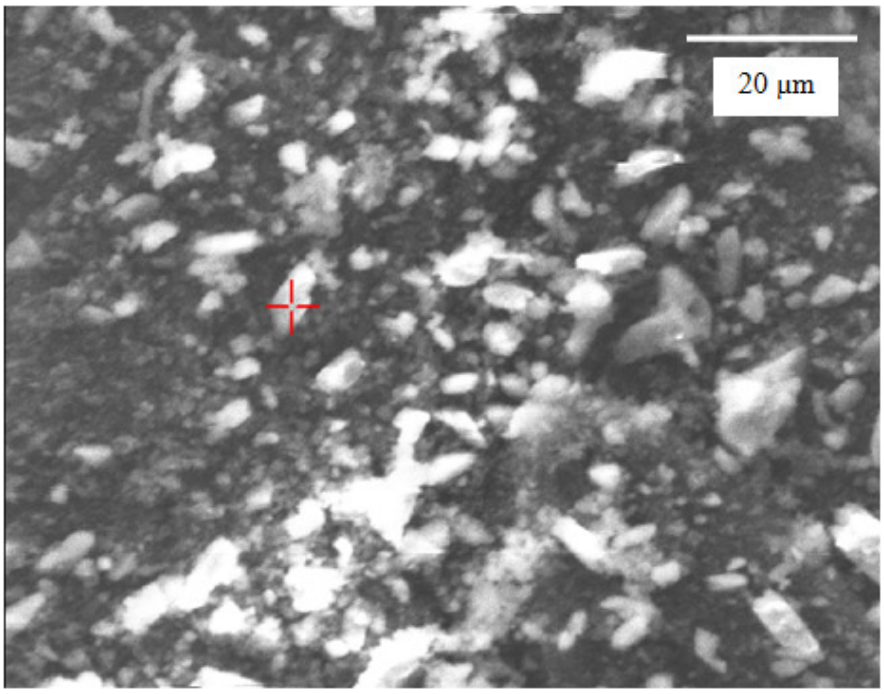

Figure 4.13. SEM Image of dried lime softening flocs

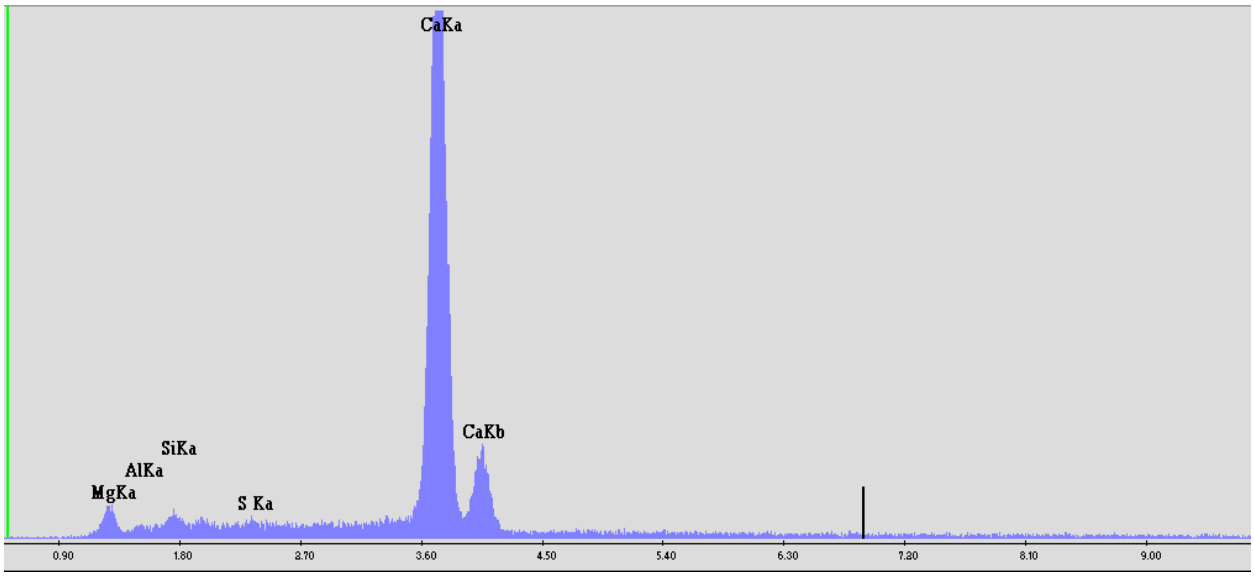

Figure 4.14. Analysis of elements of lime softening flocs by Energy Dispersive Spectrometry (EDS).

The SEM and EDS results confirm that the lime flocs are mainly composed of calcium compounds. There are also some other elements such as Al, Mg and Si and S. Since alum is

added in the pre-treatment process their existence is expected. The source of silica can be the sand that is used in sand ballasted flocculation in pre-treatment process.

4.2.1.3. Results of ICP for lime flocs

The Ion Chromatography Inductivity-Coupled Plasma (ICP) showed that the metals in the samples of lime flocs were mainly calcium (85%), Mg (9%), Fe (5%) and small amount of other elements including Al (1% total). Therefore, it was decided that the flocs were mainly composed of calcium carbonate and the density of primary particles is equal to the density of calcium carbonate particles.

4.2.2. Results of size distribution analysis of lime softening flocs

The size distributions of lime softening flocs collected from the clarifier obtained from dynamic light scattering and Malvern Mastersizer are presented in Figure **4.15** and Figure **4.16**.

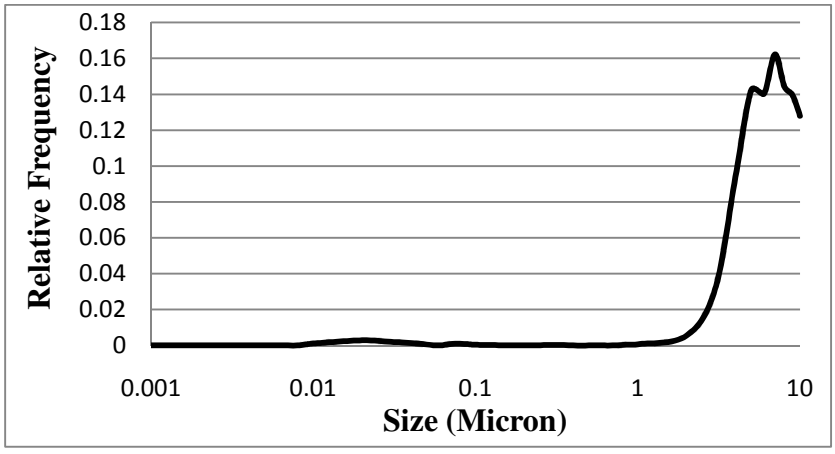

Figure 4.15. Size (ECD) distribution of lime softening flocs obtained using light scattering DSL Photocor (range: 0.001-10µm)

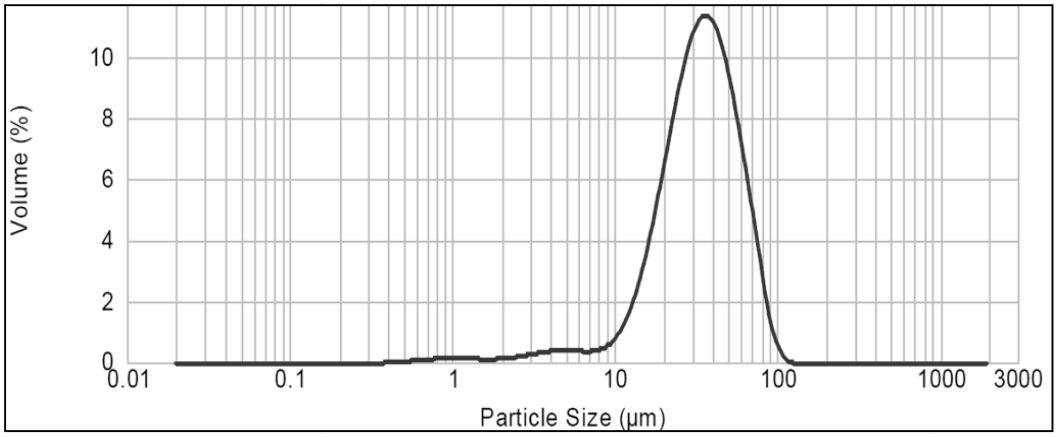

Figure 4.16. Volumetric size distribution of the lime softening flocs obtained using Malvern Mastersizer 2000 (range: 0.01-2000µm)

The measurements from these instruments showed that in the studied samples the number of flocs smaller than 2 µm was not significant and so it was decided to analyze only flocs larger than 2 µm. The size distributions of lime softening flocs obtained from microscopy, Spectrex and DPA particle counters are presented in Figure **4.17**- 4.19.

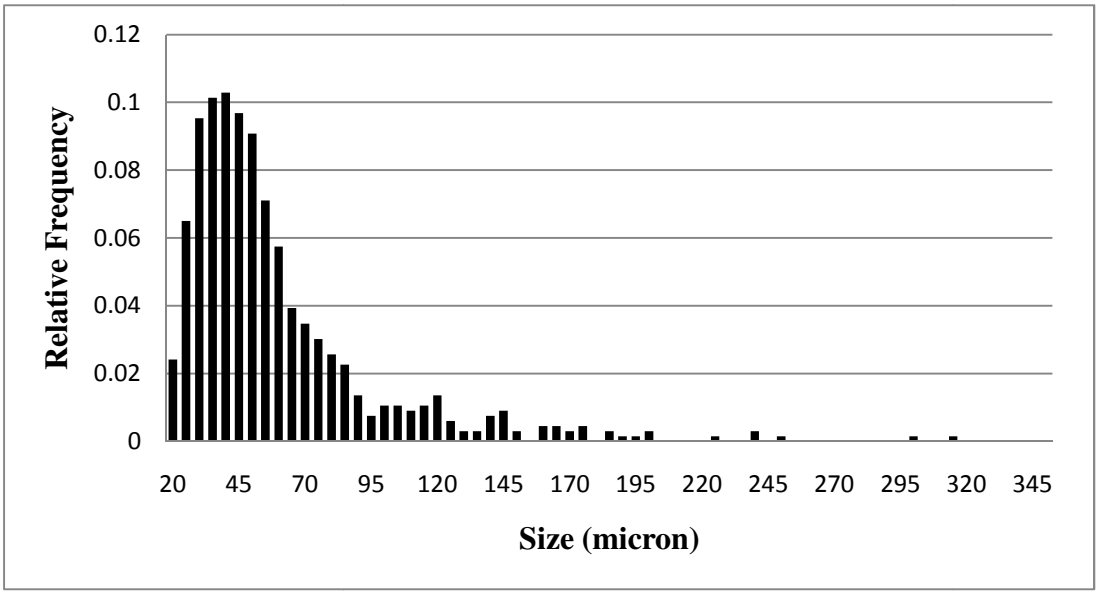

Figure 4.17. Size distribution of lime softening flocs obtained by microscopy (range: 20-350µm)

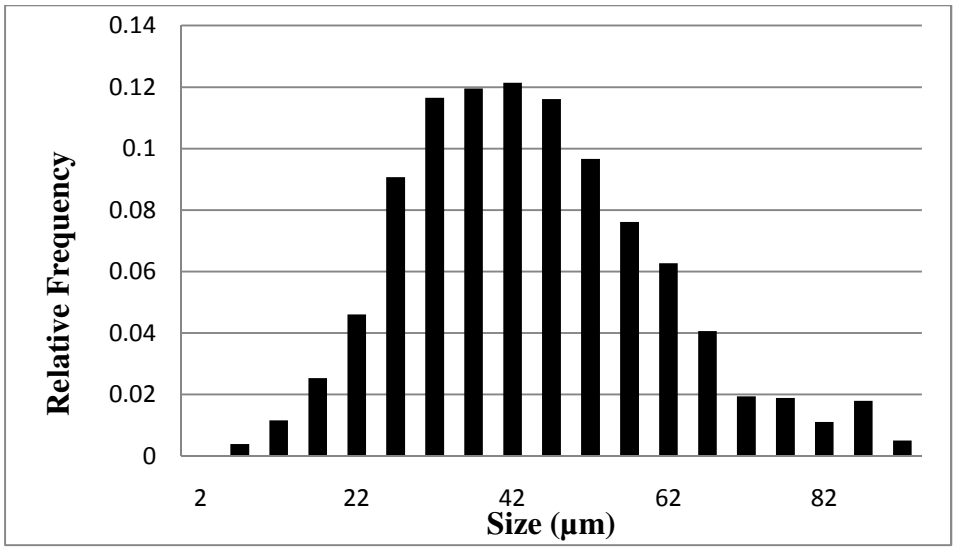

Figure 4.18. Size distribution of lime softening flocs obtained by Spectrex 2200 (range: 2-92µm)

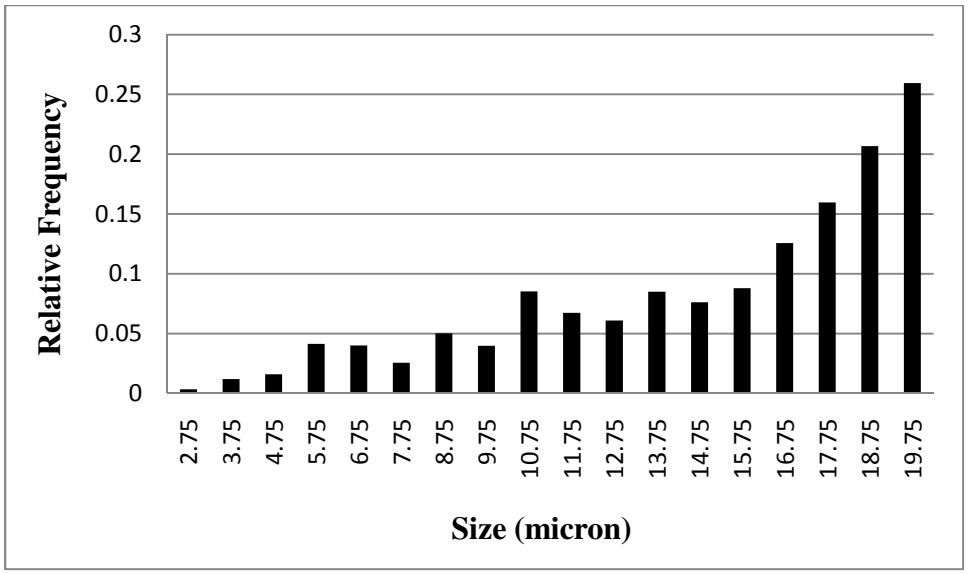

Figure 4.19. Size distribution of lime softening flocs obtained using DPA (range: 2-20µm)

Figure **4.20** shows the equivalent diameter distribution obtained as a result of combining the data from microscopy, DPA and Spectrex. The equivalent circular diameters (ECD) of the flocs

ranged from 2 µm to 250 µm with the arithmetic mean of 49 µm and standard deviation of 36 µm. There are only few very large flocs (>250 µm) in the sample.

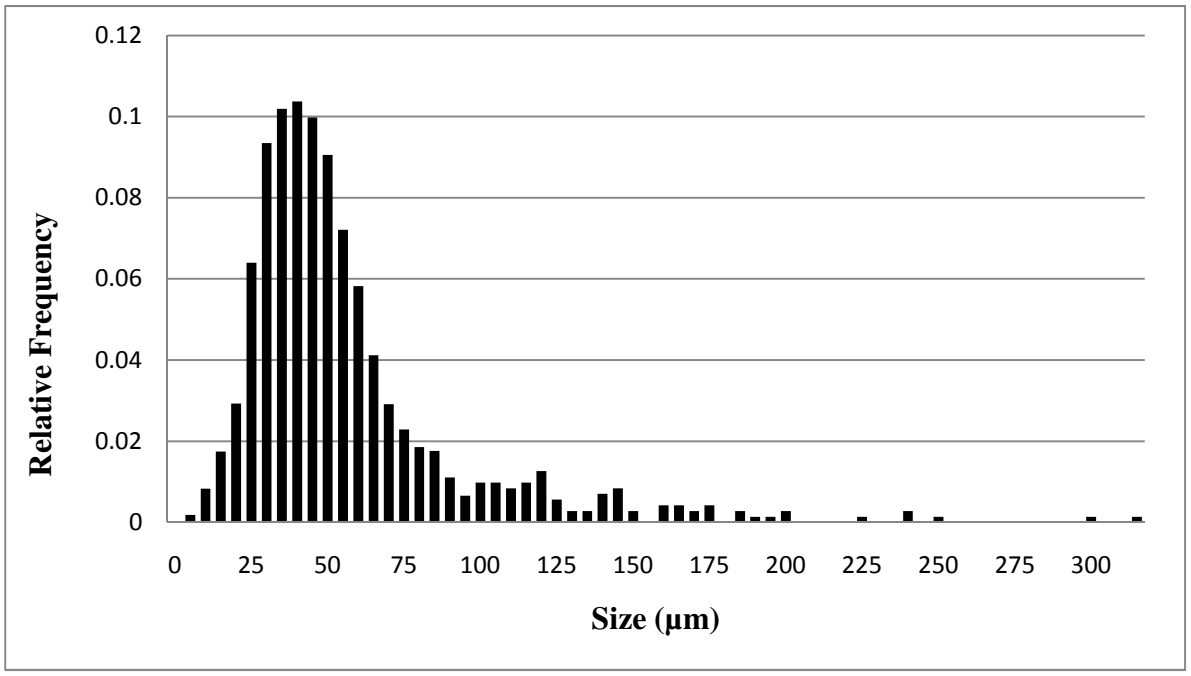

Figure 4.20. Size distribution of lime softening flocs

4.2.3. Floc fractal dimensions determined directly on the floc images.

Figure **4.21** shows the images of cross-sections of a lime softening floc at different focal planes as obtained with the Zeiss AxioImager Z1. Note that this figure is only for illustration of cross-section images. The actual number of cross-section images was 50-75 images for each floc.

Figure **4.22** shows the binary (bi-level) sectional images of a lime softening floc at different focal planes obtained by the Zeiss AxioImager Z1 and processed in MATLAB. The 3D reconstructed floc is shown in Figure **4.23**.

Figure 4.21. A lime softening floc viewed at different depths in bright field.

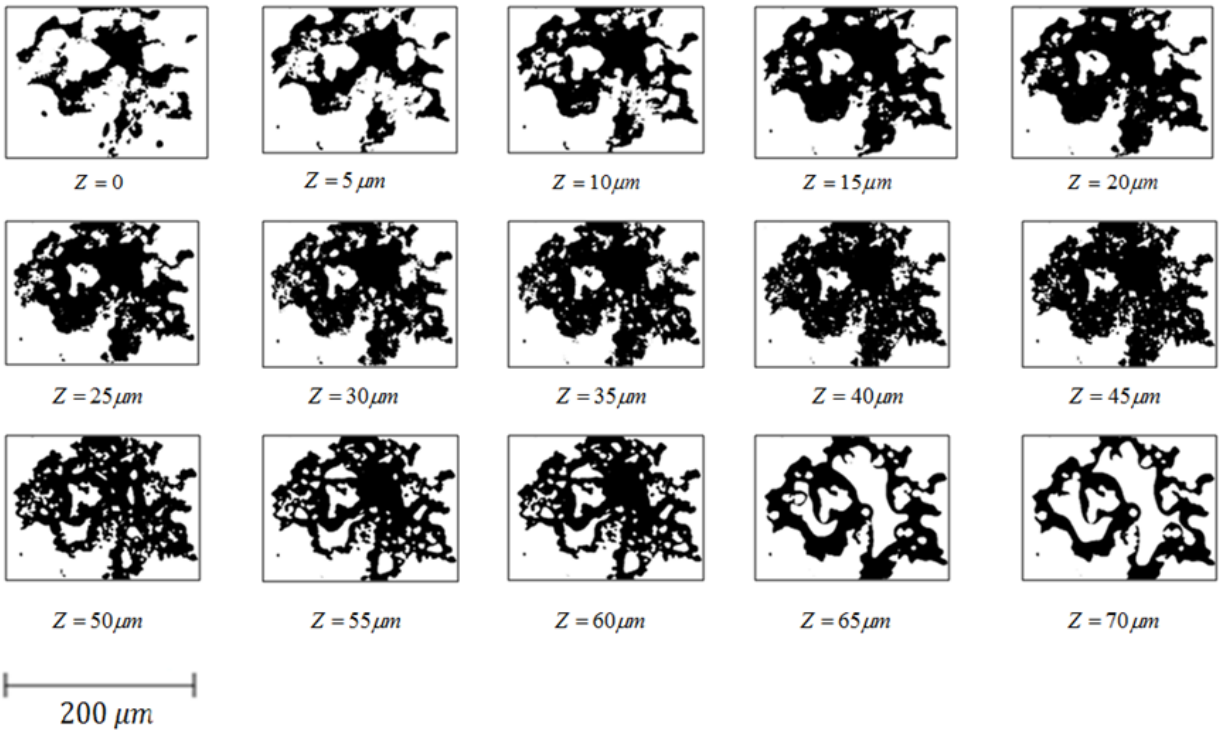

Figure 4.22. Binary images of cross-sections of a lime softening floc.

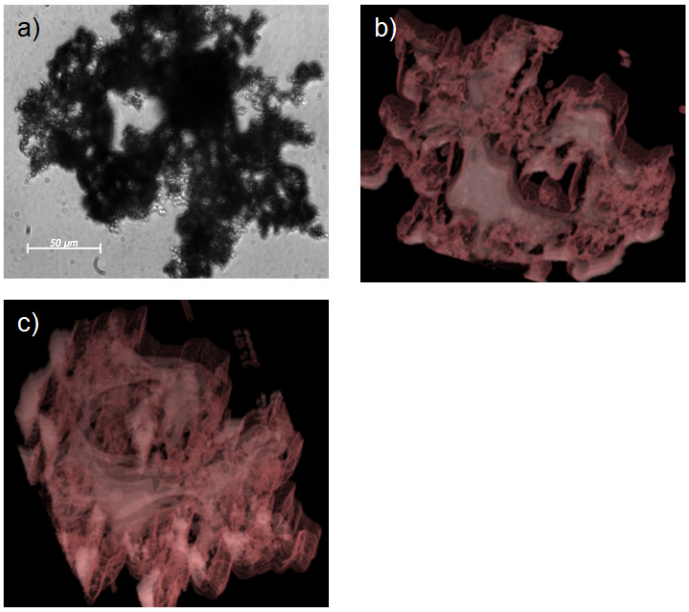

Figure 4.23. (a) 2D and (b, c) 3D images of the floc from Figure 4.22 using 3D doctor software

Note that in Figure **4.22** only 15 images out of 75 cross-sectional images are shown. There are some holes in cross-section images that might not be visible in 3D image. The reason is that some holes may not be parts of conduits continuing through different imaging planes; therefore, even though the holes are visible in all section images they are not visible in some 3D views. For the same reason the outlines of 3D and 2D images might look different.

The summary results of the box-counting fractal analysis for about 80 individual flocs in the range of 8.2-261 µm are listed in Table **4.5**.

Table 4.5. Fractal dimensions of lime softening flocs

Fractal dimension	Range	Average
Boundary (D_B)	1.15-1.27	1.20
Cross-sectional surface area (D_S)	1.49-1.90	1.90
Perimeter-based (D_P)	1.21-1.38	1.27
Volume (D_V)	2.55-2.99	2.73

4.2.4. Variation of floc fractal dimension with size

Figure **4.24** shows the measured volume fractal dimensions for the lime softening flocs. It is clear that in general, the fractal dimension decreases as the floc size increases. Two different relationships (power law and two-stage linear relationship) for flocs size and volume fractal dimension are investigated.

The power law relationship of Eq. (2.20) was applied to the measured volume fractal dimensions. A constrained optimization was performed to find values of δ (the volume fractal dimension of the primary particles) and γ according to Eq. (2.20). The method of Lagrange Multipliers was used for the optimization:

$$min\left\{\sum_i \left(D_{v_i} - \delta {l_i}^{\gamma}\right)^2\right\} \ , \ \ \delta \leq 3 \tag{4.5}$$

where D_{vi} and l_i are the volume fractal dimension and dimensionless size of the *i*th floc. The calculated values for δ and γ were 2.999 and -0.0153 respectively; therefore the relationship between the size and volume fractal dimension of lime flocs can be written as:

$$D_V = 2.999\, l^{-0.0153} \tag{4.6}$$

According to Eq. (4.6) the volume fractal dimensions of the lime softening flocs decrease as the floc size increases and become nearly constant for floc large flocs sizes. The resulted curve from Eq. (4.6) has the coefficient determination (R^2) of 0.554 and covers the range of estimated fractal dimensions from 2.68-2.83.

If the constraint of $\delta \leq 3$ is released, the following power law will be obtained:

$$D_V = 3.579\, l^{-0.044} \tag{4.7}$$

The resulted curve from Eq. (4.7) has the coefficient determination (R^2) of 0.92 and seems to fit the data very well. However, for very small flocs, the volume fractal dimension approaches 3.579 that is larger than 3 that is not possible. Therefore, the relationship of volume fractal dimensions and floc size cannot be estimated by Eq. (4.7).

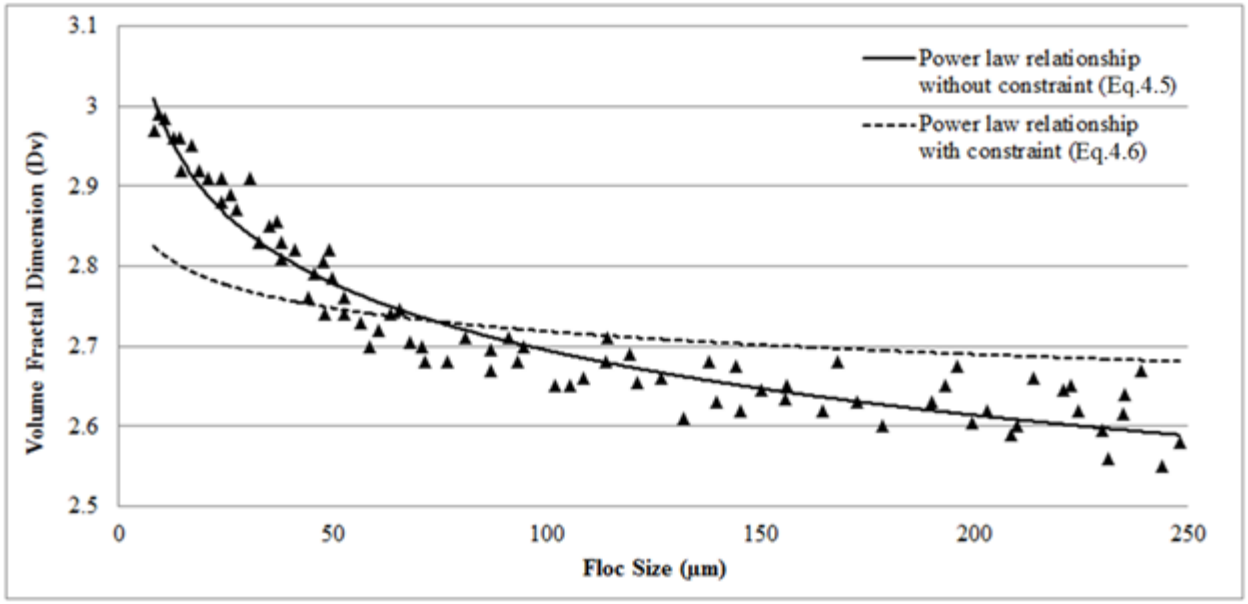

Figure 4.24. The variation of volume fractal dimension with the floc size

A two stage linear regression was also applied to the volume fractal dimension data (Figure **4.25**). The flocs were divided into two groups of small flocs (≤ 60µm) and large flocs (>60 µm) and for each group a linear relationship between size and fractal dimension was derived (Eq.

(4.8)). Note that different cut off points (50 µm, 60 µm and 70 µm) were tried and the 60 µm cut off point exhibited in the highest coefficient determination (R^2) for linear regression lines.

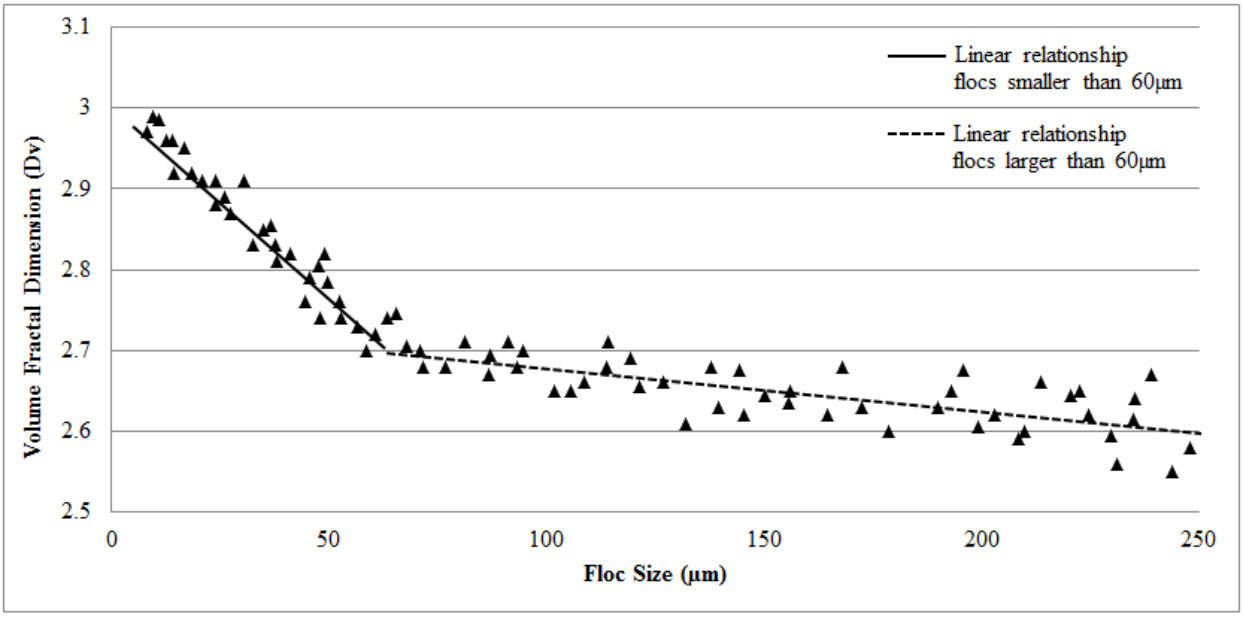

Figure 4.25. The variation of volume fractal dimension with size and two-stage relationship

$$D_V = \begin{cases} -0.0051d + 3.01 & d \leq 60\mu m \quad R^2 = 0.94 \\ -0.0006d + 2.74 & d > 60\mu m \quad R^2 = 0.60 \end{cases} \tag{4.8}$$

4.2.5. Estimations of volume fractal dimension

Figure **4.26** shows the estimation of volume fractal dimensions according to Eq. (2.12) (Maggi and Winterwerp 2004). The perimeter-based fractal dimensions were calculated simply from $A=P^{2/Dp}$. The results are compared with the measured values of volume fractal dimension of flocs.

Figure **4.27** shows the estimation of volume fractal dimension of lime softening flocs according to Eq. (2.11) (Thill et al 1998). The results are compared with the measured values of volume fractal dimension of flocs.

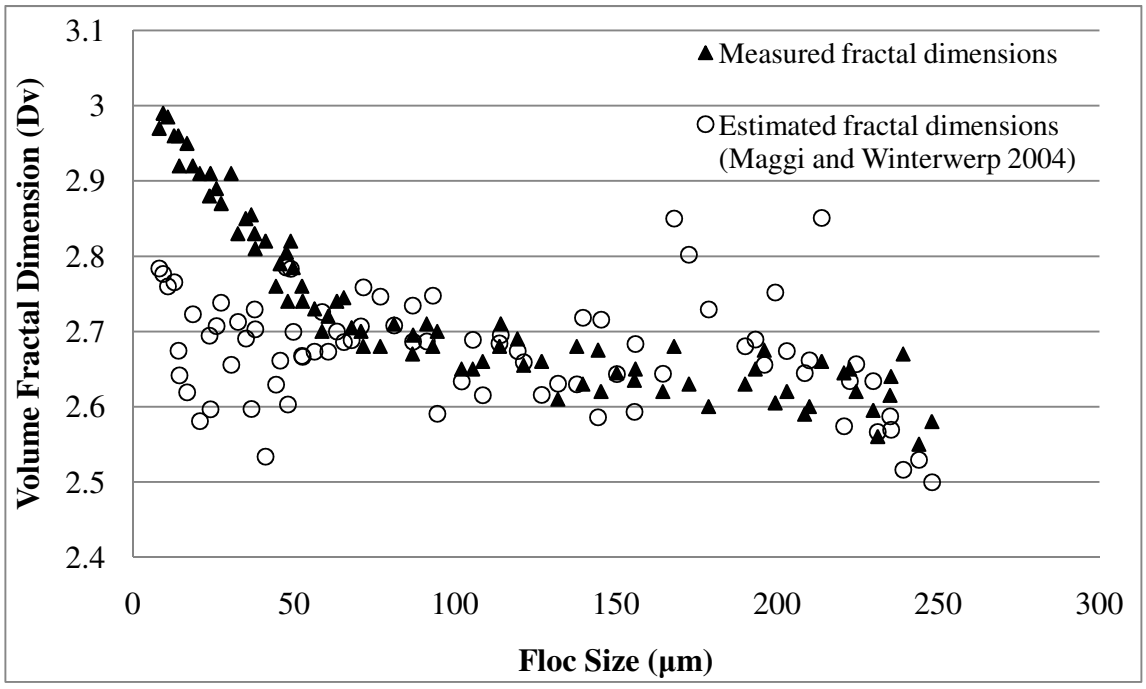

Figure 4.26. Estimation of volume fractal dimensions of lime flocs by using perimeter-based fractal dimensions according to Maggi and Winterwerp (2004).

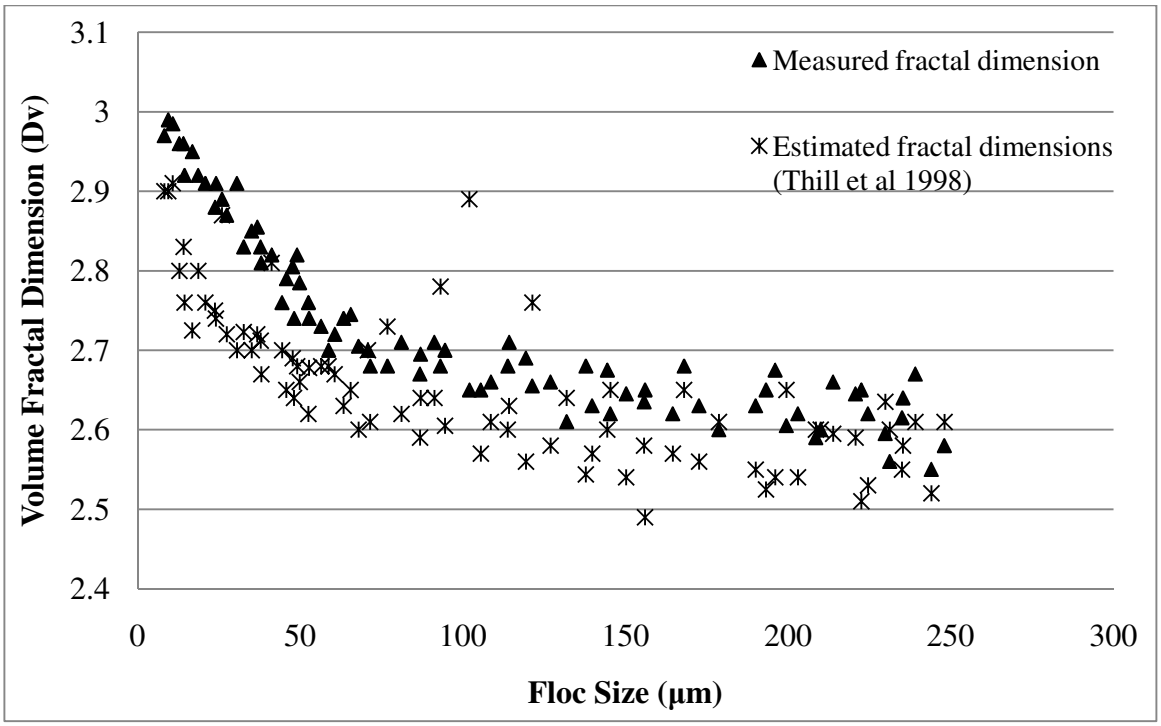

Figure 4.27. Estimated volume fractal dimensions of lime flocs by using the cross-sectional surface area fractal dimensions (Thill et al 1998)

4.2.6. Floc settling rates and mass fractal dimension

The measured settling velocity of flocs ranged from 0.1 to 7.1 mm/s (average of 2.37 mm/s) for the flocs with equivalent diameters from 10 µm to 260 µm (average 124 µm). The mass fractal dimension of flocs calculated by using Eq. (2.17) was about 2.10. Figure **4.28** shows the settling velocities of lime softening flocs.

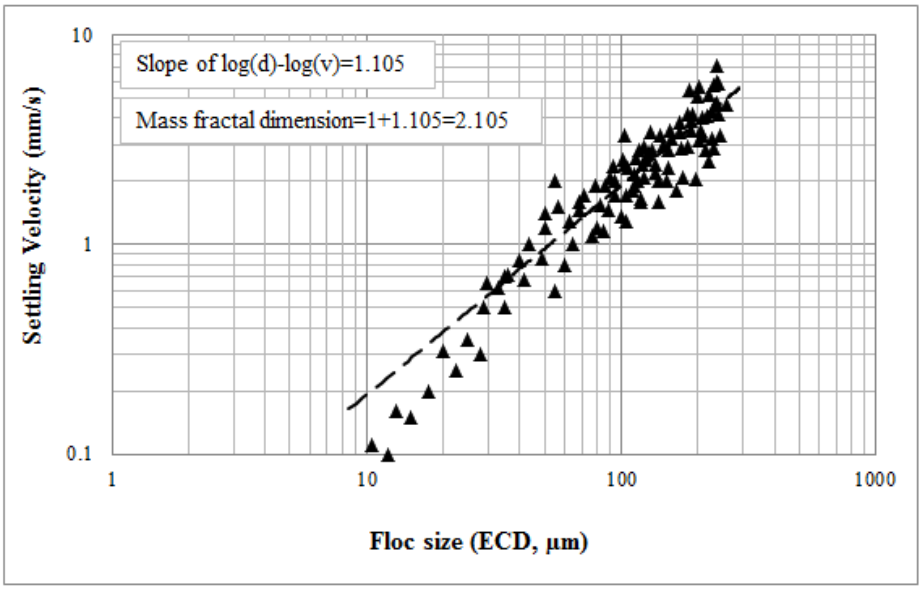

Figure 4.28. Settling velocity of lime softening flocs and indirectly determined mass fractal dimension

4.2.7. Predicting the settling velocity of flocs

The model suggested by Khelifa and Hill (2006) presented in Eq. (2.54) was applied to fit the data of the settling velocity of lime softening flocs. Based on the chemical composition analysis of flocs, the primary particles were assumed to be mainly composed of calcium carbonate. The density of calcium carbonate is usually around 2700 kg/m^3 (Kamiti and Van de Ven 1995). In this study it was assumed that the primary particles were monosized (Φ =1). Using trial and error, fitting of different sizes of primary particles was tested and four primary particles sizes (0.5 µm, 1 µm, 2 µm, 5 µm) that fitted the data well were selected for the model. The volume fractal dimension (D_V) was estimated for each floc using relationships in Eq. (4.8). The settling velocity of the flocs was also fitted with the modified Stokes' law (Eq. (2.35)). Based on the suggested values by Bushell et al. (2002), a correction factor (Ω) of 0.9 was used for the lime softening flocs. All the floc settling models are shown in Figure **4.29**.

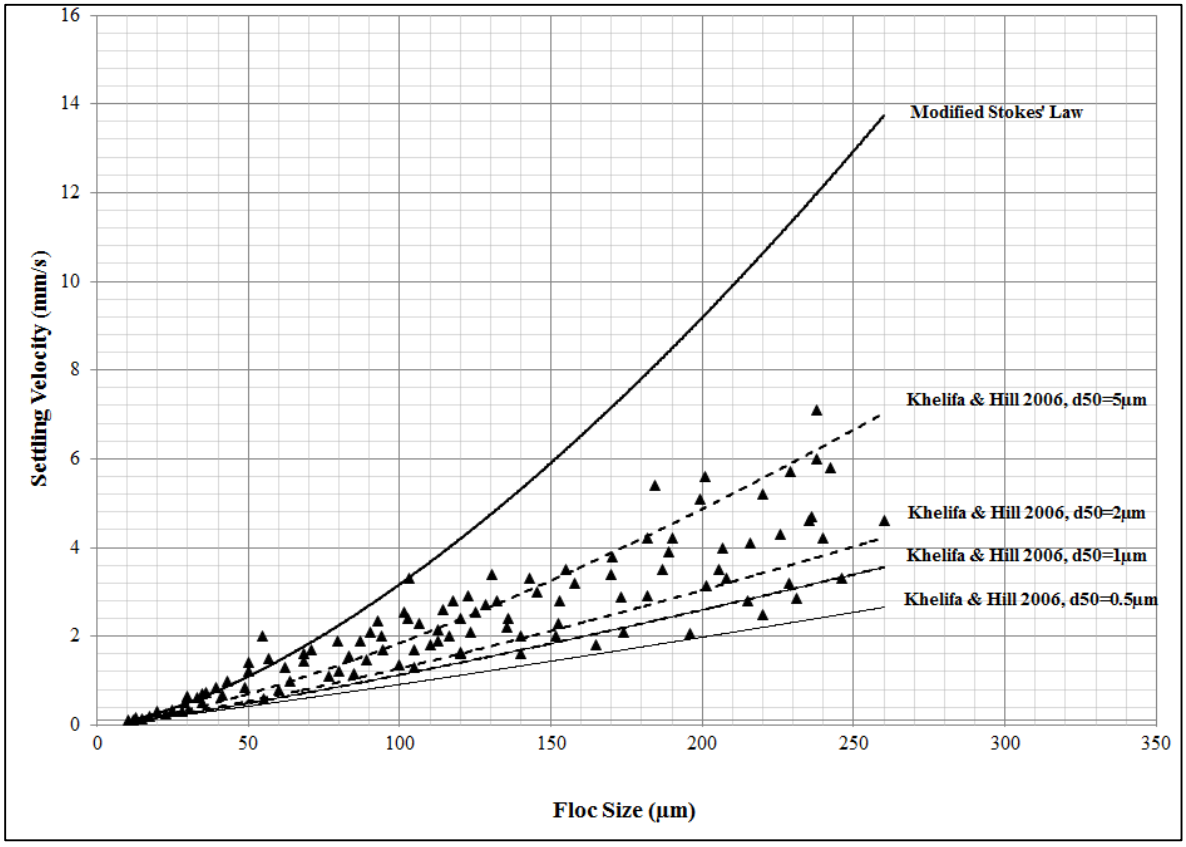

Figure 4.29. Predictions of lime floc settling velocities by Stokes' law and Khelifa et al. (2006) model

The upper bound of the Khelifa and Hill (2006) model for $D_V=3$ is the Stokes' law that was presented in Eq. (1.9). The lower bound can be determined for d_{50}=0.5 µm and lowest possible value for D_V.

4.3. Discussion

4.3.1. Settling velocities of lime flocs

Table **4.6** shows the average size and settling velocity of the lime flocs compared to other flocs encountered in water and wastewater treatment. Since the lime flocs were collected from the upper portion of the clarifier, their average size is smaller than settled alum and activated sludge flocs analyzed in other studies. Lime softening flocs analyzed in this study had settling rates lower than biological flocs (activated sludge) but settled faster than alum coagulation flocs.

Table 4.6. Average size and settling velocity of the lime flocs and some other flocs

Type of the aggregate	Average size (μm)	Average settling velocity (mm/s)
Lime softening flocs (this study)	124	2.37
Alum coagulation flocs Gorczyca, 1991,Gorczyca & Ganczarczyk 1996, 1999	339	0.7
Activated sludge flocs Ganczarczyk, 1995	700	3.8

4.3.2. Floc fractal dimensions

In Table **4.7**, the average box-counting fractal dimensions as well as the mass fractal dimension of the lime softening flocs are compared with the results of other types of flocs. Overall, the fractal dimensions of lime flocs were comparable to fractal dimensions of alum flocs and activated sludge flocs.

Table 4.7. Fractal dimensions in this study and some previous studies

Type of aggregate and source of data	Fractal Dimensions				
	D_B	D_S	D_P	D_V	D_{ST}
Lime softening flocs (this study)	1.15-1.27 (1.20)	1.49-1.90 (1.68)	1.21-1.38 (1.27)	2.55-2.99 (2.73)	2.10
Ferric coagulation flocs Bahrami 1997	1.11-1.16	1.94-1.99	N.A.	N.A.	N.A.
Alum coagulation flocs Gorczyca, 1991,Gorczyca & Ganczarczyk 1996, 1999	1.13-1.25	1.91-1.99	N.A.	N.A.	1.37-1.79
Activated sludge flocs Li and Ganczarczyk 1989 Ganczarczyk and Rizzi, 1996	N.A.	1.88-1.97	1.21	N.A.	1.45-2.0
Activated sludge flocs Ganczarczyk, 1995	N.A.	N.A.	1.04-1.32	N.A.	N.A.
Activated sludge flocs Cousin and Ganczarczyk 1998	N.A.	1.83-1.99	1.28-1.4	N.A.	N.A.
Activated sludge flocs Chu et al., 2004	N.A.	1.72-1.81	1.35-1.48	2.46-2.70	1.3-1.55

4.3.3. Estimation of 3D volume fractal dimensions from 2D fractal dimensions

Figure **4.26** and Figure **4.27** show that for flocs larger than 60µm, the Eq. (2.12) (Maggi and Winterwerp 2004) gives a better estimation of volume fractal dimension than Eq. (2.11) (Thill et al 1998) while for flocs smaller than 60 µm, Eq. (2.11) gives a closer estimation of volume fractal dimension of flocs.

In general it appears that Eq. (2.11) provides a good and easy tool for the estimation of volume fractal dimensions. However, the estimated fractal dimensions seem to be slightly lower than the measured volume fractal dimensions. In the derivation of Eq. (2.11), D_S was assumed to be the

fractal dimension of cross-sectional surface area resulting from the intersection of a plane and the floc in 3D space. If the primary particles are relatively homogeneously distributed within the aggregate, then intersection of any plane with the floc will result in cross-sectional surfaces with similar morphology. However, for a very complex and irregular floc this assumption may not be correct.

4.3.4. Variation of volume fractal dimension with floc size

It seems that the relationship between the size and volume fractal dimension of lime softening flocs can be explained by a two-stage flocculation model (Figure **4.25**). The smaller flocs (≤60 μm) have fractal dimensions close to Euclidean dimension (Eq. (4.8)) while the fractal dimensions of larger flocs deviate from Euclidean dimension i.e. 3. This result is consistent with previous studies for alum and activated sludge flocs (Snidaro et al. 1997, Gorczyca and Ganczarczyk 2001). Initial clusters are simply bundles of few primary particles and their fractal dimension is very close to Euclidean dimension (Eq. (4.8)). It seems that smaller flocs (<60 μm) are formed by aggregation of clusters and as the floc grows, the fractal dimension decreases.

Eq. (4.8) and Figure **4.25** show that there is a strong linear relationship between the size and fractal dimension at the first stage of flocculation but the linear correlation is not so strong for large flocs. Many factors such as breakup, restructuring and precipitation of calcium carbonate particles in the pores and around the aggregate specifically affect larger flocs and cause the discrepancy from the simple linear correlation. For example, the precipitation of primary lime particles inside the flocs or their penetration inside the aggregate may be modeled by the Diffusion Limited Aggregation (DLA) mechanism. According to Witten and Sander (1981) model, the diffusion limited particle-cluster aggregation can generate fractals with volume

fractal dimension of about 2.45 which is close to the fractal dimensions of large lime flocs in this study. Therefore, the relationship between the floc size and fractal dimension appears to be determined by the floc formation mechanism.

4.3.5. Discrepancy between D_{ST} and D_V

In this study, the lime flocs were mainly composed of calcium carbonate; therefore, of constant density. It was expected that the mass fractal dimension and volume fractal dimension of these flocs to be at least similar. Table **4.7** shows that for different types of flocs the indirectly determined mass fractal dimension from settling tests (D_{ST}) significantly is not within the range of directly determined volume fractal dimensions (D_V). Therefore the power law relationship in Eq. (2.17) that was used for indirect determination of mass fractal dimension needs to be critically evaluated. Here, we rewrite that power law relationship:

$$v_s \propto d^{D_M-1} \tag{4.9}$$

Let us review the derivation of Eq. (4.9). If we consider V_p and M_p as volume and mass of primary particles, since the mass of the aggregate is related to the number of elements in the aggregate by $M=N\times M_p$, the following power law exists:

$$N \propto d^{D_M} \tag{4.10}$$

For an aggregate made of N elements with mass of M_p and volume of V_p, the solid fraction is defined as (Johnson et al. 1996):

$$1 - \varepsilon = \frac{N\mathrm{V}_P}{V} \tag{4.11}$$

where ε is the floc porosity.

The first critical assumption that has been used in previous reviewed derivations appears at this point. It has been assumed that the settling velocity of flocs follow Stokes' law. According to Stokes' law (Eq. (2.35)) the following relationship exists:

$$(\rho_f - \rho_W) \sim \frac{C_D v_s^2}{d} \tag{4.12}$$

Assuming the floc being composed of solids of constant density (ρ_p), the following relation can be obtained by simple mass balance:

$$\left(\rho_f - \rho_W\right) = (1 - \varepsilon)\left(\rho_p - \rho_W\right) = (1 - \varepsilon)\Delta\rho \tag{4.13}$$

Combining Eqs. (4.11) - (4.13) results in the following relationship:

$$\frac{N\mathrm{V}_P}{V} \sim \frac{C_D v_s^2}{d} \tag{4.14}$$

Assuming the drag coefficient of $C_D = 24/Re$ acting on the settling floc, the following relationship can be derived:

$$C_D \sim \frac{1}{v_s d} \tag{4.15}$$

Combining Eqs. (4.14) and (4.15) produces the following relationship:

$$\frac{N V_P}{V} \sim \frac{v_s}{d^2} \tag{4.16}$$

And Eq. (4.10) and Eq. (4.16) together result in following relationship:

$$D_M \sim V \frac{v_s}{d^2} \tag{4.17}$$

The second critical assumption is needed to derive the Eq. (4.9) from Eq. (4.17) and this assumption is that the volume and size of a floc are related according to Eq. (4.18):

$$V \sim d^3 \tag{4.18}$$

As mentioned in Chapter 2, many researchers have estimated the volume fractal dimension of aggregates from their settling rates according to Eq. (4.9). However, Eq. (4.18), which is based on Euclidean geometry, contradicts Eq. (2.13) which is a fundamental relationship in fractal geometry. Also Eq. (4.12) is directly derived from Stokes' law that has been shown not to predict the settling velocity of flocs correctly.

Eq. (4.9) suggests that the mass fractal dimension is constant over a range of flocs sizes while the volume fractal dimension (D_V) determined directly on floc images decreases with increasing

flocs size. Further, according to Eq. (4.9) there has to be a unique linear relationship between the *log*(settling velocity) and *log*(size) of flocs. However, Figure **4.29** indicates that the relationship between the floc settling velocity and floc size cannot be modeled by a single curve. Figure **4.29** shows that a family of curves is needed to describe the complicated relationship between size, settling velocity and fractal dimension of lime flocs.

4.3.6. Fractal dimensions and settling velocity of lime flocs

The models suggested by Khelifa and Hill 2006 (Eq. (2.54)) and modified Stokes' law (Eq. (2.35)) were used to model the settling velocity of lime softening flocs (Figure **4.29**).

Stokes' law predicts the settling velocities of small flocs in the size range of 10-60 µm quite well. The small flocs have fractal dimensions close to Euclidean dimensions and this may be the reason that their settling velocity can be well predicted by Stokes' law. It seems that the large (>60 µm) flocs are too complex to be described by the modified Stokes' law (Eq. (2.35)) that is based on the Euclidean geometry. For larger flocs (>60 µm), the Khelifa and Hill (2006) model provides much better estimation of settling velocities than the modified Stokes' law (Figure **4.29**). In this model, primary particle size and fractal dimensions were variable according to the results of this study.

The settling velocity of some flocs in the size range of 60-250 µm are predicted with the model assuming a size for primary particles of 5µm. It is probable that these lime flocs are formed by the collision of clusters of calcium carbonate precipitates. The settling velocities of some other flocs in the size range of 60-250 µm could be modeled assuming primary particles with a size of 0.5-2 µm. This size of primary particles coincides with the size of calcium carbonate precipitates

(Nason and Lawler 2008). This would suggest that small flocs formed by Cluster-Cluster Aggregation (CCA) grow to larger flocs by Diffusion Limited Aggregation (DLA) due to precipitation of calcium carbonate.

4.3.7. Floc internal structure

The average directly determined fractal dimensions describing the volume of lime softening flocs (D_V) for the flocs in the size range of 60-120 μm was 2.72 that is similar to the fractal dimension of the ideal 3D Sierpinski sponge (Sierpinski carpet in 3D) with the constriction ratio of 3. For larger flocs in the range of 120-250 μm the average directly determined volume fractal dimension is about 2.6 that is similar to the fractal dimension of the ideal 3D Sierpinski sponge with the constriction ratio of 5. The results of this study suggest that this particular model can be used to represent internal structure and simulate the behaviour of the lime softening flocs during settling in this size range. Similar models may exist to represent the structure of other flocs. The Sierpinski model or other similar mathematically known models may also be appropriate to simulate the behaviour of cakes of flocs accumulated on filters or membranes.

4.4. Conclusions

Fractal dimensions of lime softening flocs were determined directly from floc images and indirectly from floc settling; application of the various floc fractal dimensions to model floc settling was evaluated. The following conclusions can be made from this study:

For lime softening flocs larger than 60 μm, the model incorporating variable floc fractal dimensions and variable primary particle size describes the settling better than the models assuming fixed values for these parameters (Stokes' law).

For smaller flocs (<60 μm) Stokes' law predicts the settling velocity better than the model based on the fractal structure of flocs. This suggests that Stokes' law can still be applied to aggregates with fractal dimensions close to Euclidean dimensions, such as the small lime flocs and other chemical coagulation aggregates.

It appears that two aggregation mechanisms are involved in the lime flocs formation: Cluster-Cluster Aggregation (CCA) for small flocs (<60 μm) and Diffusion Limited Aggregation (DLA) for large flocs (>60 μm). The precipitation of calcium carbonate particles on the aggregates as well as their penetration into the floc pores appears to be predominant mechanism for large lime flocs formation. This mechanism results in highly heterogeneous structure for large flocs.

Numerous assumptions contradicting the fractal nature of flocs are used in indirect determinations of mass fractal dimensions from the floc settling rates. These assumptions result in the large discrepancy found between the indirectly determined mass fractal dimension from settling tests and directly measured volume fractal dimensions of flocs.

For lime softening flocs in the size range of 60-120 μm and 120-250 μm, the directly determined volume fractal dimension are similar to the fractal dimensions of ideal Sierpinski sponges (Sierpinski carpet in 3D) with the constriction ratios of 3 and 5 respectively.

Chapter 5

General Model for Flocs' Settling Velocity

In this chapter we will try to derive a general model for the settling velocity of lime softening flocs that considers multiple fractal dimensions for each floc size. In the previous study we applied different primary particles sizes in the Eq. (4.1) in order to explain why flocs with the same size settled at different velocities. However, the results of this study demonstrated that the volume fractal dimensions of flocs generally deviate from Euclidean dimensions more as the floc size increases and the wide range of settling velocities, especially for large flocs, may be attributable to the multiple fractal dimensions describing these flocs.

5.1. Floc formation mechanism and floc fractal dimensions

In Chapter 4, two suggested models for variation of fractal dimensions with floc size were discussed: power law relationship (Eq. (4.6)) and two-stage linear relationship (Eq. (4.8)). It was shown that the relationship between the size and volume fractal dimension of studied lime flocs can be estimated by two lines. However, it appeared that for large flocs the linear model exhibited a poor correlation between size and fractal dimension (R^2=0.60 for flocs larger than 60 μm). In fact, as the floc size increased the fractal dimensions tend to deviate from the fitted line.

According to the results of Chapter 4, as the floc size increases, the value of fractal dimensions decreases while the complexity and therefore the range of fractal dimensions increases.

5.2. Flocculation of small and large flocs

In Chapter 4, the possible aggregation mechanisms of lime softening flocs were discussed; it was suggested that most likely two mechanisms, cluster-cluster aggregation (CCA) and diffusion limited aggregation (DLA) are involved in the flocculation of lime flocs. In all aggregation mechanisms, primary particles attach to each other and form a cluster; the first structural level of the floc aggregate. A cluster consists of fewer primary particles than the entire aggregate. The number of primary particles within the cluster determines the possible arrangements of the internal particles. For instance, assuming cubic primary particles can attach to each other only on their edge, for 4 primary particles there are 7 possible arrangements of primary particles within the cluster (Figure **5.1**).

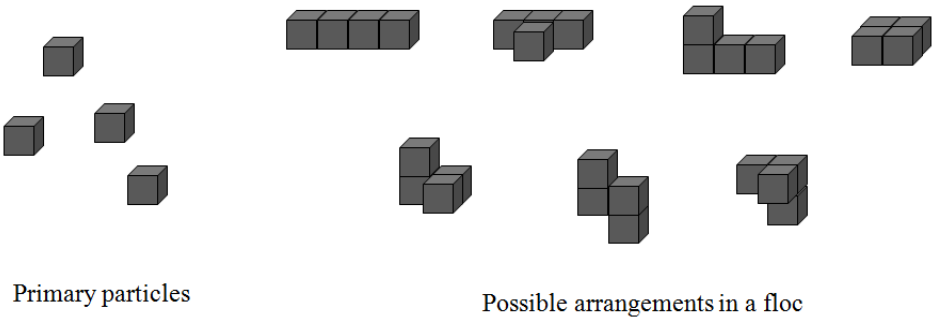

Figure 5.1. Possible arrangements of 4 primary particles in a floc

For 3 primary particles there are only 2 possible arrangements and for 5 primary particles there are 28 possible arrangements. As the number of primary particles increases, the number of possible arrangements of primary particles inside the cluster increases dramatically. As the number of primary particles increases, it is possible to have a cluster with opening (pores) within

its structure. For a cluster with few primary particles, porosity is almost zero, but for a cluster built of a large number of primary particles (large floc), porosity may assume a significant value. As the floc size increases, the random arrangements of primary particles can form a heterogeneous aggregate (Figure **5.2**).

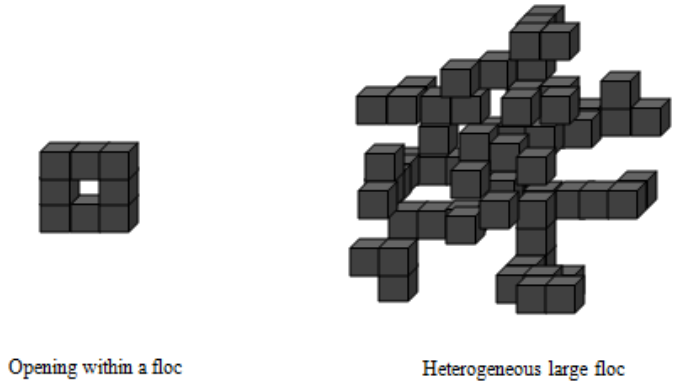

Figure 5.2. Formation of porosity and heterogeneity in large aggregates

When a few primary particles form a cluster i.e. a very small floc, the resulting structure is unlikely fractal. The self-similar fractal structure requires the repetition of a certain pattern and that is not possible for a cluster containing a limited number of primary particles. Therefore, very small flocs may not exhibit fractal properties and their measured fractal dimensions may be very close to Euclidean dimensions.

As the number of primary particles increases, various patterns of cluster, primary particles attachments and different self-similarity patterns result in flocs with variety of fractal dimensions. For example, clusters can act as primary particles for the next level of aggregation

(Figure **5.3**). This cluster-cluster aggregation increases the possible arrangements of particles and clusters.

According to Figure **4.25** of Chapter 4, two different aggregation mechanisms were identified in flocculation of lime softening flocs in this study. A wide range of floc fractal dimensions, especially for large flocs may be the combined result of larger number of primary particles and different aggregation mechanisms.

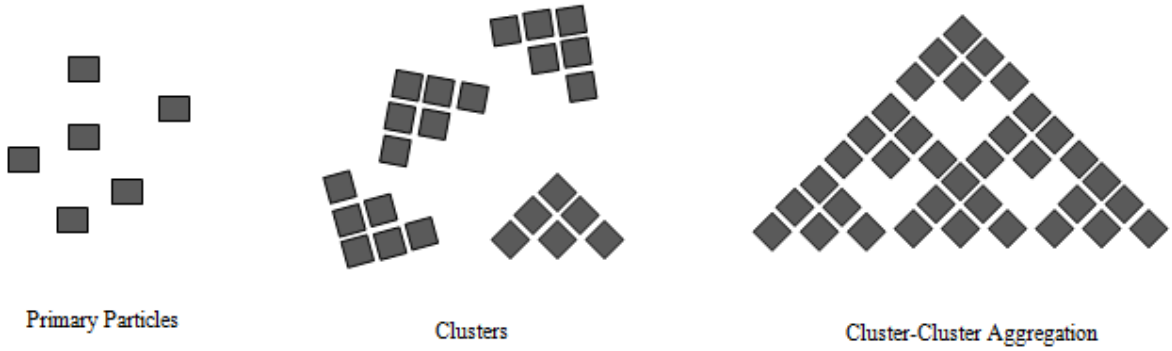

Figure 5.3. Cluster-Cluster Aggregation (CCA) in flocculation processes

5.3. Theoretical fractal dimensions of flocculated aggregates

Some researchers have attempted to analytically derive the fractal dimensions of flocculated aggregates (Witten and Sander 1981, 1983, Meakin 1983, Brown and ball 1985, Turkevich and Scher 1985, Tan et al 1999, Hasley 2000, Weipeng et al 2009). These studies are based on the possible mechanisms of aggregation i.e. diffusion limited aggregation (DLA) or cluster-cluster aggregation (CCA).

Witten and Sander (1981) developed a random-walk model to simulate the mechanism of aggregation of colloidal aggregates. In another study (Witten and Sander (1983)) used a lattice model to simulate the aggregation. A lattice model is a physical model that is defined on a lattice

as opposed to the space-time or continuum of space. According to their model, the Hausdorff fractal dimension of diffusion limited aggregates in 2D yields to about 1.7. They suggested that primary particles form clusters and the particles randomly move and stick to other particles or clusters to form a bigger aggregate. Their results were later confirmed by other studies (Meakin 1983[a], Halsey 2000). The model suggested by Witten and Sander (1981) only allowed one particle to move and attach to other particles at any time. Meakin (1983[b]) developed a model in which all particles and clusters were allowed to move and stick to each other and found that fractal dimensions of aggregates yield to 1.45-1.5. This situation seems to be more realistic in an actual aggregation process.

In 3D space, the model suggested by Meakin (1983[a]) resulted in aggregates with fractal dimensions of about 2.51. A parameter called "sticking coefficient" can be added to the model that is the probability that a primary particle sticks to the available spots on the current aggregated particles and clusters when it randomly walks into the lattice. Meakin (1983[a]) concluded that even though the decrease in sticking coefficient results in a denser aggregate, it does not have a significant effect on the fractal dimension of the aggregate. I personally disagree with this conclusion because when the sticking coefficient approaches zero, the aggregate essentially will be a solid accumulation of particles and the fractal dimension must yield to the Euclidean dimension, i.e. 3.

Some studies also only considered cluster-cluster aggregation or reaction-limited aggregation. Kolb et al. (1983) found the fractal dimension of about 1.38 in 2D. For cluster-cluster aggregation, Meakin (1984) found the fractal dimensions of about 1.5 and 1.9 in 2D and 3D respectively. The random-walk algorithm is one of the models used for simulation of aggregation mechanism. There are other models that can yield different results.

It is important to note that the fractal dimensions derived in the studies mentioned above are the minimum (yield) fractal dimensions for the aggregates that are formed solely by DLA or CCA aggregation. Other factors affecting the value of the fractal dimension, such as variable turbulence level, a combination of different mechanisms of aggregation and floc break-up were not considered in these studies.

5.4. Modelling of floc settling revisited

As described in the previous section, small flocs that are formed by few primary particles cannot be very porous or fractal and therefore they can be considered as solid particles and their settling can be modelled by the Stokes' law. However, larger flocs exhibit fractal properties and their settling velocity can be described best by models that incorporate fractal dimensions.

In Chapter 4, a family of curves were used to model the settling velocity of lime softening flocs (Figure **4.29**). The model that was suggested by Khelifa and Hill (2006) uses different primary particles sizes to cover the wide range of settling velocities. However, the wide range of settling velocities, especially for large flocs, is most likely attributable to the multiple fractal dimensions describing these flocs.

As discussed in Chapter 4, for large flocs, there are numerous possible fractal dimensions and therefore a wide range of settling velocities is possible. Since the fractal dimensions can take any value in a wide range, the settling velocities can be any value in a wide range and therefore a limited number of curves may not be sufficient for modeling the settling velocity of flocs. This has been confirmed experimentally (Li and Logan 2001, Khelifa and Hill 2006).

In this chapter, a model incorporating a distribution of fractal dimensions for each floc size is used to predict the settling velocities of lime softening flocs. The suggested model is in fact a more general form of the Khelifa and Hill (2006) model.

According to the theoretically determined fractal dimensions by Meakin (1983[a], 1984), the 3D fractal dimensions should range from 1.9 to 3.0 for cluster-cluster aggregation and from 2.5 to 3.0 for diffusion limited aggregation. Depending on the characteristics of the system the distribution may be different.

In Chapter 4, the fractal dimensions of lime softening flocs were measured in 3D. The measured fractal dimensions were in the range of 2.55-2.99 that is in good agreement with the theoretically determined fractal dimension for diffusion limited aggregates. As discussed in Chapter 4, the small flocs (<60 μm) seem to follow the cluster-cluster aggregation mechanism. If we assume that the cluster-cluster aggregation resulted in the steep slope of the fractal dimension and the size regression line for small flocs (<60 μm) in Figure **4.25**, then one can extrapolate the regression line for largest flocs and find 1.73 for the fractal dimension of the floc of equivalent diameter of 250 μm. This value is close to the theoretically determined fractal dimension for cluster-cluster aggregation.

5.5. General model for floc settling

In Chapter 4, we used Eq. (5.1) to model the settling velocity of lime softening flocs:

$$v_s = \frac{1}{18}\theta g \frac{\rho_s - \rho_w}{\mu} d_{50}^{3-D_V} \frac{d^{D_V-1}}{1 + 0.15Re^{0.687}}\phi \qquad (5.1)$$

In Eq. (5.1), the primary particle size (d_{50}) and volume fractal dimension (D_V) of flocs were variable. The variation of volume and fractal dimension with size was modeled by using a two-stage linear model. The model was able to cover a range of settling velocities (See Figure **4.29** of Chapter 4).

According to the results of Chapter 4, the general relationship between the size and volume fractal dimension of flocs can be written as:

$$D_V = f(d) \tag{5.2}$$

where f is a linear function over a certain range of floc size (d). However, as the floc size increases the fractal dimensions disperse. In other words, when the floc size increases the magnitude of fractal dimensions can occur in a wider range. Here, we assume that a distribution of fractal dimensions exists for each individual floc size. For simplicity, assume that the fractal dimensions for a given floc size have a normal distribution. Therefore, for a given floc size, the distribution of fractal dimensions can be written as:

$$D_V = \mu_d + \sigma_d . \frac{1}{\sqrt{2\pi}} e^{-\frac{x^2}{2}} \tag{5.3}$$

where μ_d and σ_d are the mean and standard deviation of fractal dimensions for flocs of size d, and x is a real number.

It has been shown that in general the fractal dimensions of flocs decrease as the floc size increases (Maggi and Winterwerp 2004, Vahedi and Gorczyca 2011). Also as discussed earlier in

this paper, as the floc size increases, a broader range of fractal dimensions can be expected. Accordingly, we assume that in Eq. (5.3), the mean (μ_d) decreases and variance (σ_d) increases as the floc size increases.

According to Meakin (1983b, 1384), the minimum mass fractal dimension of diffusion limited aggregation and cluster-cluster aggregation in 3D are 2.5 and 1.9 respectively. We have reported earlier that both mechanisms occur in the flocculation of lime softening flocs. We also know that the maximum mass fractal dimension in 3D embedding space is 3. Therefore, the fractal dimensions describing an individual flocs must fall within [1.9 3.0] interval.

The likelihood of occurrence of a large floc with the fractal dimension of 3.0 is very low. According to our previous study (Vahedi and Gorczyca 2011), the aggregation of the large lime flocs (>50 μm) is mainly controlled by diffusion limited aggregation; consequently the probability of occurrence of a big floc with the fractal dimension of 1.9 is also very low. Therefore, the normal distribution of possible fractal dimensions in the range of 1.9 -3.0 is well justified.

Fractal dimension decreases as the floc size increases and as the floc size approaches zero, the fractal dimension yields to the Euclidean dimension (3). Here for simplicity we assume that for the average mass fractal dimension of largest studied flocs (d=d_{max}) in 3D is the midpoint of the [1.9 3] interval i.e. 2.45. Therefore, we propose the following simple linear relationship between the mean fractal dimension and floc size for flocs in the range of *0*-d_{max}:

$$\mu_d = 3 - \frac{0.55}{d_{max}} d \tag{5.4}$$

Note that, here we did not use the suggested equation for the variation of fractal dimensions in Eq. (4.8) of chapter 4 because we are trying to simulate the settling velocity of flocs simply and only by using the information about their aggregation mechanism.

As mentioned earlier, the results of previous chapter showed that for large flocs the linear model exhibited a poor correlation between size and fractal dimension (R^2=0.60 for flocs larger than 60 μm in Figure **4.25**). In fact, as the floc size increased the fractal dimensions tend to deviate from the fitted line. Since for each floc size only few measured fractal dimensions are available it is not possible to analytically determine the variation of the variance of fractal dimensions. Therefore, here for simplicity we assume that the variance of fractal dimensions increases linearly with floc size.

As the floc size approaches zero, it is logical to expect that the fractal dimension is equal to the Euclidean dimension (3) and is unique (σ = 0). For a normal distribution, the interval [μ-4σ μ+4σ] accounts for more than 99.9% of the data. For the largest floc ($d = d_{max}$) we assumed that the fractal dimensions have a normal distribution within [1.9 3] interval. Therefore $\sigma(d_{max})$=1.1/8=0.1375 and the relationship between the variance of fractal dimensions and floc size is written as:

$$\sigma_d = \frac{0.1375}{d_{max}} d \tag{5.5}$$

Consequently, for a floc size d, the normal distribution of fractal dimensions of flocs will be written as:

$$D_V = 3 - \frac{0.55}{d_{max}} d + \frac{0.1375}{d_{max}} d . \frac{1}{\sqrt{2\pi}} e^{-\frac{x^2}{2}} \quad (5.6)$$

The suggested distribution of fractal dimensions in Eq. (5.6) is used in Eq. (5.1) to simulate the possible settling velocities of the flocs. All primary particles were assumed to be the original primary particles (lime particles) with the size of 0.5-1µm. The effect of the formed clusters that may act as primary particles is already seen in the distribution of fractal dimensions.

The "rand" and "icdf" MATLAB toolboxes were used to generate 30 random points of fractal dimensions distribution for each floc size. The generated fractal dimensions were used in Eq. (5.1) in order to simulate the settling velocity of aggregates. The simulation was carried out in MATLAB 2009a.

The simulated fractal dimensions are compared to measured fractal dimensions in Figure 5.4. The results of the simulation are presented and compared to measured settling velocities in Figure **5.5**

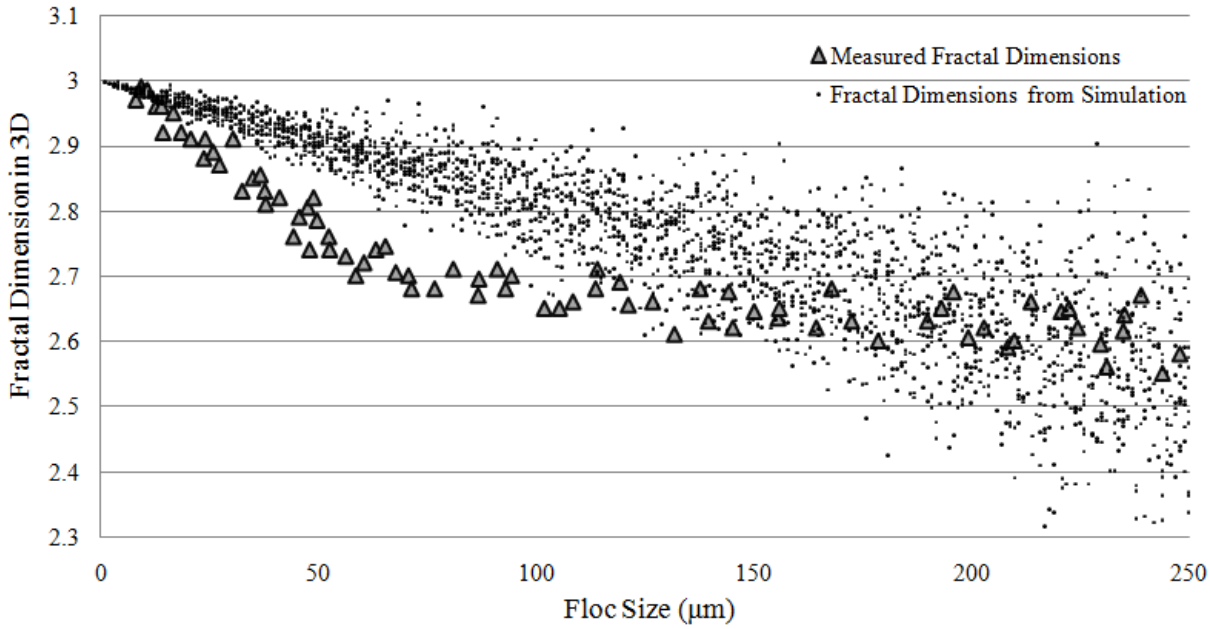

Figure 5.4. Measured and estimated fractal dimensions of lime softening flocs

For this simulation we did not use any measured fractal dimensions of lime softening flocs. We only used the theoretically determined fractal dimensions and estimated the settling velocity of flocs and found it in good agreement with the measured settling velocities.

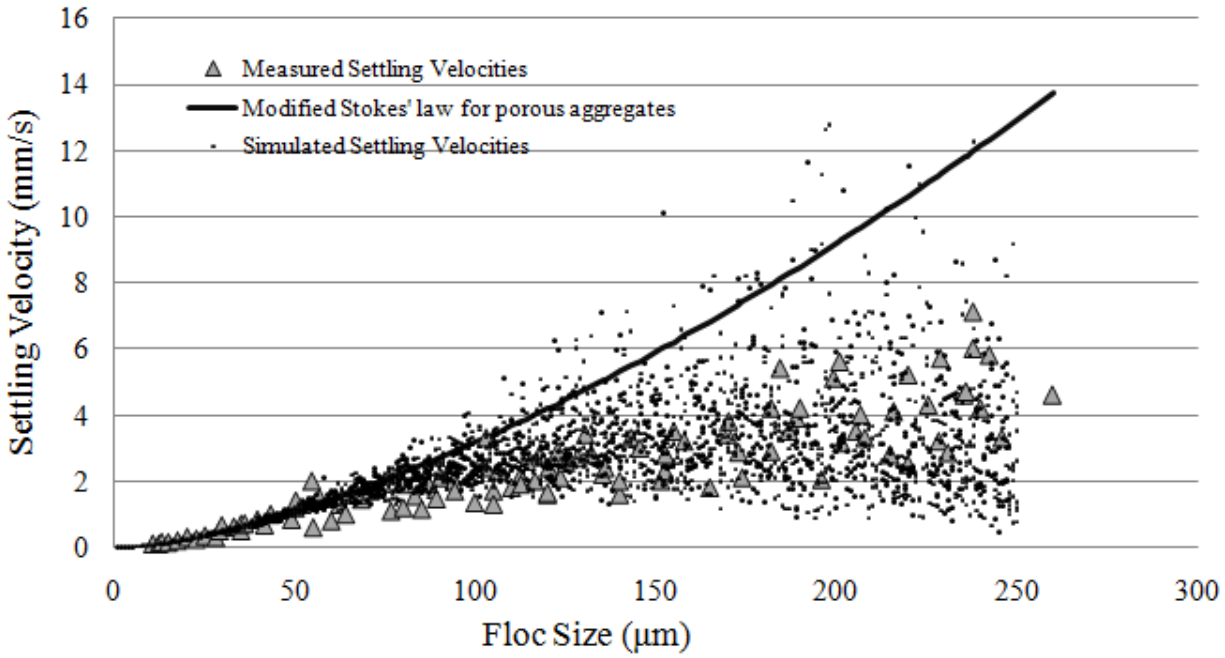

Figure 5.5. Simulated settling velocities for lime flocs by using simple normal distribution for fractal dimensions

5.6. Discussion

The calculated floc settling velocities are presented and compared to measured settling velocities in Figure **5.5**. No experimentally determined fractal dimensions were used for the simulation of the floc settling velocity. Instead, the floc fractal dimensions were generated according to normal distributions described by Eq. (5.6). Figure **5.5** shows that the predicted settling velocities using the generated floc fractal dimensions are in good agreement with the measured settling velocities.

The fractal dimensions were generated assuming that a floc can assume any fractal dimension, normally distributed in a certain range determined by the mechanism of floc aggregation. Consequently, a single floc exhibits a range of different settling velocities. Therefore, the

relationship between the settling velocity and the size of flocs is not unique, but rather in a form of a cloud where several settling velocities are possible for one floc size (Figure **5.5**).

The results of this study generally show that the Stokes' law significantly overestimates the settling velocity of lime flocs. Therefore, the sedimentation tanks that are designed according to Stokes's law are not large enough to remove the flocs.

Figure **5.6** shows the simulated settling velocities with 68% and 95% calculated confidence intervals, which can provide guidelines for designing the sedimentation tanks. For example, according to the data of Portage la Prairie water treatment plant, the maximum inflow to one clarifier is about 10000 m^3/day. If the designer wants to remove the lime flocs with 95% confidence, the surface overflow should be about 1 mm/s and the required surface area of the clarifier can be calculated as follows:

$$S = \frac{10000\left(\frac{m^3}{day}\right) \times \frac{1}{24 \times 3600}\left(\frac{day}{s}\right)}{0.1\left(\frac{mm}{s}\right) \times \frac{1}{1000}\left(\frac{m}{mm}\right)} = 1157.4\, m^2 \qquad (5.7)$$

Assuming a circular clarifier, the required diameter of the clarifier will be about 34 m. According to Table **3.2**, this diameter is significantly larger than the diameters of the existing clarifiers at the plant (14-16.5 m). The surface overflow rates for the clarifiers at Portage la Prairie plant have been recently improved with 60º 0.5m tall ABS tube settlers (See the Figure **3.15** in Chapter 3). However, as discussed in chapter 3, the plant still has a significant problem with sand filter clogging due to the inefficient sedimentation of lime flocs.

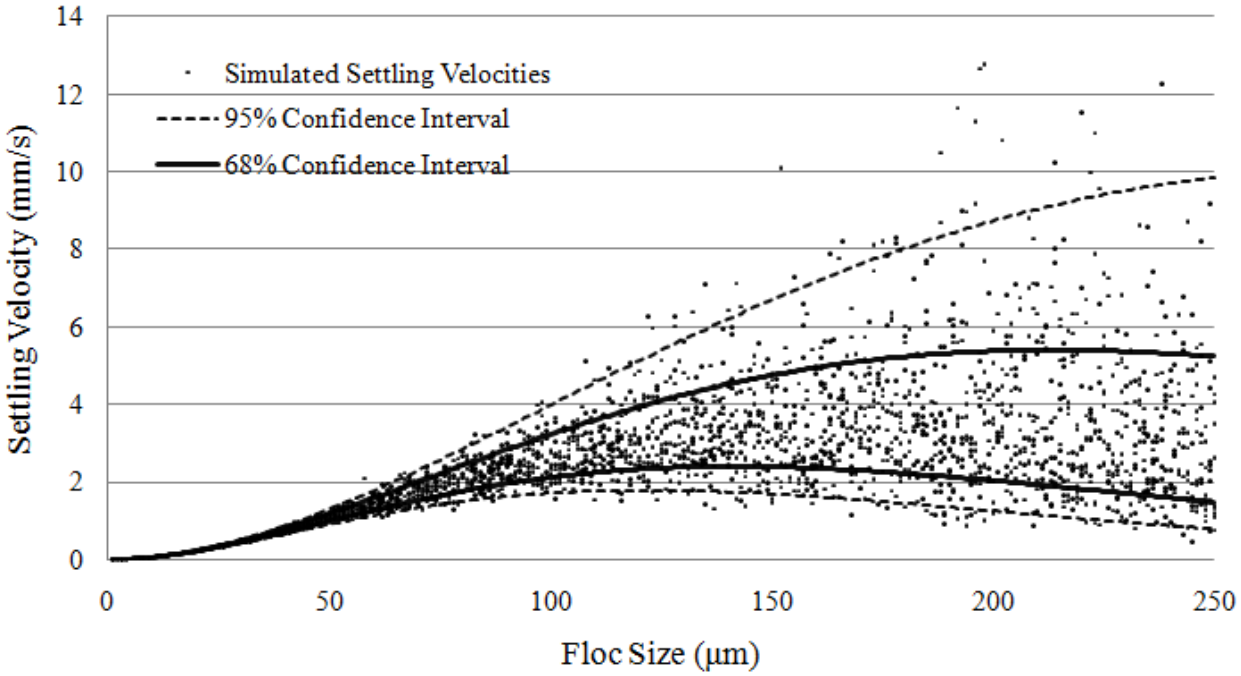

Figure 5.6. Simulated settling velocities and confidence curves

Figure **5.6** suggests that the settling tanks surface overflow rates may be quite low even for larger flocs. This is an important finding that has been confirmed by results of this study and also previous studies (Maggi and Winterwerp 2004). This finding suggests that forming large flocs size does not guarantee improved sedimentation as the settling velocity of flocs can vary with the floc fractal dimension which is controlled by aggregation mechanisms.

5.7. Conclusions

The settling velocity model that incorporated calculated, normally distributed fractal dimensions for each floc size fitted well the measured settling velocities of lime softening flocs.

Fractal dimensions were generated assuming that a floc can assume any fractal dimension in a certain range, determined by the floc aggregation model. Consequently, a single floc can have a

range of different settling velocities. As a result, the relationship between the settling velocity and size of flocs is not unique, but rather in the form of a cloud where several settling velocities are possible for one size of the floc.

Stokes' law significantly overestimates the settling velocity of lime flocs. The settling tank's surface overflow rates may be quite low even for larger lime flocs. The settling velocity of flocs seems to be mainly controlled by aggregation mechanisms and forming large flocs does not guarantee improved sedimentation.

Chapter 6

Multifractal Analysis of Lime Flocs

The box-counting fractal dimension of lime flocs discussed in the previous chapter is a morphology-based fractal dimension. Highly heterogeneous structures, such as flocs, can be described by a number of different fractal dimensions, i.e. spectrum of fractal dimensions. In this chapter a variety of other fractal dimensions (multifractal spectrum) of lime softening flocs are determined on 2D section images of these aggregates.

6.1. Analytical procedures

The floc images obtained and processed for measurement of box-counting fractal dimensions were also used for multifractal analysis. The procedure of imaging was described in Section 4.1.3 of Chapter 4 of this thesis.

The multifractal analysis of lime softening flocs was performed by using FracLac 2.5 that is a freely available plugin for ImageJ. ImageJ is a public domain, also freely available, Java-based image processing program. FracLac plugin was written by Audrey Karperien at the School of Community Health, Faculty of Science, Charles Sturt University, Australia (Karperien 2007). ImageJ was developed at the National Institutes of Health, USA (Rasband 1997-2009).

The multifractal analysis toolbox of FracLac plugin is based on the method developed by Chhapra and Jensen (1989) that is a probability-based approach for multifractal analysis. The details of this method were presented in Section 2.3.3 of Chapter 2 of this thesis.

For a 2D digital image, the object density P_{rj} is defined in Eq. (6.1) as the relative image density in any box *j* of size *r* covering a part of the image:

$$P_{rj} = \frac{M_{rj}}{M} \tag{6.1}$$

where M_{rj} is the mass of the image included in the *jth* element and *M* is the total mass. The whole image is a large matrix of grey-scale values and therefore a binary matrix of 0s and 1s; each covering element can be related to one block of the matrix. For each covering element, M_{rj} is the sum of 1s of that element's matrix and *M* is the sum of all 1s of the floc image matrix. FracLac 2.5 uses Eq. (6.1) and Eqs. (2.31)-(2.33) to determine the bounded singularity spectrum (Eq. (2.27)) of the floc images.

6.2. Results

For about 20 lime softening flocs with different sizes (10-230 μm) the singularity spectrum and Rényi dimension (Eq. (2.27)) were determined. Results of multifractal analysis of 4 individual lime softening flocs are presented in this section.

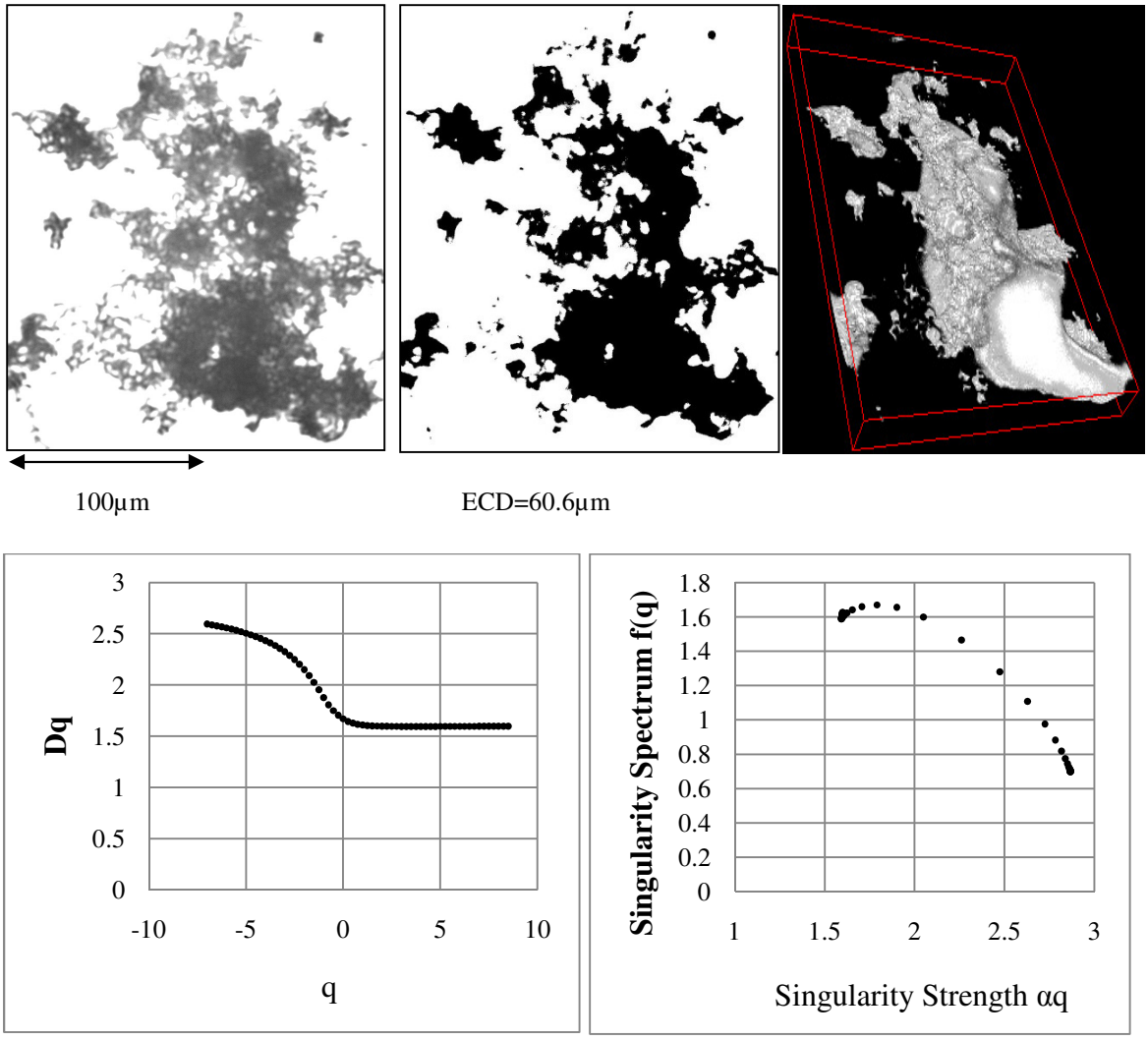

Figure 6.1. Original, binary and 3D image of a lime softening floc #1 (up); Rényi dimension (D_q) and singularity spectrum of the 2D binary image of the floc (down)

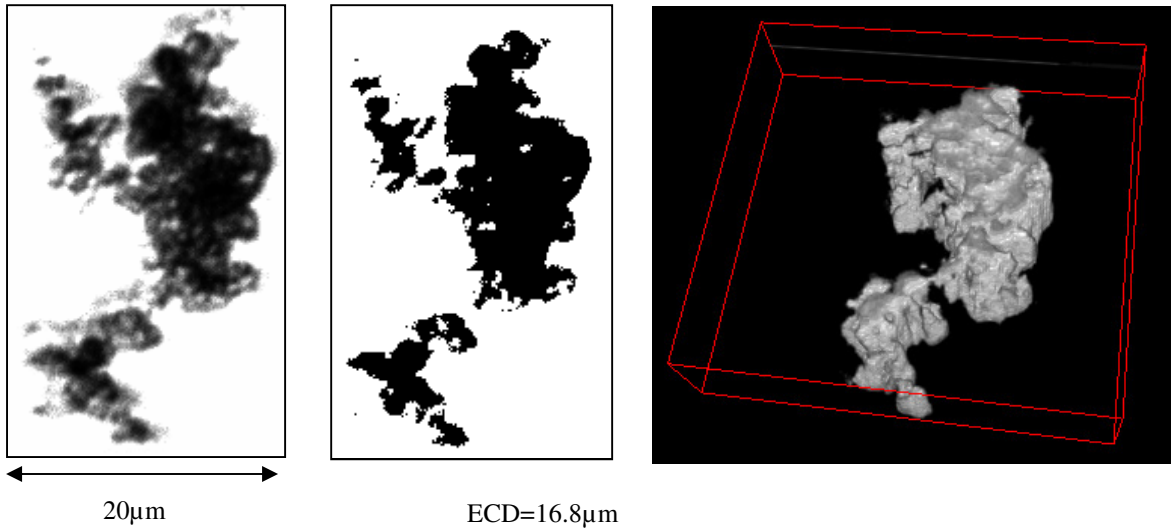

Figure 6.2. Original, binary and 3D image of a lime softening floc #2 (up); Rényi dimension (D_q) and singularity spectrum of the 2D binary image of the floc (down)

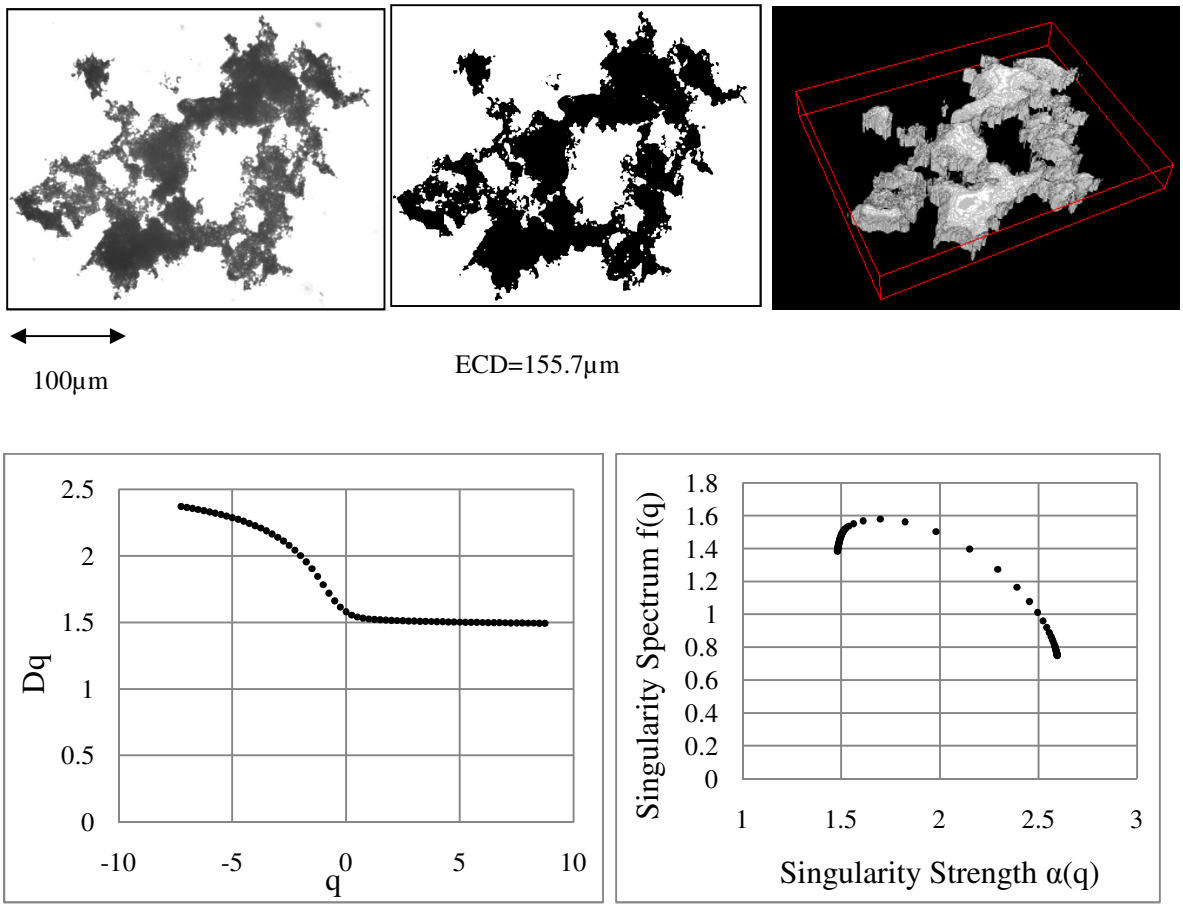

Figure 6.3. Original, binary and 3D image of a lime softening floc #3 (up); Rényi dimension (D_q) and singularity spectrum of the 2D binary image of the floc (down)

In some cases, the multifractal analysis did not yield to an expected spectrum. Eq. (6.2) shows the Rényi dimension (D_q).

$$D_q = \lim_{r \to 0} \frac{1}{q-1} \frac{log \sum_{j=1}^{N_r} \left(P_{rj}^q\right)}{log(r)} \qquad -\infty \leq q \leq +\infty \tag{6.2}$$

In Eq. (6.2) the object densities are less that 1 and by increasing the value of q, the numerator decreases while the denominator increases; therefore the Rényi dimension (D_q) must decrease as

q increases. In this study, in some cases, when q increased and approached infinity, the multifractal analysis resulted in a spectrum that exhibited an increase in Rényi dimension (D_q). An example of such cases is presented below and it can be observed that the Rényi dimension (D_q) first decreases and then increases as q increases.

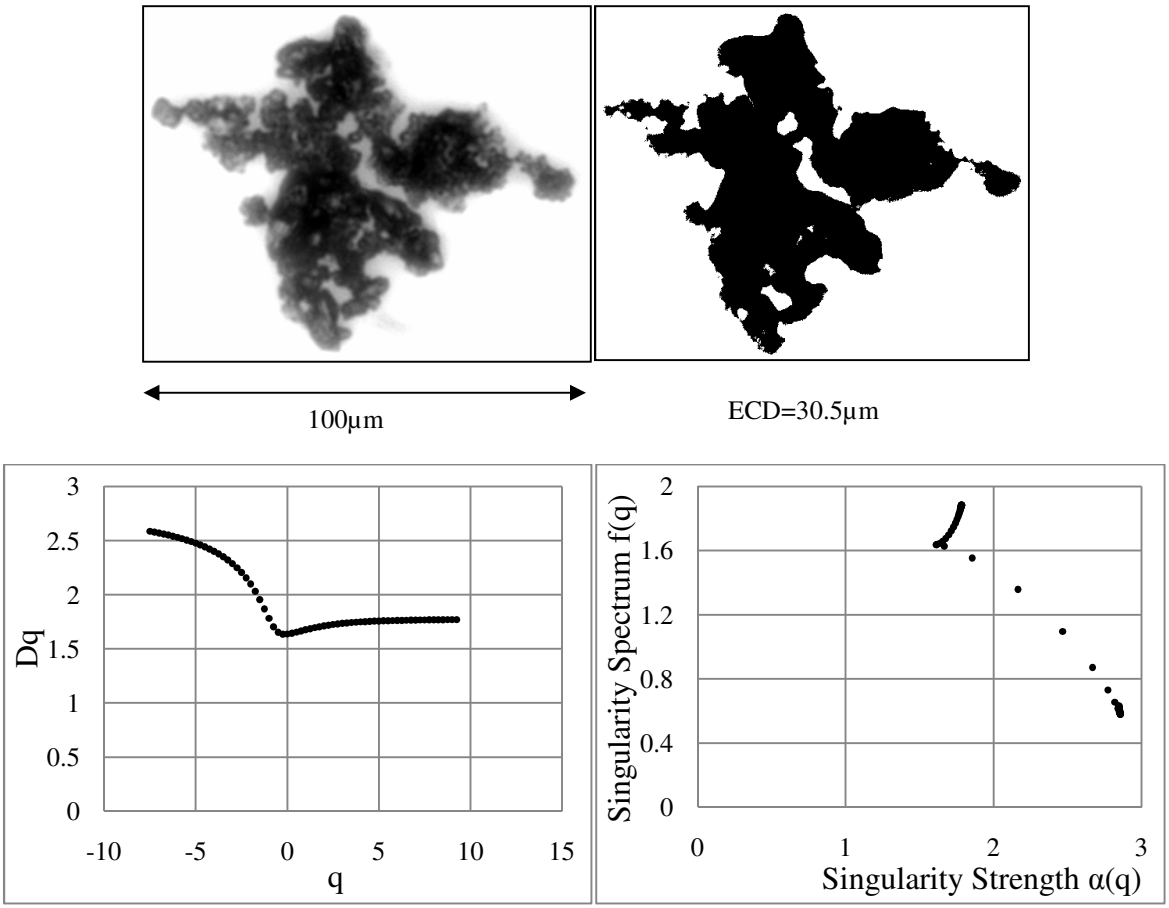

Figure 6.4. An example of multifractal analysis of lime flocs that does not exhibit accepted spectrum

Several factors may cause the unexpected increase of Rényi dimension (D_q) when q increases. In some cases, the imaging and image processing can cause such a problem. We should not forget that what we analyze is only an image of a floc as obtained by using imaging instruments.

Extremely uneven mass distribution inside the floc may cause the unexpected increase of Rényi dimension (D_q) in multifractal analysis. For example, overlapped flocs, trapped sands inside the lime softening flocs or reflection of water drops might result in structures with uneven materials.

The summary of results of multifractal analysis of 15 lime softening flocs is presented in Table **6.1**.

Table 6.1. The results of 2D multifractal analysis of lime softening flocs

Floc #	Size (ECD), µm	D_0	$D_1=D_I$	$D_2=D_C$	D_q range for $0\leq q\leq 5$
1	9.4	1.9	1.87	1.862	1.856-1.9
2	16.8	1.725	1.69	1.67	1.66-1.725
3	25.9	1.87	1.85	1.84	1.827-1.87
4	41.2	1.81	1.763	1.75	1.74-1.81
5	60.6	1.67	1.608	1.597	1.595-1.67
6	70.8	1.7	1.605	1.59	1.572-1.7
7	87	1.64	1.54	1.523	1.499-1.64
8	91.2	1.64	1.572	1.545	1.51-1.64
9	102	1.89	1.78	1.756	1.737-1.89
10	121.3	1.76	1.66	1.638	1.605-1.76
11	145.3	1.65	1.55	1.537	1.49-1.65
12	155.7	1.58	1.525	1.515	1.502-1.58
13	168	1.65	1.52	1.508	1.478-1.65
14	210	1.60	1.46	1.441	1.422-1.60
15	229.5	1.635	1.419	1.4	1.394-1.635

6.3. Discussion

In this chapter, a probability-based method was used for multifractal analysis of 2D images of lime softening flocs. The results indicate that the 2D images of studied lime softening flocs are multifractal and exhibit a spectrum of fractal dimensions.

It is critical to note that the spectrum of the fractal dimensions derived in this chapter is for one individual floc and is different from the distribution of the fractal dimensions that was suggested

in the previous chapter for each floc size. It is important to note that the multifractal spectra are not the origin of various settling velocities for large flocs.

The mass fractal dimension that was estimated by the Housdorff fractal dimension for volume of the aggregate in Chapter 4 is only one point on the multifractal spectrum that was derived in this chapter. All settling models and the one that were presented in this thesis only use the self-similarity dimension of flocs and therefore may not adequately describe the behaviour of multifractal flocs. It may not be easy to incorporate the spectrum of fractal dimensions into floc settling models. However, the multifractal spectrum of flocs may provide valuable explanation of the complexity of such models.

One of the basic parameters in formulation of multifractals is the probabilistic measure, p_{rj} that can show the degree of fullness of each pixel in the image of the studied fractal. In the measurement of Hausdorff dimension in Chapter 4, each pixel could be either black (1) or white (0), while for multifractal analysis the probability of existence of the floc in a certain pixel can be anything from 0 to 1. In fact, the probabilities somehow show the distribution of the mass over the floc image. Therefore, there is a linkage between the singularity spectrum and uniformity of a fractal. Uniform systems are characterized by a parabolic function of multifractal spectrum ($f(\alpha)$) and systems with a higher degree of heterogeneity correspond to a higher deviation of the function of multifractal spectrum from a parabola (Vertyagina 2006). Therefore, we may be able to assess the homogeneity of a fractal by assessing the square approximation of the function of multifractal spectrum by a parabola. For a uniform system, the approximation has the factor of reliability of $R^2=1$ and systems with higher degrees of heterogeneity exhibit the factor of reliability of $0<R^2<1$.

In general the aggregation mechanisms determine the morphology of flocs and their homogeneity or heterogeneity. If flocs are formed by only one aggregation mechanism, it is very likely to have a homogeneous morphology. On the other hand when multiple aggregation mechanisms are involved in formation of flocs, the resulted flocs may have more complex and heterogeneous structure.

The heterogeneity or complexity of fractals can be also assessed by the shape of the Rényi dimension function (D_q). The homogeneous fractals exhibit a narrow range for Rényi dimension, while the complex heterogeneous fractals exhibit a wide range of dimensions (Posadas et al. 2001).

Let us define D_0-D_5 as a parameter that represents the range of Rényi dimension (D_q) for the studied lime softening flocs for $0 \leq q \leq 5$. Fig.6.5 shows the variation of D_0-D_5 with size for 15 studied lime softening flocs.

Figure **6.5** indicates that the large lime softening flocs exhibit a wider deviation of Rény dimensions from D_0 and therefore they may be more heterogeneous than small flocs.

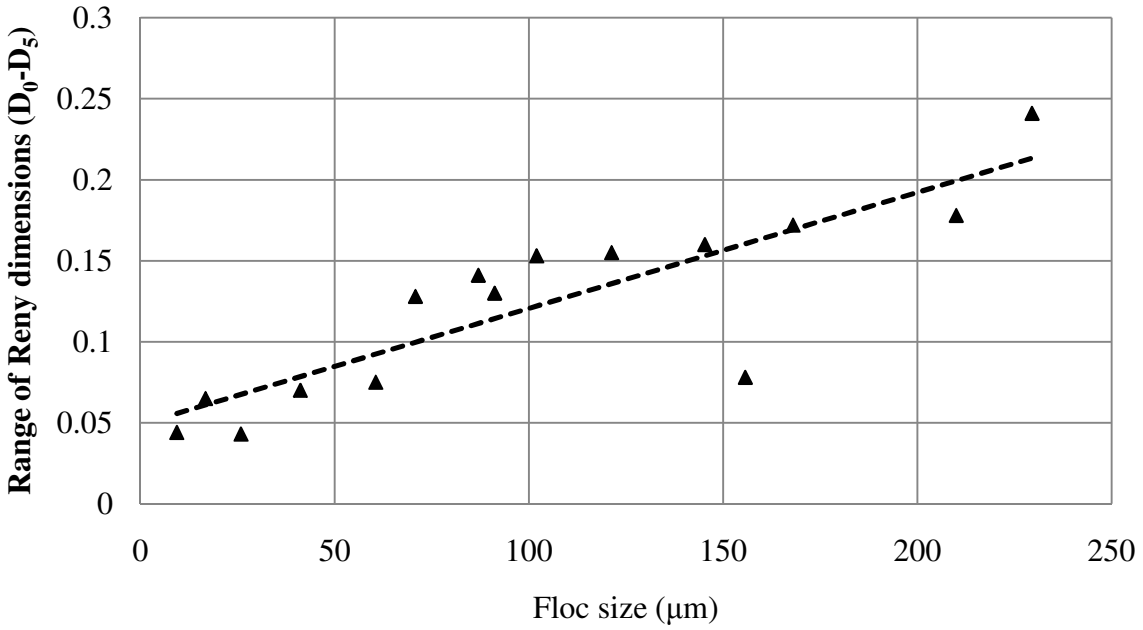

Figure 6.5. Variation of range of Rényi dimension with floc size for lime softening flocs

As mentioned it may be possible to assess the heterogeneity of flocs and the distribution of the mass over the images of the flocs by analyzing the shape of the Rényi dimension (D_q) or singularity spectrum ($f(\alpha)$). It might be possible to use the range of Rényi dimensions or the deviation of singularity spectrum from a parabolic function in the settling model. Such applications need analysis of multifractal structure of flocs in 3D and further investigation of effect of these factors on settling velocity models that are beyond the scope of this thesis and are recommended for the future work in this area.

6.4. Conclusions

The multifractal analysis of lime softening flocs showed that these aggregates are multifractal and a spectrum of fractal dimensions is needed to fully characterize them.

As the floc size increases, the complexity of internal structure of flocs increases as well and the multifractal spectrum of the floc exhibits a wider range for the Rényi dimension.

It may be possible to assess the heterogeneity of flocs and the distribution of the mass over the images of the flocs by analyzing the shape of the Rényi dimension (D_q) or singularity spectrum ($f(\alpha)$).

Chapter 7
Remarks

In this chapter the main conclusions and the significance of this research are briefly listed. Finally the recommendations for future research will be presented.

7.1. Conclusions

Based on the results of the experimental investigations, mathematical modeling, literature studies, and comparison of experimental results with the mathematical models and previous studies the following conclusions can be drawn:

The flocs formed in the lime softening process are responsible for clogging of the sand filters and deposition inside the pipes at the Portage la Prairie water treatment plant.

The flocs not removed by the clarifier are allowed to flocculate to the size of about 40 μm during the recarbonation and ozonation processes.

Increasing the effectiveness of clarifiers and filtering water prior to recarbonation and ozonation units may reduce the chance of sand filter clogging.

Improving the mixing conditions in the recarbonation and ozonation tanks by decreasing the water detention time in each process and rapid mixing may reduce the chance of sand filter clogging.

Changes in pH during the recarbonation as well as ozone dose did not affect the number or the size of the particles. This finding is important because the plant also has a problem with pH and lead corrosion control.

For lime softening flocs larger than 60 μm the model incorporating variable floc fractal dimensions and variable primary particle size describes the settling better than the models assuming fixed values for these parameters (Stokes' Law).

For smaller flocs (<60 μm) Stokes' Law predicts the settling velocity better than the model based on the fractal structure of flocs. This suggests that Stokes' Law can still be applied to aggregates with fractal dimensions close to Euclidean dimensions, such as the small lime flocs and other chemical coagulation aggregates.

It appears that two aggregation mechanisms are involved in the lime flocs formation: Cluster-Cluster Aggregation (CCA) for small flocs (<60 μm) and Diffusion Limited Aggregation (DLA) for large flocs (>60 μm). The precipitation of calcium carbonate particles on the aggregates as well as their penetration into the floc pores appears to be predominant mechanism for large lime flocs formation. This mechanism results in a highly heterogeneous structure for large flocs.

Numerous assumptions contradicting the fractal nature of flocs are used in indirect determinations of mass fractal dimensions from the floc settling rates. These assumptions result in the large discrepancy found between the indirectly determined mass fractal dimension from settling tests and the directly measured volume fractal dimensions of flocs.

For lime softening flocs in the size range of 60-120 µm and 120-250 µm, the directly determined volume fractal dimensions are similar to the fractal dimensions of ideal Sierpinski sponges (Sierpinski carpet in 3D) with the constriction ratios of 3 and 5 respectively.

The settling velocity model that incorporated calculated, normally distributed fractal dimensions for each floc size fitted well the measured settling velocities of lime softening flocs.

Fractal dimensions were generated assuming that a floc can assume any fractal dimension in a certain range, determined by the floc aggregation model. Consequently, a single floc can have a range of different settling velocities. As a result, the relationship between the settling velocity and size of flocs is not unique, but rather in the form of a cloud where several settling velocities are possible for one size of the floc.

Stokes' law significantly overestimates the settling velocity of lime flocs. The settling tank's surface overflow rates may be quite low even for larger lime flocs. The settling velocity of flocs seems to be mainly controlled by aggregation mechanisms and forming large flocs does not guarantee improved sedimentation.

The multifractal analysis of lime softening flocs showed that these aggregates are multifractal and a spectrum of fractal dimensions is needed to fully characterize them.

As the floc size increases, the complexity of internal structure of flocs increases as well and the multifractal spectrum of the floc exhibits a wider range for the Rényi dimension.

It may be possible to assess the heterogeneity of flocs and the distribution of the mass over the images of the flocs by analyzing the shape of the Rényi dimension (D_q) or singularity spectrum ($f(\alpha)$).

7.2. Significance

According to the conclusions, the main objective of this research that was modeling the settling velocity of lime softening flocs by using fractal geometry was accomplished well. The full size distribution of lime softening flocs was derived by using multiple instruments. Also the fractal dimension of lime softening flocs was directly determined on the 3D images of flocs. The application of high speed camera with appropriate image resolution was successful for accurate determination of settling velocity of individual flocs. The results indicated that the major trends and experimental results were consistent with the previous studies on similar aggregates.

Many attempts had been undertaken to model the settling velocity of flocs in water and wastewater treatment processes. It was shown in this thesis that the settling velocity of flocs does not follow any specific curve and the data of settling velocity will be always in a cloud-shaped form due to the various possibilities for arrangement of primary particles within the floc. Based on the results of this thesis a modification of the settling velocity model for fractal aggregates was suggested. The new model that considers the variable heterogeneity of flocs is able to regenerate the cloud-shape relationship of size and settling velocity of flocs.

In this research, the studied flocs were taken directly from an actual water treatment plant; therefore it was possible to connect the results with the practical problems that the water treatment plant faces. For instance, the inefficient removal of lime softening flocs causes filter clogging at the plant that can be directly related to the settling behaviour of individual flocs. The clogging cake on the sand filters is essentially accumulated individual lime softening flocs and therefore the flow through the individual floc may provide information about the hydraulic conductivity of the cake.

A number of recommendations for future research can be made based on the results of this research. The recommendations are presented in the following section of this chapter.

7.3. Recommendations for future work

The work on measuring the fractal dimensions of flocculated aggregates has been an interesting topic for many researchers in past few years. The linkage of fractal dimensions and the settling velocity and other hydrodynamic behaviours of flocs makes the topic even more interesting. Here are my recommendations for future work:

Mathematical modeling of structure and flow through flocs

It seems that the different arrangements of primary particles within the flocs that results in different values for fractal dimensions is similar to some mathematically known structures such as Sierpinski carpets. It would be interesting to study the patterns of arrangement of primary particles inside the flocs and model them with the figures that can be reproduced by computer for further studies. For instance, the flow through a Sierpinski gasket can be mathematically calculated. One interesting work would be investigating the correlation between the fractal dimensions and flow through flocs and comparing the results with flow through the Sierpinski gaskets with similar fractal dimensions. The flow-through flocs can be modeled by using simulation software such as FLUENT or COMSOL.

Modeling the flow through the clogging cake on the filters or membranes

The clogging cake on the filter or membrane is often the accumulation of flocs formed in preceding processes. The flow through individual flocs may also determine the flow through the

cake of flocs. The texture of the clogging layer will depend on the internal pattern of individual flocs as well as the arrangement of accumulated flocs. It is logical to assume a random trajectory at which an individual floc is added to other flocs; therefore a probability distribution for the different possibilities of trajectory of flocs can be assumed for simulating the clogging layer. The modeled flow-through can be compared to experimentally measured flow-through determined from pressure drop or flux of a certain flow through a bench scale filter or membrane.

Application of fractal properties of particles in modeling and optimizing the GAC filters

The granular activated carbon particles are in fact highly porous carbon particles that have a huge internal surface area. GAC filters are usually used as the final stage of water treatment plants. Usually in water treatment plants, a certain level of disinfectant is injected in the finished water in order to control the bacteria growth in the reservoir and distribution system. GAC filters play an important role in controlling the organic content of water. The organic material can react with disinfectants such as chlorine and form THMs that is known to be carcinogenic.

The adsorption capacity of activated carbon particles depends on the porosity that can be related to the fractal dimension of the particles. My recommendation is to analyze the adoption capacity of different types of activated carbon particles and find the correlation between the adsorption capacity of activated carbon particles and their fractal dimension.

There is much evidence showing that only some fractions of organic carbon content of water can cause THMs formation in contact with chlorine. In this research the precursors of THMs are identified by using fractionation technique. The analysis of adsorption capacity can be performed for each THM precursor.

REFERENCES

Alder, P.M., 1986. Transport process in fractals. VI. Stokes flow through Sierpinski carpets, Physics of Fluids **29**, 15-22.

Allen, T., 1997. Particle Size Measurement Volume I: Powder Sampling and Particle Size Measurement, Springer, New York, USA.

Annadurai, G., Sung, S.S., Lee, D.J., 2003. Floc characteristics and removal of turbidity and humic acid from high-turbidity storm water, Journal of Environmental Engineering **129**, 571-575.

APHA, AWWA, WEF, 2005. Standard Methods for the Examination of Water and Wastewater, American Public Health Association, 21st edition, American Public Health Association

Arneodo, A., Grasseau, G., Holschneider, M., 1988. Wavelet transform of multifractals, Physical Review Letters, **61**, 2281-2288.

Aslan, S., Cakici, H., 2007. Biological denitrification of drinking water in a slow sand filter, Journal of Hazardous Materials, **148 (1-2)**, 253-258

Barbot, E., Moustier, S., Bottero, J.Y., Moulin, P., 2008. Coagulation and ultrafiltration: Understanding of the key parameters of the hybrid process, Journal of membrane science, **325**, 520-527.

Bartby, J., 2006. Coagulation and flocculation in water and wastewater treatment, IWA Publishing, London, UK.

Batchelor, G.K., 1967. An Introduction to Fluid Dynamics, Cambridge University Press.

Benefield, L.D., Judkins, J.,F., Weand, B.L., 1982. Process chemistry for water and wastewater treatment.

Bouyer, D., Line, A., Dp-Quang, Z., 2004. Experimental analysis of floc size distribution under different hydrodynamics in a mixing tank, AICHE Journal, **50(9)**, 2064-2081.

Brown, W.D., Ball, R.C., 1985. Computer simulation of chemically limited aggregation, J. Phys. A: Math. Gen., 517-521.

Brown, P.P., Lawler, D.F., 2003. Sphere drag and settling velocity revisited, Journal of Environmental Engineering ASCE **129**, 222-231.

Bugni, D., 2007. Experimental and numerical investigation of settling and synthetic fractal aggregates. IWA International Conference on Particle Separation July 9-12 Toulouse France.

Bushell, G.C., Yan, Y.D., Woodfield, D., Raper, J., Amal, R., 2002. On technique for the measurement of the mass Fractal dimension of aggregates. Advanced Colloid and Interface Science **95**, 1-50.

Chakraborti, R.K., Gardner, K.H., Kaur, J., Atkinson, J.F., 2007. In situ analysis of flocs. Journal of Water Supply: Research and Technology – AQUA **56**, 1-11.

Chavez, P., Yarleque, C., Piro, O., Posadas, A., Mares, V., Loayza, H., Chuquillanqul, C., Zorogastua, P., Flexas, J., Quiroz, R., 2010. Applying multifractal analysis to remotely sensed data for assessing PYVV infection in potato (solanum tuberosum L.) corps, Remote Sensing, **2**, 1197-1216.

Chhabra, A., Jensen, R.V., 1989. Direct determination of singularity spectrum Physical Review Letters **62 (12)**, 1327-1330.

Choi, Y.H., Kim, H.S., Kweon, J.H., 2008. Role of hydrophobic organic matter flocs on the fouling in coagulation-membrane processes, Separation and Purification Technology, **62**, 529-534.

Chu, C.P., Lee, D.J., Peng, X.F., 2004. Structure of conditioned sludge flocs, Water Research **38**, 2125-2134.

Chu, C.P., Lee, D.J., Tay, J.H., 2005, Floc model and intrafloc flow, Chemical Engineering Science **60**, 565-575.

Chung, H.Y., Lee, D.J., 2003. Porosity and interior structure of flocculated activated sludge flocs. Journal of Colloid and Interface Science **267**, 136-143.

Coufort, C., Dumas, C., Bouyer, D., Line, A., 2008. Analysis of floc size distributions in a mixing tank, Chemical Engineering and Processing, **47**, 287-294.

Cousin, C.P., Ganczarczyk, J.J., 1998. Effects of salinity on the physical characteristics of activated sludge flocs. Water Quality Research **33**, 565-587.

Darby, J.L., Lawler, D.F., 1990. Ripening in depth filtration: effect of particle size on removal and head loss, Environmental Science and Technology, **24**, 1069-1079.

Daubechies, I., Lagarias, J.C., 1992. Two-scale difference equations II. Local regularity infinite products of matrices and fractals, SIAM Journal of Mathematical Analysis, **23(4)**, 1031-1079.

De Julio, M., Gregory, J., 2009. Effect of included particles on hydroxide floc properties, IWA nanoparticle and particle separation conference, Durham, NC, USA.

Dong, Y.J., Wang, Y.L., Feng, J., 2011. Rheological and fractal characteristics of unconditioned and conditioned water treatment residuals, Water Research, In Press.

Ekama, G.A., Barnard, J.L., Gunthert, F.W., Krebs, P., McCorquodale, J.A., Parker, D.S., Wahlberg, E.J., 1997. Secondary settling tanks: theory, modeling, design and operation. International Association on Water Quality, London.

Gao, R.X., Yan, R., 2010. Wavelets: theory and application for manufacturing, Springer, New York, USA.

Ganczarczyk, J.J., 1995. A correlation between external surface characteristics and settling velocity of activated sludge flocs. Newsletter of the International Association on Water Quality, Specialist Group on Activated Sludge population Dynamics **8**, 4-6.

Ganczarczyk, J.J., Rizzi, M., 1996. Mechanism of sludge formation and dewatering. CSCE 4th Environ. End Conference Edmonton.

GENIVAR, 2010. Water system infrastructure and water supply source assessment for the City of Portage la Prairie.

Grassberger, P., 1985. Generalization of the Hausdorff dimension of fractal measures, Physical Letters A, **107(3)**, 101-105.

Gomes, C., Selman, B., 1999. On the fine structure of large search spaces. 11th IEEE ICTAI Conference Proceeding, IEEE Computer Society, Washington, DC, USA.

Gorczyca, B., Ganczarczyk, J.J., 1996. Image analysis of alum coagulated mineral suspensions. Environmental Technology **17**, 1361-1369.

Gorczyca, B., Ganczarczyk, J.J., 1999. Structure and porosity of alum coagulation flocs. Water Quality Research **34**, 653-666.

Gorczyca, B., Ganczarczyk, J.J., 2001. Fractal analysis of pore distributions in alum coagulation and activated sludge flocs. Water Quality Research **36(3)**, 687-700.

Gorczyca, B., Ganczarczyk, J.J., 2002. Flow rate through alum coagulation and activated sludge flocs. Water Quality Research **37**, 389-398.

Gorczyca, B., Klassen, P., 2008. Optimization of solid separation in dissolved air flotation. Water Research **43**, 239-247.

Gorczyca, B., London, D., 2003. Characterization of particles in slow sand filtration at North Caribou water treatment plant, Water Quality Research, **38(1)**, 153-168

Govoreanu, R., Saveyn, H., Van der Mearen, P., Nopens, I., Vanrolleghem, P.A., 2009. A methodological approach for direct quantification of the activated sludge floc size distribution by using different techniques, Water Science and Technology, **60(7)**, 1857-1867.

Graf, W.H., 1977. Hydraulics of sediment transport. McGraw-Hill Book Company, New York

Gregory, J., 2009. Optical monitoring of particle aggregates, Journal of Environmental Sciences, **21**, 2-7.

Halsey, T.C., 2000. Diffusion limited aggregation: a model for pattern formation, Physics Today, 36-41.

Health Canada, 2008. Guidelines for Canadian Drinking Water Quality: http://www.hc-sc.gc.ca/ewh-semt/water-eau/drink-potab/guide/index_e.html, November 2010

Hentschel, H.G.E., Procaccia, I., 1983. The infinite number of generalized dimensions of fractals and strange attractors. Physica D:Nonlinear Phenomena, **8(3)**, 435-444.

Hilligardt, D., Hoffmann, E., 1997, Particle size analysis and sedimentation properties of activated sludge flocs", Water Science and Technology **36**, 167-175.

Holschnieder, M., 1988. On the wavelet transformation of fractal objects, Journal of Statistical Physics, **50(5/6)**, 963-993.

Hribersek, M., Zajdela, B., Hribernik, A., Zadravec, M., 2011. Experimental and numerical investigations of sedimentation of porous wastewater sludge flocs, Water Research, **45**, 1729-1735.

Huang, C., Lin, J.L., Lee. W.S., Pan, J.R., Zhao, B., 2011. Effect of coagulation mechanism on membrane permeability in coagulation-assisted microfiltration for spent filter backwash water recycling, Colloids and Surfaces A: Physicochemical and Engineering Aspects, **378**, 72-78.

Huisman, L., Wood (F.I.C.E.), W.E., 1974. Slow sand filtration, World Health Organization, Geneva, Belgium

Imre, A.R., 2006. Artificial fractal dimension obtained by using perimeter-Area relationship on digitalized images, Applied Mathematics and Computation **173**, 443-449.

Jarvis, P., Jefferson, B, Parsons, S.A., 2005. How the natural organic matter to coagulant ratio impacts on floc structural properties. Environmental Science and Technology **39**, 8919-8924.

Ji, J., Qui. J., Wong, F.S., Li, Y., 2008. Enhancement of filterability in MBR achieved by improvement of separation and floc characteristics visa filter aids addition, Water Research, **42**, 3611-3622.

Johnson, C.P., Li, X., Logan, B.E., 1996. Settling Velocities of fractal aggregates, Environmental Science and Technology **30(6)**, 1911-1918.

Jullien, R., Botet, R., Mors, M., 1987. Computer simulation of cluster-cluster aggregation. Faraday Discussions of Chemical Society 83, 125-137.

Kamiti, M., Van de Ven, T.G.M., 1995. Impinging jet studies of the kinetics of deposition and dissolution of calcium carbonate particles. Collides and Surfaces A: Physiochemical and Engineering Aspects **100**, 117-129.

Karperien, A., 2007. Fraclac advanced user's manual, Charles Sturt University, Australia.

Kaye, B., 1993. Chaos and complexity. VCH Publishers, New York.

Khelifa, A., Hill, P. S., 2006. Models for effective density and velocity of flocs. Hydraulic Research **44(3)**, 390-401.

Kim, S.H., 2001. Effects of PH and dosage on pollutant removal and floc structure during coagulation. Micro chemical Journal **68**, 197-203.

Kinsner, W., 2005. A unified approach to fractal dimensions, Proceedings of the Fourth IEEE International Conference on Cognitive Information (ICCI), Irvine, CA, August 2005. IEEE Computer Society, pp. 55-72.

Kolb, M., Botet, R., Jullien, R., 1983. Scaling of kinetically growing clusters, Physical Review Letters, **51**, 1123-1126.

Kranenburg, C., 1994. The fractal structure of cohesive sediment aggregates, Estuarine, Coastal and Shelf Science, **39**, 451-460.

Lawler, D.F., Nason, J., 2006. Granular media filtration: old process, new thoughts, Water Science and Technology, **53(7)**, 1-7.

Lee, D.J., Chen, G.W., Liao, Y.C., Hsieh, C.C., 1996. On the free-settling test for estimating activated sludge flocs density. Water Research **30(2)**, 541-550.

Li, D.H., Ganczarczyk, J.J., 1987. Stroscopic determination of settling velocity, size and porosity of activated sludge flocs, Water Research **21**, 257-261.

Li, D.H., Ganczarczyk, J.J., 1989. Fractal geometry of particle aggregates generated in water and wastewater treatment processes. Environmental Science and Technology **23**, 1385-1389.

Li, D.H., Ganczarczyk, J.J., 1992. Advective transport in activated sludge flocs. Water Environment Research **64**, 236-240.

Li, X.Y., Logan, B.E., 2001. Permeability of fractal aggregates. Water Research **35**, 3373-3380.

Li, X., Yuan, Y., 2002. Settling velocities and permeability of microbial aggregates, Water Research **36**, 3110-3120.

Li, X., Yuan, Y., Wang, H., 2003. Hydrodynamics of biological aggregates of different sludge age: an insight into the mass transport mechanism of bioaggregates, Environmental Science and Technology **37(2)**, 292-299.

Liao, J.Y.H, Selomulya, C., Bushell, G., Blackert, G., Amal, R., 2005. On different approaches to estimate the mass fractal dimension of coal aggregate, Particle and Particle Systems Characterization **22(5)**, 229-309.

Logan, B.E., 1999. Environmental Transport Processes. John Wiley and Sons Inc., New York.

Maggi, F., Winterwerp, J.C., 2004. Method for computing the three-dimensional capacity dimension from two-dimensional projections of fractal aggregates. Physical Review **E69**, 011405.

Maggi, F., 2005, Flocculation dynamics of cohesive sediment. PhD thesis, University of Delft, Netherlands.

Maggi, F., Manning, A.J., Winterwerp, J.C., 2006, Image separation and geometric characterisation of mud flocs, Journal of Hydrology **326**, 325-348.

Maggi, F., Mietta, F., Winterwerp, J.C., 2007. Effect of variable fractal dimension on the floc size distribution of suspended cohesive sediment. Journal of Hydrology **343**, 43-55.

Mallat, S.G., 1989. Theory for multiresolution signal decomposition: the wavelet representation, IEEE Transcription on Pattern Analysis and Machine Intelligence, **11(7)**, 674-692.

Mandelbrot, B. B., 1982. The fractal geometry of nature. W.H. Freeman, New York.

Mandelbrot, B.B., 1985. Self-affine fractals and fractal dimension, Physica Scripta, **32**, 257-260.

Manning, A.J., Baugh, J.V., Spearman, J.R., Whitehouse, R.J.S., 2010, Flocculation settling characteristics of mud: sand mixtures, Ocean Dynamics, **60**, 237-253.

Markus, H.G., 2009. Particle Size Measurement, Springer, New York, USA.

Meakin, P., 1983[a]. Diffusion-controlled cluster formation in 2-6 dimensional space, Physical Review A, **27**, 1495-1507.

Meakin, P., 1983[b]. Formation of fractal clusters and networks by irreversible diffusion-limited aggregation, Physical Review Letters, **51**, 1119-1122.

Meakin. P., 1984. Effects of cluster trajectories on cluster-cluster aggregation: A comparison of linear and Brownian trajectories in two and three-dimensional simulations. Physical Review A **29(2)**, 997-999.

Meakin. P., 1985. The effects of random bond breaking on diffusion limited cluster-cluster aggregation. Journal of Chemical Physics **83(7)**, 3645-3649.

Meakin, P., Jullien, R., 1988. The effects of restructuring on the geometry of clusters formed by diffusion-limited, ballistic, and reaction-limited cluster-cluster aggregation, Journal of Chemical Physics, **89(1)**, 246-251.

Mikeš, D., 2011. A Simple Floc-Growth Function for Natural Flocs in Estuaries, Mathematical Geosciences, **43(5)**, 593-606.

Motta, M.D., Pons, M.N., Roche, N., 2001, Automated monitoring of activated sludge in a pilot plant using image analysis, Water Science and Technology **43**, 91-96.

Murguia, J.S., Urias, J., 2001. On the wavelet formalism of multifractal analysis, Chaos, **11(4)**, 858-863.

Namer, J., Ganczarczyk, J.J., 1993. Settling properties of digested sludge particle aggregates. Water Research **27**, 1285-1294.

Nason, J., Lawler, D.F., 2008. Particle size distribution dynamics during precipitative softening constant solution composition, Water Research, **42(14)**, 3667-3676.

Neal, G., Epstein, N., Nader, W., 1973. Creeping flow relative to permeable spheres, Chemical Engineering Science **28**, 1865-1874.

Nies, U., Tiehm, A., 1997. Particle size analysis in primary and secondary wastewater effluents, Water Science and Technology **36**, 151-158.

Parker, B., 1970. Characteristics of biological flocs in turbulent regimes. PhD thesis, University of California, Berkeley.

Parker, D., Kaufman, W.J., Jenkins, D., 1972. Floc breakup in turbulent flocculation processes, Journal of Sanitary Engineering Division, **98(1)**, 79-99.

Perrier, E., Tarquis, A.M., Dathe, A., 2006. A program for fractal and multifractal analysis of two-dimensional binary images: Computer algorithms versus mathematical theory, Geoderma, **134**, 284-294.

Platzer, C.H.R., Mauch, K., 1997. Soil clogging in vertical-flow reed beds – mechanisms, parameters, consequences and ….. solutions, Water Science and Technology, **35(5)**, 175-181

Posadas, A.N.D., Gimenez, D., Bittelli, M., Vaz, C.M.P., Flury, M., 2001. Multifractal characterization of soil particle-size distribution, Soil Science Society (American Journal), **65**, 1361-1367

Rattanakawin, C., 2005. Aggregate size distribution in sweep flocculation, Journal of Science and Technology, **27(5)**, 1095-1101.

Reddi, L.N., Ming, X., Hajra, M.G., Lee, I.M., 2000. Permeability reduction of soil filters due to physical clogging, ASCE Journal of Geotechnical and Geoenviornmental Engineering, **126(3)**, 236-246

Reidi, R.H., Crouse, M.S., Riebeiro, V.J., Baraniuk, R.G., 1999. A multifractal wavelet model with application to network traffic, IEEE Transactions on Information Theory, **45(3)**, 992-1018.

Rooklidge, S.J., Burns, E.R., Bolte, J.P., 2005. Modeling antimicrobial contaminant removal in slow sand filtration, Water Research, **39**, 331-339

Schmid, M. Thill, A., Purkhold, U., Walcher, M., Bottero, J.Y., Ginestet, P., Nielsen, P.H., Wuertz, S., Wagner, M., 2003. Characterization of activated sludge flocs by confocal laser scanning microscopy and image analysis. Water Research **37**, 2043-2052.

Shannon, C.E., 1948. A mathematical theory of communication, The Bell System Technical Journal, **27**, 379-423, 623-656.

Son, M., Hsu, T.J., 2008. Flocculation model of cohesive sedimen using variable fractal dimension. Environmental Fluid Mechanics, **8**, 55-71.

Snidaro, D., Zartarian, F., Jorand, F., Bottero, J.Y., Block, J.C., Manem, J.,1997. Characterization of activated sludge flocs structure. Water Science Technology **36(4)**, 313-320.

Spicer, P.T., Pratsinis, S.E., 1996. Shear-induced flocculation: the evolution of floc structure and the shape of the size distribution at steady state, Water Research, **30**, 1049-1056

Stanley, H.E., Meakin, P., 1988. Multifractal phenomena in physics and chemistry, Nature, **335(29)**, 405-409.

Sterling, Jr. M.C., 2005. Application of fractal flocculation and vertical transport model to aquatic sol–sediment systems. Water Research **39**, 1818–1830.

Stone, M, 1961. Linear opinion pool. The Annuals of Mathematical Statistics **32(4)**, 1339-1342.

Tan, Z.J., Zou X.W., Zhang W.B., Jin Z.Z., 1999. Influence of particle size on diffusion limited aggregation, Physical Review E, **60**, 6202-6205.

Tang, P., Greenwood, J., Raper J.A., 2002. A model to describe the settling behaviour of fractal aggregates. Journal of Colloid and Interface Science **247**, 210-219.

Thill, A., Veerapaneni, S., Simon, B., Wiesner, M., Bottero, J.Y., Snidaro, D., 1998. Determination of structure of aggregates by confocal scanning laser microscopy. Journal of Colloid and Interface Science **204**, 357-362.

Thirunavukkarasu, O.S., Viraraghavan, T., Subramanian, K., S., 2003. Arsenic removal from drinking water using iron oxide-coated sand, Water, air and soil pollution, **142**, 95-111.

The City of Portage La Prairie, 2009. [http://www.city.portage-la-prairie.mb.ca/]

Thomas, D.G., 2004. Turbulent disruption of flocs in small particle size suspensions, AICHE Journal, **10(4)**, 517-523.

Thouy. R., Jullien. R., 1994. A cluster-cluster aggregation model with tunable fractal dimension. Journal of Physics A: Mathematical and General **27**, 2953-2963.

Turkevich, L.A., Scher, H., 1985. Occupancy-probability scaling in diffusion limited aggregation, Physical Review Letters, **55**, 1026-1029.

Vahedi, A., Gorczyca, B., 2009. Fractal analysis of flocs formed in lime softening process, ACE09, AWWA conference, San Diego, CA, USA.

Vahedi, A., Gorczyca, B., 2010. Analysis of Particle Formation and Filter Fouling at Portage La Prairie and RM of Macdonald Water Treatment Plants, CSCE 11th annual conference, Winnipeg June 9-12.

Vahedi A., Gorczyca B., 2011, Application of fractal dimensions to study the structure of flocs formed in lime softening process, Journal of Water Research, **45(2),** 545-556.

Van Gelder, A.M., Chowdhury, Z.K., Lawler, D.F., 1999. Conscientious particle counting, American Water Works Association Journal, **91(12)**, 64-78.

Vertyagina, E.N., 2006. Research of open systems evolution by the method of multifractal analysis, Proceedings of the Conference of Chaos and Structures in Nonlinear Systems: Theory and Experiment, Astana, Kazakhstan.

Wang, D., Wu, R., Jiang, Y., Chow, C.W.K., 2010. Characterization of floc structure and strength: Role of changing shear rates under various coagulation mechanisms, Colloids and Surfaces, **379**, 36-42.

Weipeng, H., Nun, J., Song, J., Song, X., 2009. Application of numerical simulation to investigate fractal structure of flocs formed in flocculation process of water treatment, ICEET, **2**, 441-445, International Conference on Energy and Environment Technology.

Weiying, X., Gao, B., Yue, Q., Bo, X., 2011. Influence of pH on flocs formation, breakage and fractal properties-the role of Al_{13} polymer, Journal of Water Sustainability, **1(1)**, 45-57.

Winterwerp, J.C., 1998. A simple model for turbulence induced flocculation of cohesive sediment. Journal of Hydraulic Research **36**, 309-326.

Witten, T.A.Jr., Sander. L.M., 1981. Diffusion-limited aggregation, a kinetic critical phenomenon. Physical Review Letters **47**, 1400-1403.

Witten, T.A.Jr., Sander. L.M., 1983. Diffusion-limited aggregation, Physical Review B, **27**, 5686-5697.

Wotton, R.S., 2002. Water purification using sand, Hydrobiologia, 469, 193-201

Wu, R.M., Lee, D.J., 2003. Estimation of floc permeability and porosity, Journal of Chinese Institute of Chemical Engineers **34(2)**, 275-280.

Wu, R.M., Tsou, G.W., Lee, D.J., 2000. Estimation of the interior permeability of polymer-flocculated sludge flocs, Advances in Environmental Research **4**, 163-167.

Wu, J., He, C., 2010. Experimental and modeling investigation of sewage solids sedimentation based on particle size distribution and fractal dimension, Journal of Environmental Science and Technology, **7(1)**, 37-46.

Yang, Z., Peng, X.F., Lee, D.J., Ay, S., 2007. Advective flow in spherical floc, Journal of Colloids and Interface Science, **308**, 451-459.

Yang, Z., Lee, D.J., Mujumdar, A.S., Peng, X.F., Su, A., Hsu, C., 2008. Probing heterogeneous structure of aggregates, Drying Technology **26(8)**, 1018-1023.

Yu, W.Z., Gregory, J., Campos, L., Li, Guibai, 2011. The role of mixing conditions on floc growth, breakage and re-growth, Chemical Engineering Journal, In Press.

Zhang, Z.B., 2007. Particle size distribution and removal by a chemical-biological flocculation process, Journal of Environmental Sciences **19**, 559–563.